
From the: *Helmholtz Zentrum München*



Dissertation

zum Erwerb des Doctor of Philosophy (Ph.D.) an der Medizinischen
Fakultät der

Ludwig-Maximilians-Universität zu München

Cathepsin B,
a new player in the progression of
Bronchiolitis Obliterans Syndrome

vorgelegt von:

Carmela Morrone

aus:

Italy

Jahr:

2020

First supervisor: Dr. Dr. Alexey Dashkevich

Second supervisor: Dr. Dr. Nikolaus Kneidinger

Co-supervisor: Dr. Ali Önder Yildirim

Third TAC member: Dr. Dr. Sebastian Michel

Fourth TAC member: Prof. Dr. Dr. Wolfgang Jungraithmayr

Dean: Prof. Dr. med. dent. Reinhard HICKEL

Datum der Verteidigung:

19th October 2020

Affidavit

Morrone, Carmela

Surname, first name
Street

Munich

Zip code, town

Germany

Country

I hereby declare, that the submitted thesis entitled

**Cathepsin B, a new player in the progression of
Bronchiolitis Obliterans Syndrome**

is my own work. I have only used the sources indicated and have not made unauthorised use of services of a third party. Where the work of others has been quoted or reproduced, the source is always given.

I further declare that the submitted thesis or parts thereof have not been presented as part of an examination degree to any other university.

Munich, 06Nov2020

Place, date

Carmela Morrone

Signature doctoral candidate

ABBREVIATIONS

A

A1ATD	Alpha 1 Anti Trypsin Deficient
ABO	ABO blood group system
aCatB	active Cathepsin B
AMs	Alveolar Macrophages
ANOVA	Analysis of Variance
APCs	Antigen Presenting Cells
Asn	Asparagine

B

B	B cells/ B lymphocytes
B6	Black 6, abbreviation of C57BL/6J
B6→ B6	Black 6 implanted in Black 6
BAL	Broncho Alveolar Lavage
BALF	Broncho Alveolar Lavage Fluid
BCA	Bicinchoninic acid assay
BOS	Bronchiolitis Obliterans Syndrome
BOS 0	Bronchiolitis Obliterans Syndrome grade 0
BOS 1	Bronchiolitis Obliterans Syndrome grade 1
BOS 2	Bronchiolitis Obliterans Syndrome grade 2
BOS 3	Bronchiolitis Obliterans Syndrome grade 3
BSA	Bovine serum albumin

C

CA074	inhibitor of Cathepsin B activity
CAST	Computer Assisted Stereological Toolbox
CatB	Cathepsin B
CatH	Cathepsin H
CatL	Cathepsin L
CatS	Cathepsin S
CD3	Cluster of Differentiation 3, specific for T cells
CD45R	Cluster of Differentiation 45R, specific for B cells
CD4 +	Cluster of Differentiation 4, specific for T-helper cells
CF	Cystic Fibrosis
CLAD	Chronic Lung Allograft Dysfunction
COPD	Chronic Obstructive Pulmonary Disease
CT	Computer Tomography
<i>Ctsb</i>	Cathepsin B gene name
<i>Ctsb</i> -/-	Cathepsin B deficient mouse strain
<i>Ctsb^{tm1Jde}/J</i>	Cathepsin B deficient mouse strain
CXCR3	CXC chemokine receptor expressed on activated T cells
CysC	Cystatin C

D

DAB	3, 3' diaminobenzidine tetrahydrochloride substrates
DAPI	4',6-diamidino-2-phenylindole fluorescent dye

DBD	Donor after Brain Death
DCD	Donor after Circulatory Death
ddcfDNA	donor derived circulating cell free DNA
DLTx	Double Lung Transplantation
DMEM	Dulbecco's Modified Eagle Medium
DMEM/F12	Dulbecco's Modified Eagle Medium with F12 Supplements
CM	Conditioned Medium
DMSO	Dimethyl sulfoxide
dNTPs	Desoxyribonucleotides
DS	Deviation Standard
DSAs	Donor Specific Antibodies
dsDNA	double strand Deoxyribonucleic acid

E

ECL substrate	Enhanced Chemiluminescence substrate
ECM	Extracellular Matrix
EDTA	Ethylenediaminetetraacetic acid
ELISA	Enzyme-linked immunosorbent assay
EMT	Epithelial Mesenchymal Transition
EVLP	<i>Ex Vivo</i> Lung Perfusion

F

F	Female
FBS	Fetal Bovine Serum
FEV1	Forced Expiratory Volume in 1 second %
FK 506	Tacrolimus, immunosuppressive drug for transplantation
FN1	Fibronectin 1
FRC	Functional Residual Capacity
FRET	Fluorescence Resonance Energy Transfer
FVC	Forced Vital Capacity

G

Gal3	Galectin 3, marker for macrophage
------	-----------------------------------

H

H ₂ O ₂	Water
hBALF	human Broncho Alveolar Lavage Fluid
HLA	Human Leukocyte Antigen
HLA→ B6	HLA implanted in Black 6
HLA→ <i>Ctsb</i> -/-	HLA implanted in Cathepsin B deficient mice
HLA.A2	Human Leukocyte Antigen class A2
HE	Hematoxylin Eosin
His	Histidine
HPRT	Hypoxanthine Phosphoribosyltransferase
HRCT	High Resolution Computed Tomography
HRP-conjugated	Horseradish Peroxidase

I

I-airway	Inter-airway
----------	--------------

I-septa	Inter-septa
I-vessel	Inter-vessel
IL4	Interleukin 4
IL13	Interleukin 13
IFN- γ	Interferon gamma
ILD	Interstitial Lung Disease
IMs	Interstitial Macrophages
IPF	Idiopathic Pulmonary Fibrosis
IPD	Interstitial Pulmonary Disease
IRI	Ischemia Reperfusion Injury

J

JHLT	Journal of Heart and Lung Transplantation
------	---

L

L9-V10-G11	Leucin 9-Valine 10-Glycine 11
LAP	Latency Associated Protein
LNC-NS-629	Liposomal nanocarrier, CatB inhibitor
L(p)	Line per point
LPS	Lipopolysaccharides
LTx	Lung Transplantation
Ly6G	Lymphocyte antigen 6 complex locus G6D

M

M	Molar
M	Male
M0	Macrophages not differentiated
M1	Pro-inflammatory Macrophages
M2	Anti-inflammatory Macrophages
mCatB	mature Cathepsin B
MCL	Mean Chord Line
MEF	Mouse Embryonic Fibroblast
MgCl ₂	Magnesium chloride
Mregs	regulatory Macrophages
MW	Molecular Weight
mM	nano Molar
μ M	microMolar
μ m	micrometer

N

NaCl	Sodium Chloride
NOS2	Nitric Oxide Synthase 2

P

P	p-value, probability value
PAH	Pulmonary Arterial Hypertension
PBS	Phosphate-buffered saline
PBSA	Phosphate-buffered saline supplemented with BSA
PBS-T	Phosphate-buffered saline supplemented with Tween
PGD	Primary Graft Dysfunction

Pen/Strep	Penicillin-streptomycin
pH	power of Hydrogen
PH	Pulmonary Hypertension
proCatB	Pro-form of Cathepsin B
pSMAD3	phosphorilation of signal transducers proteins of TGF-B1RI
R	
RAS	Restrictive Allograft Syndrome
Raw	Airway Resistance
Raw264.7	Abelson murine leukemia virus transformed macrophage
reLTx	re-lung transplantation
RIPA	Buffer for cell lysis and protein solubilization
RT	Room Temperature
RV	Residual Volume
S	
S	Stable
SB431542	inhibitor for Alk 5 receptor
SDS	Sodium dodecyl sulphate
SDS-PAGE	Sodium dodecyl sulphate-PolyAcrylamide Gel Electrophoresis
SEM	Standard Error of the Mean
SMA	Smooth Muscle Actin
SMAD	signal transducers protein of TGF-B1RI
SLTx	Single Lung Transplantation
SYBR Green	Dye for the quantification of double stranded DNA
T	
T	T cells/ T Lymphocytes
TBB	Transbronchial Biopsy
TBLB	Transbronchial Lung Biopsy
TBS	Tris-buffered saline solution
TGF- β 1	Transforming growth factor beta 1
TGF- β 1RII	TGF- β 1 type-II-receptor
TLC	Total Lung Capacity
TNF α	Tumor Necrosis Factor alpha
Tx	Transplantation
Z	
Z-Arg-Arg-AMC	fluorogenic substrate specific for Cathepsin B

Table of Contents

ABBREVIATIONS	2
SUMMARY	7
1. INTRODUCTION	8
1.1 Lung Transplantation	8
1.2 Clinical Diagnosis after LTx.....	11
1.3 Complications of LTx	12
1.4 Lung allograft dysfunctions	12
1.5 Lung allograft biomarkers.....	17
1.6 Lung macrophages	18
1.7 Other molecular lung allograft features	19
1.8 Cystatin C and Cathepsin B	21
1.9 Experimental murine models of LTx	23
2. AIM OF THE PROJECT	25
3. MATERIALS AND METHODS	27
3.1 List of materials	27
3.2 Molecular biological methods.....	35
3.3 Protein analysis	36
3.4 Protease activity assay	38
3.5 ELISA	39
3.6 Mouse experiments	40
3.7 Lung tissue staining	42
3.8 Signal quantification	44
3.9 Cell culture.....	45
4. RESULTS AND FIGURES	47
4.1 Demographics of patients involved in the study	47
4.2 Newly formed collagen levels increased in BOS patients	51
4.3 Cystatin C levels decreased in BOS patients	52
4.4 Cathepsin B activity increased in BOS patients.....	53
4.5 Cathepsin B expression increased in BOS patients.....	55
4.6 Enhanced Cathepsin B activity in IPF patients	57
4.7 Infiltrating macrophages are the main source of CatB in BOS.....	58
4.8 Cathepsin B expression increases in a murine model of LB.....	62
4.9 Genetic deletion of Cathepsin-B protected lungs from BOS development	66
4.10 Cathepsin B expression in pro-inflammatory macrophages	69
4.11 Cathepsin-B contributed to fibroblast activation via TGF β 1-maturation	71
5. DISCUSSION	74
6. REFERENCES	79
7. LIST OF TABLES	87
8. LIST OF FIGURES	88
9. LIST OF PUBLICATIONS	90
ACKNOWLEDGMENT	91

SUMMARY

Bronchiolitis obliterans syndrome (BOS) is a major chronic complication after lung transplantation (LTx). BOS is characterized by massive fibrosis in areas surrounding small airways that leads to air trapping induced pulmonary dysfunction. Several cellular and molecular features of BOS have been described in the latest stage of the disease, however, triggers that promote airway fibroproliferation and the disease-progression have not yet been sufficiently investigated.

Cathepsin-B (CatB), a lysosomal cysteine-protease, is able to exert its activity under acidic and neutral pH conditions, cleaving its targets intracellularly and extracellularly. CatB has been described in association with several fibrotic diseases and was shown to enforce fibrotic pathways *in vitro* conditions. Furthermore, the relevance of CatB in BOS progression has not yet been investigated.

In this study, we aimed to elucidate the role of CatB as potential trigger of BOS pathogenesis and its contribution to the progression of the disease.

CatB expression and its activity in lung tissue and bronchoalveolar lavage fluid (BALF) were determined using Western blotting, staining and a FRET-based activity assay, respectively. Pro-collagen levels were analysed in BALF samples via ELISA. To further investigate the impact of Cathepsin-B in the pathophysiology of BOS, we used an *in vivo* orthotopic left-lung transplantation mouse model of early-stage of BOS development, called lymphocytic bronchiolitis (LB). Mechanistical studies were performed *in vitro* using macrophage and fibroblast cell lines.

With our study, we demonstrated that CatB protein levels were increased in BALF samples and in lung tissue of patients who developed BOS, as well as in our murine model of LB. Interestingly, CatB activity was increased in BALF from BOS patients, already at early stages of the disease. Remarkably, the activity of CatB negatively correlated with the lung function over the progression of BOS disease, and was associated with an increased biosynthesis of pro-collagen. We furthermore identified infiltrating pro-inflammatory macrophages being the main source of CatB in BOS. Mechanistically, we demonstrated that CatB contributed to TGF- β 1-dependent activation of fibroblasts, and its inhibition prevented BOS phenotype.

In conclusion, infiltrating macrophages, in areas surrounding airways, release CatB that promotes fibroblast-activation and subsequent collagen deposition, driving BOS progression. CatB may represent a potential therapeutic target to prevent BOS progression.

1. INTRODUCTION

1.1 Lung Transplantation

The lung, differently from other organs, is constantly exposed to external and internal insults, and must handle air pollution particles, bacteria, virus, gastro-intestinal reflux/aspiration, but also immunological factors that are released from the immune system after tissue-injury (1). Despite high dosage of immunosuppressants, the organ can be recognised as foreign, and donor molecules are presented as antigen by innate immune cells to the adaptative immune system, causing the release of donor specific antibodies (DSAs) (2). DSA are known to be risk factors of organ failure (3-4). Patients affected by long-term lung disease rely on lung transplantation (LTx) as the only therapeutic intervention for a longer survival (5). Depending on the underlying disease, patients may require single or double LTx. During LTx, a diseased or failing lung is replaced by a healthy lung (**Figure 1**), usually derived from donors after brain death (DBD), which represents the largest source of lungs (6), or from donors after circulatory death (DCD). DCD source remains considerably underutilized, although there are no studies showing significant differences in primary graft dysfunction (PGD) risk and freedom from chronic lung allograft dysfunction (CLAD) between DCD and DBD (7-8). However, DCD markedly increases the pool of donor lungs, especially when coupled with the *ex vivo* lung perfusion (EVLP). In some situations, the lungs may be transplanted together with a donor heart. While lung transplantation is a complex operation that can involve many complications, it can significantly improve the quality of life and the survival of patients affected by end-stage lung diseases.

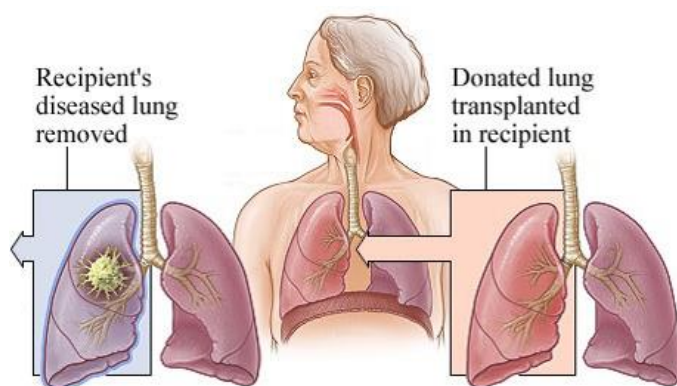


Figure 1. Schematic representation of single lung transplantation

Graphical representation of single lung transplantation in human patients. The image is derived from Gregory Thompson, MD et al. Medical Review 2018

The first cardiopulmonary transplantation was successfully performed by a team in Stanford University in 1981; in 1983 the first single LTx was performed in a patient with idiopathic

pulmonary fibrosis (IPF), who survived for 7 years (9). Later, in 1986, the first double LTx (10), and in 1990 the first double sequential transplantation was performed with the surgical technique that is nowadays used all over the world (11). The main difference between the double LTx and the double sequential LTx, which is currently used, refers to the type of airway anastomosis. While in the double LTx the anastomosis was performed in the trachea, provoking several post-surgery complications, in the double-lung sequential LTx, the anastomoses are made in each primary bronchus (left and right), in order to one lung ventilated while the other is implanted, and by that reducing the complications of the airway anastomoses (12-14). Approximately 30% of LTx is still single. Although the survival rate of single LTx is significantly lower when compared with double LTx (4.8 years in SLTx vs 7.8 years in DLTx) (15), it represents a good strategy to address the shortage of donor organs. This approach offers the possibility of transplanting two recipient patients with only one donor lung, in order to bypass the shortage of donor organs.

Patients affected by end-stage lung disease are selected for LTx according to the lung allocation score (LAS), with a scale from 0 to 100. This score considers the survival probability of the recipient patient in the following year, while the patient is on the waiting list, and the predicted one year after LTx (16). Among the underlying diseases before LTx, chronic obstructive pulmonary disease (COPD) and alpha-1 anti-trypsin deficient patients (A1ATD) represent 36.5% of the cases, idiopathic pulmonary fibrosis (IPF) 29.7%, cystic fibrosis (CF) 15.8%, bronchiectasis not associated to CF 2.7%, pulmonary hypertension (PH) for 4.4%, re-transplantation for 4.1%, and some cases of sarcoidosis (17) (**Figure 2**).

Adult Lung Transplants Major Diagnoses by Year (Number)

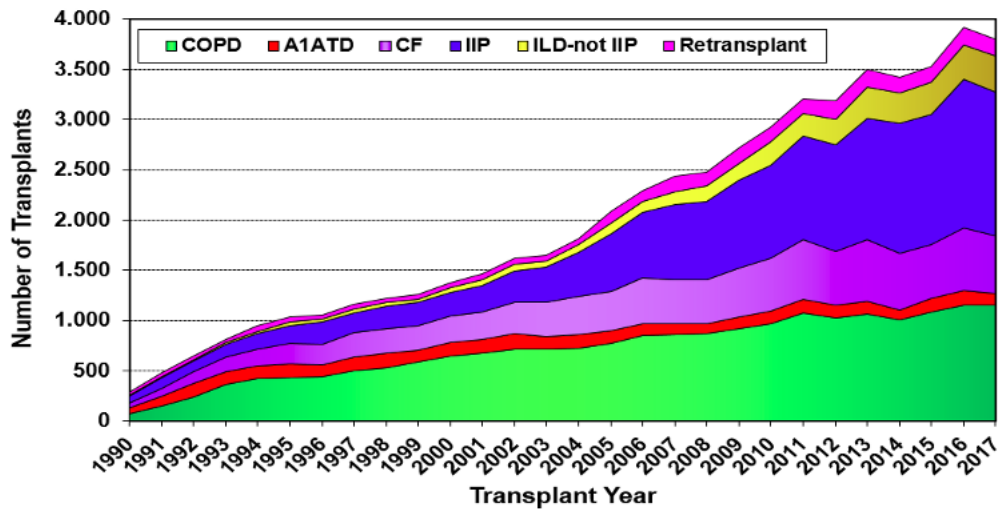


Figure 2. Underlying lung diseases incidence in adult patients before LTx.

Graphical representation of the incidence of underlying lung disease before LTx in adult patients in the period between 1990 and 2017. Chronic obstructive pulmonary disease (COPD), Alpha1 anti-trypsin deficiency-patients (A1AT), cystic fibrosis (CF), interstitial lung disease (ILD), patients that underwent a second transplantation (Retransplant). Source: JHLT Registry 2019

While waiting for a donor lung, approximately 50% of patients die from their underlying lung disease because of the organ shortage (18). The donor organ shortage is mainly caused by the moderate number of declined donor lungs that are not considered suitable for LTx. In fact, donors that are selected being suitable for LTx must derive from patients with an age less than 55 years, with excellent blood gas parameters, remote or no history of smoking, and a clear chest imaging (19). To overpass this problem, recently, the EVLP system has been introduced in Sweden and in the United States and introduced in the routine of several worldwide transplantation units for its ability to recondition lungs *ex vivo* before implantation. This system consists of a device capable of perfusing the graft through the vascular circulation with preservative solutions, reducing the formation of pulmonary edema and, by that bypassing an initial exclusion of the donor organ from the gas exchange criteria (20).

Strict criteria are also followed for the recipient patients. Patients with advanced and progressive lung disease that, despite all medical treatments, have a reduced life expectancy, are indicated for LTx. Since older patients have shown a worse survival than younger patients (21), only patients under 65 years old are considered eligible for LTx. Moreover, physical and social criteria play a crucial role in the selection of proper recipients for LTx. Additionally, the candidates should be conscious of the pre and post-surgery procedures, should show good

conformity to the medical treatments, and should have adequate familiar environment. Before LTx, patients are aware that LTx is not a curative approach but will guarantee a longer life expectation. On the other hand, LTx is not indicated for patients with recent history of chronic infections and malignancy, because of the post-surgery immunosuppressive therapies.

1.2 Clinical Diagnosis after LTx

When LTx patients develop symptoms (e.g. dyspnoea, cough, fatigue, with or without fever) and persistent reduction (20% from the baseline FEV₁ which persists for 3 weeks) in forced expiratory volume in 1 second (FEV₁) at clinic follow-ups that may indicate allograft dysfunction, further examinations are required to determine the cause of lung function decline. One of the key lung function tests used in the clinic is spirometry. The spirometry measures FEV₁, which is the amount of air that can be blown out in the first second of a forced exhalation. Most importantly for LTx patients is the total body plethysmography that provides detailed information about functional parameters, in particular functional residual capacity (FRC), airway resistance (Raw), total lung capacity (TLC) and residual volume (RV). As the body box is rigid and locked, variation of air pressure that is released during the test is converted in volume variation that represents the lung volume (22). Over the first years after LTx, the spirometry is measured at regular intervals (1-3-6-12-18-24 months) to establish the new baseline value for the implanted lung(s), and to evaluate the presence of a pathological condition. A chest x-ray or a computer tomography (CT) scan, and the high-resolution computed tomography (HRCT) are often able to detect lung parenchymal changes and air trapping that are usually not detectable via a normal chest radiography (23-25).

For further analysis, surveillance bronchoscopy associated with transbronchial lung biopsy (TBLB) is an useful tool to detect infections, other inflammatory responses and rejection that are maybe causing the organ dysfunction. BAL collection is performed by squirting sterile 100 ml of saline solution into the airways through the fibroelastic bronchoscope and suctioning it back to use it for tests. These tests evaluate the inflammatory response and a potential infection. The airway biopsies use special forceps through the bronchoscope to get small pieces of the airway tissue. These are evaluated by pathologists to assess and grade any sign of rejection. While the clinical evaluation of acute rejection is often built on TBLB (25), airway biopsies are not sensitive enough to identify changes of chronic rejection, due to the technical challenges of reaching small and peripheral airways (26). The final decision about the diagnosis of chronic

lung dysfunction is based on the clinical judgment, and the results of other testing are needed to exclude other potential causes of the decline in FEV₁.

1.3 Complications of LTx

Post-surgery complications are grouped into early and late ones according to the time of their appearance after LTx. The presence of preformed antibodies to donor organ-specific HLA and/or ABO blood antigens have been described as central players in hyperacute rejection, since they appear within 24h and quickly (27). Ischemia-reperfusion injury (IRI) represents the most common early complication after LTx, by occurring within 3 days after the surgery. IRI pathology is defined with tissue edema, thickening of the alveolar septum, of the peri-bronchial and perivascular wall, ground glass opacifications at CT scan (24), and pulmonary dysfunction. Intermediate complications that occur between 1 week and 2 months are represented by acute rejection, and bacterial infections, whereas viral infections start appearing in later stages. Late post-LTx complications are mainly represented by signs of chronic lung allograft dysfunction (CLAD), that occurs already at the first year post-LTx.

1.4 Lung allograft dysfunctions

1.4.1 Acute rejection and lymphocytic bronchiolitis (LB)

In organ transplantation, the terms “acute” and “chronic” are referred to two concepts: reversibility and duration. Acute rejection is potential reversible and is limited in the time; chronic rejection is irreversible and persist for long time.

Acute rejection (AR) is an early form of post-LTx rejection driven by T cells that recognize foreign major histocompatibility complex (MHC) antigens, also called human leukocyte antigen (HLA), and get activated. After activation, T cells migrate towards the allograft and prime immune responses, and by that causing tissue destruction (28). Clinical symptoms of AR are shortness of breath, cough with or without sputum and fever, associated to blood eosinophilia and neutrophilia. Pulmonary tests highlight airway dysfunctions with a decline of FEV₁ >10%, while chest imaging shows inflammation and opacities. For a proper diagnosis of AR, bronchoscopy and TBB are highly recommended (26). Histologically, depending on the inflammatory state, AR is classified in different severity grades: A0-4, for the vascular evaluation, B for the airway evaluation (26). Generally, the diagnosis of grade A1-2 and B0-BR2 is performed at high magnification, while the diagnosis of grade A2-3 and BR3 is clearly

defined at low magnification. Grade A0 refers to the absence of rejection; in grade A1, a minimal acute rejection is observed, with sparse mononuclear infiltration around small vessels, and the alveolar septum; in grade A2, a mild acute rejection is observed, with a frequent perivascular infiltration, from lymphocytes, macrophages and eosinophils that lead to sub-endothelial infiltration and endothelial hyperplasia. The alveolar septum is slightly affected. Grade A3 represents the moderate form of acute rejection, since it consists of extended perivascular and peribronchiolar cell infiltration from lymphocytes, macrophages and some neutrophils. Furthermore, a diffuse alveolar infiltration and alveolar cells hyperplasia can be observed. Grade A4 is the most severe form of acute rejection, with a diffuse perivascular, peribronchiolar and alveolar mononuclear infiltration. Importantly, the endothelium and the alveolar septum are damaged and undergo hyperplasia.

In 2006, in association to the previous classification based on the vascular assessment, pathologists decided to introduce new criteria of evaluation for the airway inflammation, also defined lymphocytic bronchiolitis (LB). B0 refers to the absence of bronchiolar inflammation; B1R defines a low grade of peribronchiolar infiltration, even though the epithelium appears hyperplastic. B2R refers to a high-grade airway inflammation, made of eosinophils and lymphocytes that extensively infiltrate the bronchial epithelium and the peribronchiolar area. Moreover, LB is considered to be an important risk factor for chronic rejection development (29).

1.4.2 Chronic lung allograft dysfunction (CLAD)

Chronic lung allograft dysfunction (CLAD) is one of the major limitations for long term survival in LTx, affecting 50% of the patients within 5 years (27). Originally, the term CLAD was used to refer to a homogeneous form of chronic rejection, whose diagnosis was based on the evaluation of FEV₁ decline (31).

In the last decade, the general knowledge in the scientific community has been based on the presence of two variants of CLAD, bronchiolitis obliterans syndrome (BOS), and restrictive allograft syndrome (RAS). The difference between the 2 phenotypes became more distinct when RAS was clinically defined with a decline in the total lung capacity (TLC) $\geq 10\%$ compared with the baseline value, with a concomitant and persistent decline in FEV₁ $\geq 20\%$ from the baseline. In RAS, lungs show clear signs of pleuro-parenchymal fibroelastosis and interstitial pneumonia. Although RAS is less frequent than BOS, accounting for 18% of CLAD

patients, this phenotype causes a poorer prognosis, with a median survival of 18 months from LTx (32).

Importantly, Verleden SE. et al. recently described, beside BOS and RAS, the presence of a third phenotype that represents 9% of the entire CLAD cohort, defined as mixed phenotype. The mixed phenotype is thought to be evolved from BOS and represents around 11% of BOS patients. This phenotype was mainly observed in patients with emphysema before LTx, that showed a decline in FEV₁, in TLC and in the forced vital capacity (FVC) \geq 20% (33). Similar to RAS, imaging scans of mixed CLAD show evident signs of parenchymal fibrosis (with an apical, basal or diffuse distribution) (33).

1.4.2.1 Bronchiolitis Obliterans Syndrome (BOS)

BOS represents the most common phenotype of CLAD, covering approximately 80% of the cases, and heavily affects the long-term outcomes of LTx patients (34). BOS, also known for its popcorn-like lungs, is a disease that results in obstruction of the small terminal airways (bronchioles) due to a chronic inflammation (35) (**Figure 3**). This phenotype has been described to occur within the first year after LTx (JHLT Registry 2018). Clinical symptoms are dry cough, shortness of breath, wheezing and general weakening, and usually worsen over time (35).

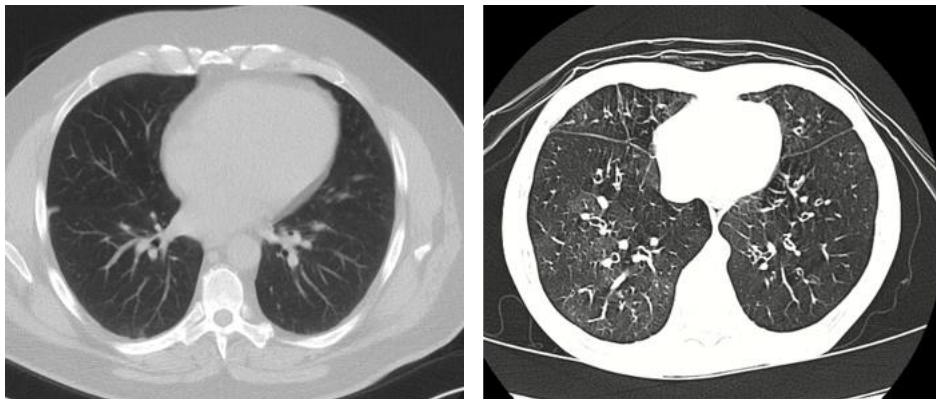


Figure 3. Lung imaging via high resolution computer tomography

Representative HRCT scan of healthy lungs (on the left)(Case courtesy of Assoc Prof Craig Hacking, Radiopaedia.org, rID: 40797), and of lungs with bronchiolitis obliterans syndrome phenotype, showing a so-called pop-corn phenotype, bronchiectasis, air trapping and bronchial thickening (on the right) (image derived from Xie BQ, et al. PLoS One 2014)

BOS pathogenesis has been shown to quickly develop, in parallel with a progressive decline of the pulmonary function. Clinically, it is defined as a persistent decline in FEV₁ \geq 20% from the

baseline, without any change in TLC. According to the decline rate of FEV₁ (31), several stages of the disease have been described (**Table 1**). BOS stages are classified according to the % decline in FEV₁ values, in BOS-0 when the FEV₁ value is >90%; in BOS-1 when the FEV₁ value is between 66 and 80%; in BOS-2 when the FEV₁ value is between 51 and 65%, and in BOS-3 when the FEV₁ value is ≤50% (23, 28).

The histological hallmark of BOS consists of fibrotic luminal obliteration and advanced mononuclear cell infiltration of the respiratory and terminal bronchioles (36) (Figure 6). HRCT scans of transplanted lungs have shown in BOS signs of bronchiectasis, air trapping and peribronchial thickening (37). Differently from the acute rejection, the heterogeneous nature of BOS makes it difficult to be diagnosed via transbronchial lung biopsies (TBB). After LTx, patients are treated with moderate dosages of immunosuppressants in order to prevent forms of rejection. Several combinations of immunosuppressive agents like tacrolimus, cyclosporine, mycophenolate, and corticosteroids (e.g. prednisone) are used to treat BOS patients. However, intensive treatment with corticosteroids (≥30 mg/day of prednisone) has shown any beneficial effect in attenuating lung function decline; in addition, numerous serious and long-lasting side effects have been associated with this therapy, such as osteoporotic fractures, cataracts and indigestion (38). Tacrolimus, also known as FK506, is a strong immunosuppressive drug that prevents the white blood cells from attacking the graft. Tacrolimus has been shown to be crucial for a longer survival after transplantation. Patients, that were previously treated with cyclosporine, switching to tacrolimus have shown to successfully reduce the lung function decline, and to inhibit BOS progression. Most importantly, replacing cyclosporine with tacrolimus also reduces the incidence of nephrotoxicity and hyperglycaemia, usually reported after long-term cyclosporine treatment (39-40). Another well-established drug for BOS treatment is Azithromycin, a potent antibiotic, which was demonstrated to efficiently prevent disease-progression. Approximately 40% of LTx patients treated with Azithromycin, showed a complete reversal of FEV₁ decline when BAL neutrophilia was detected (41). Interestingly, previous studies have highlighted the anti-inflammatory effects of Azithromycin in several organs, via its ability to drive macrophage polarization towards an anti-inflammatory phenotype (M2 macrophages) (42), and to increase the phagocytic activity of alveolar macrophages towards apoptotic bronchial-epithelial cells, limiting secondary injury damages (43). In cases where bronchiolitis obliterans syndrome is progressive and severe, extracorporeal photopheresis has also been successfully used to slow the decline in lung function from bronchiolitis obliterans syndrome (44).

Table 1. BOS severities according to the decline of FEV1

FEV ₁ %	BOS severity
81-90	0
66-80	1
51-65	2
≤50	3

1.4.2.2 Restrictive Allograft Syndrome (RAS)

In 2011, Sato et al. described for the first time a new form of CLAD, called restrictive allograft syndrome (RAS). RAS is characterized by a diffuse alveolar damage and excessive fibrosis, that affects the alveolar septum, the pleura, and can show, similar to BOS, bronchial obliterations (Figure 4 A). Importantly, the predominant fibroproliferation in the alveolar septum (Figure 4B), observed only in RAS, makes the lung stiff and causes an important decline in the total lung capacity. Clinically, RAS is diagnosed with a persistent decline in FEV₁ >20% and TLC >20%. Due to the severe phenotype, the survival of RAS patients is less than 18 months when compared with 46 months of BOS patients (30).

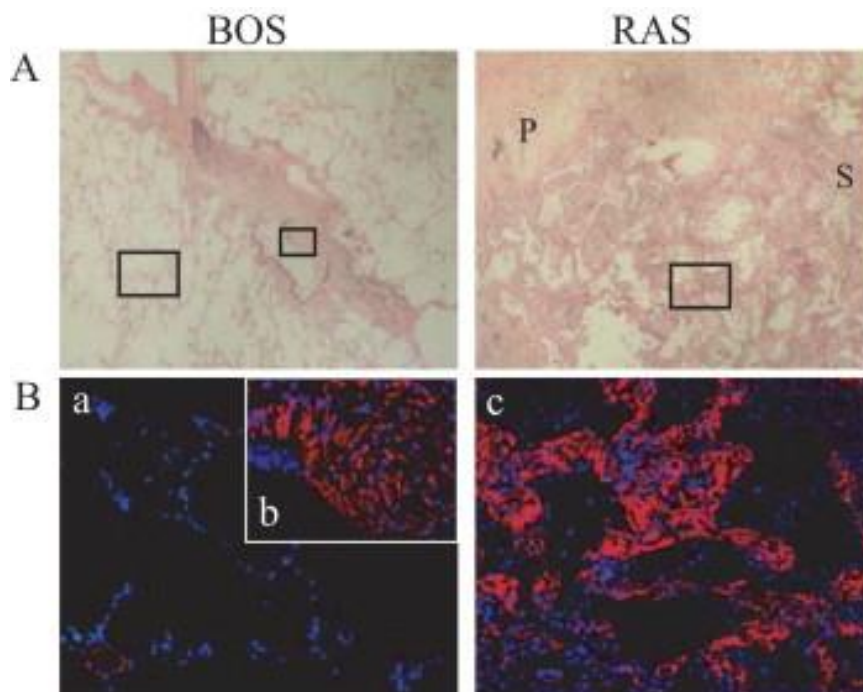


Figure 4. Histological comparison between BOS and RAS tissue

(A) Hematoxylin and eosin staining of lung tissue from explanted lung tissue (BOS in the right panel, RAS in the left panel) (original magnification $\times 100$). (B) Immunofluorescence staining for α -smooth muscle actin (α -SMA), marker of myofibroblasts (red), and nuclei (blue)

1.5 Lung allograft biomarkers

When the spirometry values of LTx patients drop, and physical symptoms are observed, further tests are required in order to exclude the presence of infections and/or rejection. Several centers adopt routine tests, to evaluate the total lung capacity (TLC) and diffusion lung capacity; blood tests, including biochemistry and coagulation; bronchoscopy with/without transbronchial biopsy; microbiological tests.

Growing evidence shows the involvement of the immune system in BOS development. BAL neutrophilia is used as marker to distinguish BOS patients from stable LTx patients. A trend towards high levels of neutrophils in BAL of stable LTx patients is used to predict the development of BOS by 3-9 months (45). RAS shows a restrictive physiology, and diffuse inflammation and fibrosis that affect alveolar septum, pleura and interlobular interstitium. RAS can be distinguished from BOS, for the presence of diffuse signs of alveolar damage, called diffuse alveolar damage (DAD). On the other hand, BOS shows an obstructive physiology, associated with air-trapping, and peri-bronchial inflammation (30).

Vanaudenaerde BM et al. sub-classified BOS patients into NRAD and fBOS. NRAD refers to the BOS patients with BAL neutrophilia that respond to Azithromycin therapy with a beneficial long-term effect and long survival (45). BAL neutrophilia was shown to be associated with LB which has been described as risk factor of BOS (28). fBOS patients do not respond to azithromycin, and have less BAL neutrophilia and tissue inflammation, but marked signs of airway fibrosis that cause air-trapping (45). However, BOS and RAS cannot be distinguished based on BAL, since both show high number of neutrophils in the BAL (46). Therefore, several soluble mediators have been described to be specific only for BOS. Elevated amount of CXCR3 ligands that bind CXCR3 receptor on the surface of several immune cells, may predict BOS development (47). Of recent discovery, donor derived circulating cell free DNA (ddcfDNA), that are released from dead cells, have been showed increased in the BAL of BOS patients (48). A BAL gene expression profile from LTx patients reported higher expression of genes encoding for T-cell receptor, for the costimulatory molecules CTLA4 and CD28, and for T-cell effectors molecules, in patients with acute rejection when compared with patients without signs of rejection (49). Active cytomegalovirus (CMV) infection is considered an important cofactor for BOS development in patients that are do not have an appropriate immune system (50). One hallmark of BOS lung tissue is the influx of immune cells into the peribronchiolar area of allograft lungs. Among these, T and B cells have been described to infiltrate the submucosa of bronchial and vascular epithelium and contribute the formation of de novo

lymphoid tissue. The presence of lymphoid tissue may lead to immune responses in terminal airways where irreversible signs of rejection are observed (51-52). However, macrophages infiltration could promote BOS progression already at early stage of the disease.

1.6 Lung macrophages

Under homeostatic conditions, lung airways are populated by macrophages, that normally account for 95% of the airspace space, about 1-4% of lymphocytes, 1% neutrophils and less than 1% of dendritic cells (53).

Macrophages originate from the bone marrow and migrate through the blood circulation towards different tissues where they differentiate into a variety of phenotypes in response to a wide spectrum of signals from the environment (54). There is a substantial heterogeneity among each macrophage population that reflects their different roles within the tissue. This heterogeneity is found in their morphology, function, as well as on the type of cytokines they secrete (55).

On the basis of the stimulation and mediators released, macrophages are usually grouped into two distinct phenotypes: the classically activated (M1), also called pro-inflammatory macrophages, that are responsive to type 1-derived cytokines (IFN- γ and LPS), and the alternatively activated (M2) macrophages respond to type 2-derived mediators IL-4 and release anti-inflammatory cytokines to support tissue regeneration (**Figure 5**).

In the lung, there are 2 distinct populations of macrophages that have the ability to self-renew locally independently of their circulating progenitors: alveolar macrophages (AMs) and interstitial macrophages (IMs), each one with specific properties and functions (56-57). Macrophages are highly plastic and are able to change their phenotype and function during pulmonary diseases. Phagocytosis and secretion of antimicrobials and pro-inflammatory mediators is the main task of alveolar macrophages, that play a central role in maintaining immunological homeostasis and host defence in the lung (58). When these activities are not successful in defending the host, macrophages may act as antigen presenting cells (APCs), presenting antigens to T and B cells, and activate their response (59). In addition to physiological conditions, the role of macrophages in various organ transplants is still controversial.

Several studies have reported deleterious effects originating from macrophages that were shown to attack the allografts and cause organ rejection in both acute and chronic conditions. In chronic rejection after kidney transplantation, macrophages are currently used as biomarkers

since their amount is strongly associated with disease worsening (60-65). On the other hand, other studies have highlighted the presence of a certain subtype of macrophages, regulatory macrophages (Mregs), that might protect the organ after implantation (66), suggesting that the functional role of macrophages is defined by their phenotype. In the context of organ rejection, after an initial phase of CD4⁺ T cells-mediated priming, macrophages showed the ability to kill graft cells independently from other lymphoid cells (67) and triggered allo-immunity (68). Accordingly, deletion or inhibition of macrophages reduced organ damage and extend transplant survival (69). Similar to pre-clinical studies, clinical studies have reported a strong association between macrophages infiltration and graft rejection (70-72). Moreover, a high incidence of pulmonary fibrosis (73) was found when pro-inflammatory macrophages infiltrate the graft (74-76). Consistent with these findings, the inhibition of pro-inflammatory mediators demonstrated the attenuation of the fibrotic phenotype (77).

Although macrophages were described to be involved in several type of diseases and in different organ transplantation models, their role in the pathogenesis of BOS has not yet been investigated.

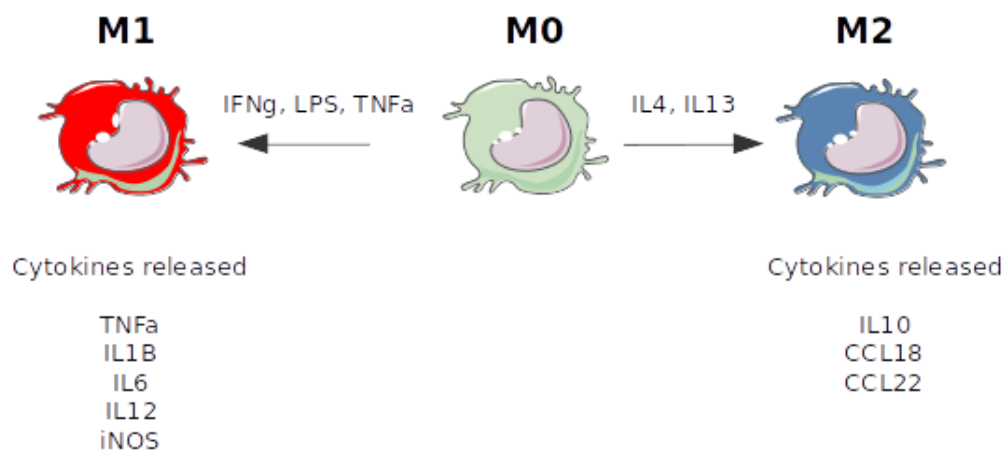


Figure 5. Macrophage polarization

Tissue macrophages differentiate into a pro-inflammatory M1 phenotype under the stimulation of IFN-gamma, LPS and TNF- α . Consequently, they release other cytokines that promote the pro-inflammatory response; under IL4 and IL13 stimulation, macrophages differentiate into an anti-inflammatory M2 phenotype, usually described in the tissue repair process

1.7 Other molecular lung allograft features

In order to identify predictive signs of BOS development, clinicians rely on clinical symptoms but also on the patchy ground glass opacity on HRCT scans as well as the state of fibrosis (**Figure 5**). The tissue fibrosis is often associated with the destruction of the airway wall, and

a severe pulmonary dysfunction (77). In particular, collagen and elastic tissue staining facilitate the identification of injured and/or obliterated airways (30).

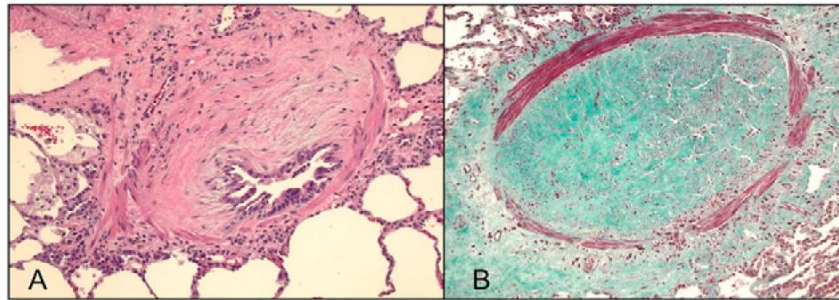


Figure 6. Histological features of BOS

Representative image of hematoxylin eosin (A) and Masson Trichrome (B) staining of BOS lung tissue, that show mononuclear infiltration and accumulation of collagen (78)

The pathogenesis of the fibrosis has been investigated in numerous studies, which defined it as a pathological feature of chronic inflammatory diseases. Don C. Rockey and his colleagues for instance suggested the presence of 4 main phases that all contribute to the tissue scarring. The first phase refers to the initiation of the response, driven by the injury of the tissue which triggers the activation of effector cells in the second phase, and lead to the synthesis and deposition of the extracellular matrix (ECM) components in the third phase, prompting the progression of fibrosis and organ dysfunction in the fourth phase (79). In general, when the injury occurs, resident epithelial cells and/or endothelial cells start releasing inflammatory mediators, such as cytokines, chemokines, and growth factors, that lead to the recruitment of a wide range of innate immune cells, mainly macrophages, neutrophils and lymphocytes (80). These inflammatory cells release other soluble mediators (e.g. transforming growth factor 1, also called TGF- β 1, interleukin 4, also called IL-4, interleukin 13, also called IL-13) and by that activate fibroblasts and myofibroblasts, which have been identified as key effector cells in many organs, responsible for the synthesis of ECM proteins (80-81). Among the ECM proteins that are usually found in fibrotic areas, interstitial collagens (types I and III) and fibronectin 1 are the most frequent. In addition, activated fibroblasts express smooth-muscle proteins (SMA) that enable that to contract (81-82), causing the alteration of the tissue structure and promoting organ failure.

On the molecular level, of all pro-fibrotic mediators reported (80), TGF- β 1 is the most intensively studied and central player in fibrotic diseases (83-85). TGF- β 1 is released in the extracellular space bound to a latency-associated protein (LAP) that prevents its rapid

activation. Separation and activation can be achieved through different triggers that are released by inflammatory cells in the extracellular space, like plasmin, calpain-1, thrombospondin, integrins and matrix metalloproteinases (86). Once released, active TGF- β 1 binds to a serine–threonine kinase type-II-receptor (TGF- β 1RII) that recruits and phosphorylates a type-I-receptor (TGF- β 1RI). TGF- β 1RI subsequently phosphorylates SMAD2/3 proteins that bind SMAD4, and by that they mediate SMAD4 translocation into the nucleus. Downstream signalling results in the up-regulation of pro-fibrotic genes expression, including ECM proteins (**Figure 6**). TGF- β 1 is synthesized and secreted by inflammatory cells (e.g. macrophages) and by effector cells (e.g. fibroblasts), thereby functioning in both in autocrine and paracrine way.

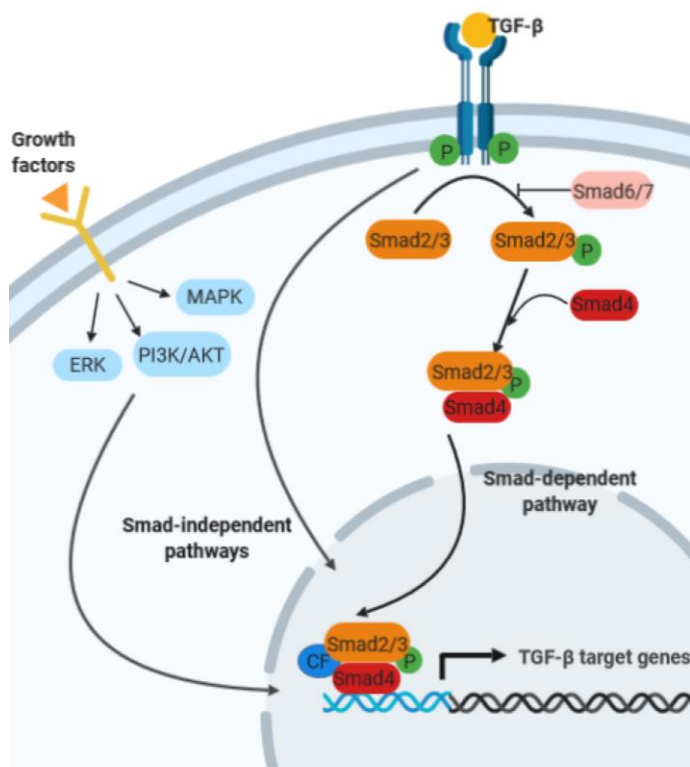


Figure 7. Schematic description of TGF- β 1 signaling

The binding of TGF- β 1 ligand to the extracellular receptor triggers the signal cascade intracellularly, through the phosphorylation of smad2/3 proteins, that build up a complex with smad4 protein and translocate into the nucleus, where the transcription of genes associated to the fibrogenesis is promoted (87)

1.8 Cystatin C and Cathepsin B

TGF- β 1 was shown to be regulated by at least five well-known endogenous molecules (86). Indeed, among them, Cystatin-C (CysC) was shown to prevent epithelial-mesenchymal transition (EMT) in cancer cells (88), through the inhibition of TGF- β 1-signaling in fibroblasts. CysC was reported to be significantly reduced in murine and human lungs when affected by interstitial fibrosis, while its restoration attenuated lung fibrosis (89). CysC belongs to the cystatin superfamily and is known to be the most relevant biological inhibitor of cysteine-proteases (cathepsins) of the papain family, such as Cathepsin B (CatB), Cathepsin L (CatL), Cathepsin S (CatS) and Cathepsin H (CatH) (90). Biologically, CysC is found in all cells, and

tissues, and is continuously secreted. Because of its size of 16 kilo Dalton and basic pH (~9.0), its half-life is particularly short, since it is rapidly cleared into lysosomes (91). CysC consists of one single domain and one signal peptide and exerts a protective role from the cathepsins that are released or leaked from lysosomes (92). To exert its inhibitory function, CysC binds to the active site of the cathepsins via a N-terminal tripeptide sequence L9-V10-G11 that interacts with the pockets S3 S2 S1 of the target cathepsins. Of relevance is L9 (Leucin) which is crucial for the binding and contribute to the formation of a V-shaped structure to occlude the active site of these protease (93).

One of the most studied targets of CysC is Cathepsin B (CatB), which is widely studied in association with chronic lung diseases and in the context of tissue fibrosis (94-95). CatB is required for the elimination of damaged organelles, for the degradation of denatured proteins by autophagy, and for the recovery of damaged cells after tissue-injury. CatB is a lysosomal cathepsin and exists in diverse organisms including bacteria, viruses, plants, and animals. Its expression is highly regulated, and the protein is synthesized in a pro-form (proCatB), in which the signal peptide is needed for further post-translational modifications. In fact, a truncated form, lacking the signal peptide and part of the pro-peptide, was reported to be found in a not functional state in the cytoplasm since it is unable to reach the Golgi apparatus neither the lysosomes (96). The secretion of proCatB occurs as a result of increased expression, however the secretion of active CatB (aCatB) depends on the activity of other pro-inflammatory proteases (e.g. Cathepsin G, and neutrophil elastase), on acidic pH conditions and autocatalysis (97). CatB plays an important role in processing proteins in lysosomes and in the extracellular space, by hydrolysing the precursor peptide, from a zymogen form into an active form. Importantly, it consists of an active site, composed of cysteine (Cys) 25, histidine (His) 159, and asparagine (Asn) 175 (98). Differently from other cathepsins, CatB is unique because it exhibits two types of enzymatic activities: it acts as exopeptidase (carboxydipeptidases) or endopeptidase, due to the presence of a sequence of ~20 amino acid (105-125), called “occluding loop” (98). The exopeptidase activity occurs at pH 5 (99) which is found in lysosomes (100). By using a fluorescence resonance energy transfer (FRET) system, a previous study was able to define arginine as preferred substrate of CatB at position P1 when it acts as exopeptidase (101). In addition, the aminoacids leucine, serine and alanine can also be recognised and bound. Importantly, CatB is active at acidic as well as neutral pH (102).

One fibrosis-associated factor and target of CatB is TGF- β 1. CatB was shown to implement TGF- β 1 signaling (103) and to be significantly increased in several fibrotic diseases, such as bleomycin-induced lung fibrosis (94) and advanced liver fibrosis (84). Interestingly, lung tissue

from BOS patients revealed remarkably increased levels of TGF- β 1 (104). However, the role of CatB in this disease have not been yet investigated.

1.9 Experimental murine models of LTx

Due to poor knowledge of BOS development and poor drug response, animal models of BOS could clarify the pathogenesis of the disease. For this purpose, mice and rats have been used as a chronic rejection model for the past 30 years.

1.9.1 Tracheal transplantation model

The first animal model used for the study of BOS development was the murine heterotopic tracheal transplant model (HTT). The HTT, based on the genetic mismatch between donor and recipient mice, was able to reproduce airway obliteration. After Tx, between day 0 and 7 an important subepithelial and peri-tracheal mononuclear infiltration started, followed at day 21 by tracheal obliteration which was comparable to human OB (105). Despite a high level of similarities between HTT model and human OB pathology, and the surgical advantages, several limitations were considered. First, the trachea does not act as a functional airway; second, the trachea does not have a primary vascularization, which is thought to play a crucial role in the rejection; third, BOS is a disease that affects small and peripheral airway, not large airways (106).

1.9.2 Orthotopic left lung transplantation mouse model

To better investigate the pathomechanism of CLAD, we used a mouse model of left LTx with a single mismatch. Donor lungs from mice having a HLA-A2–knock-in (HLA) on a C57BL/6 (B6) background were implanted in B6 recipients. B6 donor lungs implanted in B6 recipients (B6→B6 mice) were used as experimental controls. The single mismatch was able to reproduce the phenotype of LB after a period of 2 months (52). Our mouse model (HLA→B6) clearly shows pathological changes that occurs in human BOS, including ECM deposition in peri-vascular and peri-bronchiolar areas, peri-bronchial mononuclear infiltration, loss of clara cells, the formation of immune follicles around vessels and airways, bronchiolar epithelial cell dysplasia, and bronchiolar epithelial thickening (25). Plasma donor specific antibodies (DSAs) have been considered risk factor for BOS development (4) in LTx patients. In agreement with human findings, our mouse model of LB (HLA→B6) exhibited high titers of DSA (26) at 2

months post-LTx. Considering that LB is a precursor of OB in BOS (28), our mouse model of LTx is an useful tool to investigate the initiation of BOS progression. However, the main limitation of this model is the lack of airway obliteration, in particular in small and peripheral airways, as described in human.

2. AIM OF THE PROJECT

Bronchiolitis obliterans syndrome (BOS) is a major complication after LTx, affecting the long-term outcomes and life expectancy of patients. Approximately 50% of transplanted lungs develop BOS within 5 years from the surgery. Histopathological evaluations have highlighted in the late stage of the disease that distal small airways, vessels and alveolar spaces are dramatically marked by signs of inflammation and fibrosis (30) (78), that all lead to a persistent drop of FEV₁ % ≥ 20 , and organ failure. However, the main triggers that promote BOS development in human patients have not been identified yet. One of the major reasons for this scientific gap is the limitation of human samples for research. Translational studies are restricted to bronchoalveolar lavage fluid (BALF) and peripheral blood. Lung tissue sampling is mainly available from patients that have already reached a very late stage of the disease, rendering it hard to investigate early-events that may trigger disease progression. Moreover, if airway biopsies are available, these are not always a reliable specimen capable of reproducing the disease due to technical limitations.

Therefore, the objective of this study was to investigate potential markers that contribute to the development of BOS, using BALF samples collected from LTx patients at different stages of the disease. This, coupled with our LTx mouse experimental model of LB, enabled us to identify potential drivers of the disease.

Previous studies have shown Cystatin-C (CysC), the most relevant endogenous regulator of Cathepsins' activity, to prevent epithelial-mesenchymal transition (EMT) and fibrogenesis in cancer cells as well as in fibroblasts through the inhibition of TGF- β 1-signaling in fibroblasts. Consistent with this, Cathepsin B (CatB), one of the targets of CysC, was already reported to be notably increased in the context of lung fibrosis as well as in liver fibrosis.

We hypothesized that the inflammation, driven by enhanced CatB activity, leads to a progressive accumulation of collagen over the pathogenesis of BOS.

To elucidate the function of Cathepsin-B in BOS pathogenesis, we first determined the expression of CysC in lung tissue from transplanted patients, and then evaluated the activity and protein expression of CatB as well as the levels of newly formed collagen in BALF samples from LTx patients, at different time points of the disease. To investigate the impact of CatB in the pathophysiology of BOS, we used an *in vivo* orthotopic left-lung transplantation mouse model. Mechanistically, CatB-mediated BOS progression was addressed by using an *in vitro* cell culture model of BOS pathogenesis.

To elucidate the function of Cathepsin-B in BOS pathogenesis, we first determined the expression of CysC in lung tissue from transplanted patients, and then evaluated the activity and protein expression of CatB as well as the levels of newly formed collagen in BALF samples from LTx patients, at different time points of the disease. To investigate the impact of CatB in the pathophysiology of BOS, we used an *in vivo* orthotopic left-lung transplantation mouse model. Possible mechanisms of CatB-mediated BOS progression were addressed by using an

3. MATERIALS AND METHODS

3.1 List of materials

Reagents

Table 2. Solutions, reagents and cell culture media used in the study

Name	Source
0.25 % Trypsin-EDTA	Sigma Life Science
Acrylamide:N,N'- Methylene – Bisacrylamide 40% (29:1)	Carl Roth
Ammoniumsulfate (APS)	ZYTOMED Systems
Amersham ECL Prime Western blotting detection reagent	Sigma
β – Mercaptoethanol	Sigma Life Science
Blot Stripping Buffer	Thermo Scientific
Bovine serum albumin (BSA)	Life Technologies
Complete (Protease Inhibitor)	Life Technologies
Dulbecco's Modified Eagle Medium (DMEM)	Gibco, Thermo Fisher Scientific
DNase/RNase free water	Promega
Distilled water	ZYTOMED Systems
dNTP Mix 10mM 1000 μ l	Carl Roth
EDTA Buffer pH 9	Roche Diagnostics
Ethanol	Sigma
Fetal Bovine Serum (FBS)	Bio and Sell
Fluorescent Mounting Medium	Dako
Isopropanol	Carl Roth

Name	Source
4x Laemmli Sample Buffer	Bio-Rad
LPS	Sigma
IFNgamma	Biolegend
IL4	Biolegend
CA074	Sigma-Aldrich C5732
SB431542	Tocris
Methanol	Sigma-Aldrich
MuLV Reverse Transcriptase 5000U (Reverse Transcriptase)	Carl Roth
MgCl ₂ (25mM)	Life Technologies GmbH
Milk Powder	Carl Roth
Pen for histology	Dako
Protein Standards	Bio-Rad
Phosphatase Inhibitor (Vanadate)	Life Technologies
Penicillin/Streptomycin	Gibco, Thermo Fisher Scientific
PBS	Applied Biosystems
PCR Buffer II + MgCl ₂	New England Biolabs
Random Hexamers 50μM	Thermo Fisher Scientific
RNase Inhibitor 20 U/μl, 2000U	Bela-pharm
PowerUp Syber green Mastermix	Thermofisher
SDS	AppliChem
Temed	Bio-Rad
Tween-20	Sigma-Aldrich

Name	Source
Xylol	Sigma – Aldrich
H2O2 30%	H1009 Sigma Aldrich
Avidin/Biotin	SP-2001 Vector Laboratories
Peroxidase substrate	SK-4105 Vector Laboratories
Biebrich Scarlet-Acid Fuchsin Solution	HT15-1 Sigma Aldrich
Phosphomolybdic Acid Solution	HT15-3 Sigma Aldrich
Aniline Blue Solution (Collagen staining)	HT15-4 Sigma Aldrich

Buffers and Stock solutions

Table 3. Composition of buffers and stock solutions

Buffer Name	Ingredients
10x PBS	Na ₂ HPO ₄ KH ₂ PO ₄ NaCl KCl
PBS-T / Washing Buffer	1x PBS 1% Tween-20
Running	1,5M Tris – HCl pH=8.8 NaCl 150 mM Tris pH7,2 10 mM
RIPA	SDS 0,1% Triton x100 1% Deoxycholate 1% EDTA 5mM

Buffer Name	Ingredients
	150mM Glycine
Transfer	20mM Tris
	20% Methanol
Fuchsin Solution	0.9% Biebrich Scarlet 0.1% Acid 1% Fuchsin
Phosphomolybdic acid	10% Phosphomolybdic acid
Collagen staining blue solution	2.4% Aniline blue 2% Acetic acid

Primers for qPCR

Table 4. qPCR primers used in this study

Target gene	Forward	Reverse
Mouse <i>hpert3</i>	TCC TCC TCA GAC CGC TTT T	CCTGGTTCATCATCGCTAATC
Mouse <i>hpert2</i>	CCT AAG ATG AGC GCA AGT TGA A	CCA CAG GAC TAG AAC ACC TGC TAA
Mouse <i>ctsb</i>	AGCCATTTCTGACCGAACCT	TGGTAAGCAGCCTACATGAGAA
Mouse <i>tgfβ-1</i>	TGA CGT CAC TGG AGT TGT AGT TGT ACG	GGT TCA TGT CAT GGA TGG TGC

Antibodies

Primary antibodies

Table 5. Primary antibodies used in this study

Primary Antibody Name	Source
Anti-Galectin 3 (mouse)	Santa Cruz Biotechnology
Anti-Galectin 3 (rabbit)	Santa Cruz Biotechnology
Anti- β -actin	Abcam
Anti-Cystatin C (rabbit)	Abcam
Anti-Cathepsin B (mouse)	Abcam
Anti-Collagen 1 (rabbit)	Rockland
Anti-Fibronectin 1 (rabbit)	Abcam
Anti-Ly6G (rat)	Biolegend 127602
Anti-CD3	Abcam clone SP7
Anti-CD45R	Labome clone RA3-SB2
Anti-HLA.A2	Abcam
Anti-NOS2	Santa Cruz Biotechnology
Anti-pSmad3	Cell signaling

Secondary antibodies

Table 6. Secondary antibodies used in this study

Secondary antibody name	Source
DAPI	Life Technologies
Anti-rat	Abcam
Anti-rabbit	Merk Millipore
Anti-mouse	Life Technologies
Alexa Fluor 568 anti-goat	Life Technologies
Alexa Fluor 488 (anti-rabbit)	Life Technologies
Alexa Fluor 488 (anti-mouse)	Life Technologies
Alexa Fluor 555 (anti-rabbit)	Life Technologies

Commercial Kits

Table 7. List of commercial kits used in the study

Kits	Company
peqGOLD Total RNA Kit	PEQLAB Biotechnology
Pierce BCA Protein Assay Kit	Thermo Fisher Scientific
Human Pro-collagen 1a1 ELISA Kit	R&D System
Cystatin C ELISA ELISA Kit	R&D System
Active TGF- β 1 ELISA Kit	Boster Picokine

Laboratory equipment

Table 8. List of devices used in the study

Devices	Company
Centrifuge 5430	Eppendorf AG
Centrifuge Galaxy 16 DH	VWR International
Cool centrifuge, Mikro 220R	Andreas Hettich
Cool centrifuge, Rotina 35R	Andreas Hettich
Heat block HBT 130	DITABIS, Digital Biomedical Imaging Systems AG
Heat block Thermomixer Compact	Eppendorf AG
Haemocytometer Neubauer	Karl Knecht Assistent
Incubator MCO-18AC	SANYO Component Europe
Magnetic Steerer IKAMAG REO	IKA Werke
Microtome Hyrax m55	Carl Zeiss Microscopy
Microscope	Carl Zeiss Microscopy
Multiplate Reader Infinite 200 Pro	Tecan Trading AG
NanoDrop® ND-1000 spectrophotometer	Thermo Scientific
PCR Thermo cycler (Nexus Eco, Nexus Gradient)	Eppendorf AG
Pipettes	Eppendorf AG
Pipetboy	INTEGRA Biosciences
qRT – PCR Thermocycler StepOne™	Applied Biosystems
Scanner Mirax Desk	Carl Zeiss Microscopy

Shaking incubator	IKA Werke
SDS PAGE Chamber Bio-Rad	Bio – Rad Laboratories
Scale, Precisa XT 6200C-FR	Pesa Waagen AG
Voltage device Bio-Rad	Bio – Rad Laboratories
Vortexer, VM3	Ingenieurbüro CAT M. Zipperer
Vortexer, Vortex Genie 2	Scientific Industries
Western Blot Chamber, Bio-Rad	Bio – Rad Laboratories
96 wells qPCR plate	Thermo Scientific
FlexiVent	ScireQ
Myrax scanner	Zeiss
Microdismembrator	Sartorius

Fluorescence resonance energy transfer (FRET) materials

Table 9. FRET substrate used in this study

Sequence	Target	Company
Z-Arg-Arg-AMC	Cathepsin B	Bachem, 404789

Table 10. Recombinant proteins used in this study

Protein	Company
Cathepsin B	R&D System
Transforming growth factor 1 (TGF- β 1)	R&D System 40B-002/CF

3.2 Molecular biological methods

RNA isolation

RNA isolation from adherent cells was performed via PeqGOLD kit. For 12 and 24 well plates, cell lysates were obtained by adding 400 μ l of lysis buffer into each well. Cell lysate was applied to a DNA Removing Column and centrifuged for 1 min at 12,000xg. DNA Removing Columns were discarded, and the eluted solution of each sample was transferred into new 1.5 ml tubes. 400 μ l of 70% Ethanol was added into each tube and the sample was mixed via vortex, then loaded on RNA binding columns followed by a centrifugation step at 10,000xg for 1 minute. The eluted solution was thrown away and RNA binding columns were placed in 2 ml collection tubes. The columns were washed by adding 500 μ l of RNA Wash buffer 1 and centrifuged at 10,000xg for 15 seconds. The eluted solution was discarded and 600 μ l of RNA wash buffer II was added to the columns. A centrifugation step at 10,000g for 15 seconds followed by a second centrifugation for 2 min was important in order to remove all the ethanol. For an efficient elution, RNAase free water was heated to 70°C, and 40 μ l was added into each column and incubated for 5 min. The columns were centrifuged at 5000xg for 1 min and the eluted samples were collected. RNA concentration and purity were determined via Nano Drop. Samples were stored at -80°C for further use. All centrifugation steps were performed at room temperature (RT). Nucleic Acid- RNA-40 setting was used for measurements, considering for pure RNA sample a ratio of A260/A280 nm around 2.

Synthesis of cDNA via RNA-reverse transcription (RT)

The concentration of RNA was adjusted to 25-50ng/ μ l with RNase free water. Samples were incubated in a thermo-shaker (Heat block Thermomixer Compact, Eppendorf) at 70° C for 10 minutes followed by incubation on ice for 5 minutes. Master mix solution was prepared for a 20 μ l of final volume per sample: 4 μ l of 10x Buffer II, 8 μ l MgCl₂ (25mM), 2 μ l of dNTPs (10mM), 2 μ l of Random Hexamers, 1 μ l of RNase-Inhibitor, 2 μ l of Reverse Transcriptase and 1 μ l of dH₂O. The master mix (20 μ l mix per sample) was added to 20 μ l of RNA samples. Reverse transcription procedure was performed on the Thermocycler (PCR Thermo cycler, Nexus Eco, Nexus Gradient) according to the following protocol: for 10 min at 20° C, 75 min at 43° C and 5 min at 99° C. Finally, 60 μ l RNase free water was added to each tube to dilute the samples. Samples can be stored for further analysis.

Real time quantitative polymerase chain reaction (Real time qPCR)

In order to determine the expression level of genes of interest, real time quantitative-PCR was performed using SYBR® GREEN PowerUP. SYBR® GREEN is a dsDNA-binding dye that intercalates into dsDNA in a non-specific manner. Specific primer that were pre-tested bind to parts of the gene of interest and ensure the proper amplification. The newly produced double stranded DNA molecules produce a fluorescent signal with SYBR® GREEN that can be detected and quantified by the qPCR machine (PCR Thermocycler StepOne™, Applied BioSystem). For reliable results, a housekeeping gene (in this study Hprt was chosen) as a reference is used in each qPCR. qPCR reactions were prepared as followed: 10 µl of syber green buffer, 12 µl of distilled water and 1 µl of forward and reverse primer (from 1:10 stock solutions), 2 µl of cDNA was added into this master mix in 96-well qPCR plates from Applied Biosystems. The reaction was performed using a Thermocycler StepOne™ according to the following protocol: 5 min at 95°C, 5 sec at 95°C, followed by 5 sec at 59°C, 30 sec at 72°C for 45 cycles and 15 sec at 95°C. The gene amplification program provided melting curves that ensured the presence of proper DNA molecules. The relative expression of each gene was normalized to the average of the Ct value of HPRT expression using the formula $2^{-\Delta Ct}$, where $\Delta Ct = Ct_{\text{target}} - Ct_{\text{control}}$. The results were analysed in GraphPad prism 8 software and depicted as graphs.

3.3 Protein analysis

Protein isolation

In order to isolate protein from cells, medium was discarded and cells that were previously seed in either 6 or 12 well plates were washed with sterile cold PBS. Plates were put on ice and all further steps were performed on ice to avoid degradation of the proteins. 60-100 µl of cold RIPA buffer supplemented with protease inhibitors, were added into each well. Adherent cells were scratched from the plate and collected in precooled tubes. In order to enhance the protein yield, samples were snap-frozen in liquid nitrogen for 5 seconds. A thawing step followed and samples were vortexed. Samples were centrifuged at 16000 g for 15 minutes at 4°C, and supernatants were collected into new precooled tubes.

In order to isolate protein from tissue, frozen tissue needs to be powdered. 2-3 grams of the powder was dissolved in RIPA buffer supplemented with inhibitors. Incubation on ice and vortex-steps followed for 20 min. Centrifugation is performed similar to the upper paragraph.

Protein concentration detection via BCA

The Thermo Scientific™ Pierce™ BCA Protein Assay is a detergent-compatible formulation for measurement of protein concentration, that is based on chelation of bicinchoninic acid (BCA). BCA reacts with complexes between copper ions that are reduced by peptide bonds in proteins, and the end product gives purple colour depending on the concentration of protein in the reaction which absorbs light at 562 nm (Walker, 1994). Standard curve was made using serial dilutions of bovine albumin protein in RIPA buffer (from 2 mg/ml to 0.025 mg/ml). Samples were added at defined dilution factors into each well of a 96 well plate using RIPA buffer as diluent. The working buffer was prepared according to the standard-protocol by mixing 50 parts of BCA Reagent A with 1 part of BCA Reagent B, and 200 µl were added to each well. After 30 min of incubation at 37 °C, the absorbance was measured on a Tecan plate reader at 562nm.

Western blotting

In order to separate proteins according their molecular weight (MW) on SDS-PAGE, a gel was prepared consisting of two layers: stacking (5%) and separating (10 and 12% of Acrylamide). 10-20µg of protein samples supplemented with 4x Laemmli loading buffer were incubated at 95°C for 10 minutes, then centrifuged to remove bubbles and kept on ice for 5 min. Samples were loaded on gels, and run at 100 V for 10 min, then at 120 V for 60 min.

PVDF membranes were used for immunoblotting and placed into the transfer chamber filled with fresh 1x transfer buffer and was run at 100 V for 60-90 min. Blocking of the membranes was performed at room temperature for 2 hour using 5 % milk in 1x PBS-T buffer (Phosphate buffered saline + 0.1% Tween 20). Blocking was followed by primary antibody incubation at 4° C overnight. Primary antibodies were diluted in 1% milk or 1% Roti according to the recommended dilution for each antibody, as follows: primary antibody against CatB (1:400 ab58802), and (1:500 MAB965 R&D System); against phospho-smad-3 (1:1000, cell signaling 9520); against collagen 1 (1:000, Rockland 600-401-103), fibronectin-1 (1:1000, abcam ab-2413) and β-actin (abcam).

Before incubation with secondary antibodies, the membranes were washed. Washing steps with PBS-T for 5 times for 6 min followed by incubation with horse radish peroxidase (HRP)-conjugated secondary antibody in 1% milk for 1h at room temperature. The following secondary antibodies were used: the anti-rabbit IgG-HRP (dilution factor of 1:3000, 7074P2

New England Biolabs), and the anti-mouse (dilution factor of 1:3000, NA931V GE Healthcare). ECL or Femto solutions A and B were mixed equally and applied to the membrane for 5 minutes to allow the detection of the signal via a chemiluminescence reaction, and the bands were visualized using Image Lab 5.1 software (Bio-Rad Laboratories). Signals were quantified and normalized to the signal of β -actin used as control. Statistical analysis and densitometry of the bands were done using Image Lab 5.1 software.

3.4 Protease activity assay

Protease activities were evaluated using Fluorescent resonance energy transfer (FRET) with specific FRET-substrates. The fluorescent substrates consist of a quencher molecule which physically interacts and interferes with a fluorescence molecule. Once the protease cleaves the substrate, the quencher is separated from the fluorescence molecule, and this reaction produces a fluorescent signal which is detected from the plate reader. More active proteases are in the samples more fluorescence is released and detected over-time in a kinetic reaction.

Reagents

Table 11. FRET reaction buffer composition

Ingredients
50 mM Tris
150 mM NaCl
0.01% Triton X-100
pH 5

Table 12. FRET reaction solution for recombinant protein

Component	Volume
Activity assay buffer	35 μ l
Active Recombinant protein	10 μ l
Substrate (100 μ M)	5 μ l
Total	50 μ l

Table 13. FRET reaction solution for sample

Component	Volume
Activity assay buffer	35 μ l
Sample	10 μ l
Substrate (100 μ M)	5 μ l
Total	50 μ l

FRET system was used in this study to quantify the enzymatic activity of CatB. To do so, the specific fluorogenic substrate of CatB Z-Arg-Arg-7-amido-4-methylcoumarin hydrochloride (50 μ M C429 Sigma Aldrich) was used. Serial dilutions of recombinant proteins were used in order to create a standard curve. The enzymatic activity of CatB was determined in BALF samples as well as cell culture medium. For the reaction, 96 well nunc-black plates were used and 10 μ l of the sample of interest was added to the reaction buffer and incubated for 10 min at 37°C. The reaction was initiated by the addition of 10 μ l of substrate into a final volume of 50 μ l of sample. The proteolytic activity was monitored by the appearance of 7-amino-4-methylcoumarin (AMC) from the substrate by using Fluoroscan plate-reader at 450 nm for 60 min.

3.5 ELISA

Cystatin C

Cystatin C detection in human BALF was performed via an Enzyme-linked immunosorbent assay (ELISA) kit (R&D System DSCTC0). Same volume (50 μ l) of BALF samples was used.

Pro-collagen 1a1

Pro-collagen 1a1 detection in human BALF was performed via an Enzyme-linked immunosorbent assay (ELISA) kit (R&D Systems DY6220-05). Same volume (50 μ l) of BALF samples was used.

Active TGF- β 1 detection

Active TGF- β 1 was detected in cell culture medium of RAW264.7 cells via an Enzyme-linked immunosorbent assay (ELISA) kit (Boster Mouse TGF Beta 1 ELISA Kit PicoKine™). Same volume (100 μ l) of medium was used. 1% of FBS supplemented medium was used as blank.

3.6 Mouse experiments

Mouse strains

For this study, several mice strains were used. In the established mouse model of early stage of BOS HLA-A2–knock-in and C57BL/6J HLA were used; for functional studies *Ctsb* KO mice were used. Male B6, HLA (C57BL/6-Tg (HLA-A2.1)1Enge/J), and *Ctsb*^{-/-} (B6;129-*Ctsbtm1Jde/J*) mice were purchased from Jackson Laboratory.

Study approval

All human patients provided a written informed consent. The study was approved by the ethics committee of Ludwig-Maximilians University (333-10) and by the institutional ethics committee Comité de Protection des Personnes Ile-de-France VII, Le Kremlin-Bicêtre, France (protocol N8CO-08-003, ID RCB 2008-A00485-50). All mouse experiments were performed following the governmental and international guidelines and were approved by the local government of Upper Bavaria, Germany (project 55.2-1-54-2532.120.2015) and by the University of Colorado (protocol 115517(04)2D).

Orthotopic left lung transplantation model

Mice age was between 6-8 weeks at the time of the surgery. Orthotopic left lung transplantation (LTx) was performed as previously published (50). No immunosuppression was applied to recipient mice after the surgery but only 3 doses of pain killer. B6 and HLA mice were used as donors of left lungs; B6, and *Ctsb*^{-/-} mice were used as recipients. Donor mice were anesthetized with an i.p. injection of ketamine/xylazine in saline solution. When all the reflexes were absent, the cardiopulmonary system was isolated and kept cold on ice during the preparation of the left donor graft. The pulmonary artery, bronchus, and pulmonary vein were separated one by one, and then cuffed with, 24-, 20-, and 22-gauge cuffs, respectively.

The left lung was cut off from the heart and stored on ice for 1 hour before implantation. The recipient mouse was anesthetized with a reversible anesthetic, made of medetomidine (1 mg/kg), midazolam (0.05 mg/kg), and fentanyl (0.02 mg/kg), also called MMF; then was intubated with a 20-gauge cannula and ventilated with a small-mouse ventilator (Harvard Apparatus), at a respiratory rate of 120 bpm and a tidal volume of 300 μ l. The chest was incised on the left side between ribs 3 and 4, and the recipient left lung was carefully extracted with a clamp. The ventilation volume was reduced to 70 μ l. Blood and air flow of the left lung were blocked with clamps. The hilar structure was carefully separated with blunted forceps. The cuffed donor pipes were inserted into the recipient counterparts and fixed with 9-0 sutures. The recipient left lung was completely removed, and the chest was closed with a 6-0 suture, after removing all air bubbles from the chest. Antagonist was administered under the skin, and the animal was extubated only when it showed signs of spontaneous breathing. After the surgery, the recipient mice were recovering in the cage to recover at 30°C overnight and received daily administration of buprenorphine for 3 days. Mice were sacrificed at specific time points.

Left lung function measurement

FlexiVent device was calibrated prior to each experiment, and individual mouse weight was inserted. Mice were anesthetized with MMF; when reflexes were absent, mice were intubated with a 20-gauge cannula, and connected to a mechanical ventilator at a frequency of 120 breaths per minute and a volume of 300 μ l. The chest was incised, and the right bronchus was clamped in order to measure the left lung function. The tidal volume was reduced to 70 μ l. Afterwards, mice were removed from the mechanical ventilation, and their pulmonary function was analysed using the FlexiVent system. To mimic the lung volume during the natural breathing, mice were ventilated with a tidal volume of 3.5 ml/kg at a frequency of 150 breaths/min. Lung mechanical properties, such as airway compliance, airway resistance, tissue elastance and inspiratory capacity were measured via Snap-Shot, Prime-8 and Quick-prime wave perturbations. Three readings per animal were measured for a reliable result.

Bronchoalveolar lavage fluid collection (BALF)

Right bronchus was clamped, while left lung was washed three times with 200 μ l of cold 1x PBS (Gibco, Life Technologies) supplemented with a Cocktail of Protease Inhibitors (Roche Diagnostics). BAL was then separated into BALF (BAL fluid) and BAL cells via

centrifugation for 20 min at 400g at 4°C. Supernatants (BALF) were stored at -80 °C for protein detection.

3.7 Lung tissue staining

Lung tissue preparation

Lungs were perfused via the pulmonary artery with cold 1x PBS to flush out the blood from the tissue and fixated with a 4% solution of paraformaldehyde for 24 h, before embedding. Lung lobes were cut into 3 mm pieces and embedded into liquid paraffin overnight. Paraffin blocks were cut via a microtome (Hyrax) into sections of 3 µm for further staining analysis.

Deparaffinization

Tissue sections were melted for 10 minutes at 65 °C, and paraffin was removed with baths of 100% of xylene (twice), then 100%, 90%, 80% and 70% of ethanol, followed by running tap water for 5 min, and distilled water. Antigen retrieval was performed in a solution of 0.01 M citric acid (pH 6.0) in a cooker chamber for 30 minutes at 125°C, and for 10 minutes up to 90°C. Tissue was rehydrated with PBS-Tween 20 (0,1%) for 10 min.

Immunofluorescence staining

Tissue was rehydrated for 10 min with 1x PBS-Tween-20 (0,01%), PBS-T, then blocked with 3% BSA for 60 min, incubated overnight at 4 °C with primary antibodies. Tissue was washed for 3 times with PBST and incubated for 60 min at room temperature with secondary antibodies diluted in 3% BSA. For long storage, sections were embedded with Dako mounting medium (Agilent S3023). Images at defined magnifications were taken using AxioImager software with an M2 microscope (Zeiss), and processed with ImageJ.

Immunohistochemistry (DAB)

Tissue was rehydrated for 10 min with 1x PBS-Tween-20 (0,01%), PBS-T, while endogenous peroxidases were quenched by incubation in 3% H₂O₂ solution (30%, H1009, Sigma Aldrich) in 1x PBS for 10 min. Tissue was washed with PBS-T, and few drops of avidin solution (Avidin/Biotin Blocking Kit, SP-2001; Vector Laboratories) were added for 15 min, followed

by washing with PBS-T (1x PBS-Tween 20 0.1%); similarly, few drops of biotin solution were added for 15 min, washed with PBS-T; nonspecific antibody-binding sites were blocked with blocking solution consisting of 3% BSA in 1% PBS, PBSA for 1 h, and sections were incubated overnight at 4°C with the solution of primary antibody. After washing, the tissue was incubated with HRP-conjugated secondary antibody for 30 min at room temperature followed by the addition of the peroxidase substrate (ImmPACT DAB Peroxidase (HRP) Substrate, SK-4105; Vector Laboratories). After nuclear staining with Hematoxylin, dehydration and mounting, the sections were dried and scanned with Myrax scanner (Zeiss).

Immunohistochemistry (Vulcan fast red)

After deparaffinization, sections were rinsed with water, and quenched with a solution of H₂O₂ and methanol for 20 min, then washed for 3 times with 1x PBS; after antigen retrieval was completed, sections were washed for 3 times with washing buffer, blocked with 2 drops of Rodent Block M on each slide and incubated for 30 min at RT. Primary antibody solution was added on each slide and incubated overnight at 4°C. Samples were washed for 3 times, then incubated with AP Polymer from the secondary antibody for 15 min. After another washing step, 1 drop of Vulcan fast Red Chromogen solution was added on each slide and incubated up to 8 min. During the incubation, the staining was tracked overtime. Sections were washed again for 3 times, then rinsed in distilled water. Counter staining was performed with Hematoxylin solution up to 3 min followed by a fast washing in washing buffer, and the staining was fixed in 100% EtOH and Xylene. All the incubation steps were performed at RT.

Hematoxylin eosin staining (HE)

Tissue sections were stained with Hematoxylin (Hematoxylin solution, GHS-232, Sigma Aldrich) for 6 min, rinsed in distilled water, then washed under running tap water for 15 min, and again distilled water, then stained with eosin for 10 min and washed in tap water for 5 min. Then, tissue was dehydrated twice with ethanol 100% and with xylene. Mounting was performed with Entellan glue (Merk).

Collagen staining

Masson's trichrome is a three-colour staining protocol used for staining collagen fibers in tissue. This protocol produces red muscle fibers, blue collagen fibers, pink cytoplasm and proteins as well as dark purple cell nuclei.

After deparaffinization, tissue sections were stained for 8 min with hematoxylin solution (for nuclear staining), washed with running tap water for 1 minute, then rinsed with distilled water. Sections were rinsed with a solution of Ethanol (70%) and HCl (0,1%), and washed for 5 min with running tap water, then incubated with Ponceau Fuchsin solution for 6 min, and quickly rinsed in tap water and distilled water. Sections were incubated for 1 min in Phosphomolybdic acid solution, then in Light Green solution for 5 min (extracellular matrix staining, since it binds collagen components). The staining was fixed with Ethanol 100% and Xylol.

Signal Detection

Images at different magnifications were acquired using AxioImager M2 microscope (Zeiss), AxioVision software (Zeiss), and scanner (Zeiss).

3.8 Signal quantification

Computer assisted stereology toolbox (CAST)

Quantitative analysis of inflammation and collagen on samples previously stained for collagen was assessed by using the new computer assisted stereological toolbox (newCAST, Visiopharm) and an Olympus BX51 light microscope. 60 frames were randomly selected by the software with the x40 objective and defined by a line grid and points. The intercepts of lines with septal wall (I-septa), vessel wall (I-vessel), and airway wall (I-airway) and points localized on air space were counted and calculated $\text{Collagen/inflammatory cells} = \frac{\sum \text{Pair} \times L(p)}{\sum \text{Isepta} \times 0.5}$, where $L(p)$ is the line length per point. For each frame, inflammation and collagen were counted. CAST was also used for counting positive cells after Galectin 3 (Gal3) immunofluorescence staining. In order to quantify macrophages in mouse lung sections, 35 random frames were selected by the software with the 40x objective, and positive cells for Gal3 were manually recorded for each frame. Recorded data were analysed via a statistical program, GraphPad v.8.

Image J

Each single picture was analysed via ImageJ. A manual counting was used for the assessment of positive signal. An average of 20 random pictures for sample were considered for each analysis.

3.9 Cell culture

Cell lines

Abelson murine leukemia virus transformed macrophage, RAW264.7, were used as an *in vitro* model of macrophages; mouse embryonic fibroblasts, MEF, were used as an *in vitro* model of fibroblast. RAW264.7 were cultured in DMEM/F12 medium, MEF in DMEM, media were supplemented with 10% FBS and 1% Pen/Strep, respectively.

Cell seeding and stimulation

RAW264.7 cells were seeded at $1,5 \times 10^5$ in 12 well-plates. Cell pellet was used for protein and gene expression analysis; cell medium, also defined as “conditioned medium” (CM) was used for activity assay and mechanistic assays.

For gene and protein expression analysis, RAW264.7 cells were seeded one day prior experiment, and they were stimulated with and without pre-incubation with a specific inhibitor of CatB (CA074, $10 \mu\text{M}$, Sigma C5732). Stimulation was performed by adding IFN-gamma (20ng/ml), LPS ($1 \mu\text{g/ml}$), and IL4 (20ng/ml) to the medium, in a final volume of $1000 \mu\text{l}$ per well for 6, 24, 48h.

For mechanistic studies, RAW264.7 cells were seeded, then harvested for 18 hours with 1% FBS-supplemented medium; the day after they were pre-incubated with CA074 or DMSO and stimulated. Stimulation was performed adding IFN-gamma (20ng/ml), LPS ($1 \mu\text{g/ml}$), and IL4 (20ng/ml) to the medium, in a final volume of $500 \mu\text{l}$ per well for 24h (as shown in **Figure 8**). Condition medium (CM) from RAW264.7, with and without CA074 and TGF- β 1 receptor-2 inhibitor (SB431542, $10 \mu\text{M}$), was centrifuged at 300g at 4°C for 5 min in order to remove cell debris.

CM was added to mouse embryonic fibroblasts, previously seeded at 5×10^5 cells in 6 well-plates, and starved with 1% FBS-supplemented medium for 18 h. After 30 min, phosphorylation of SMAD3 protein (pSmad3) was assessed as marked of activation.

In this study negative technical controls (only medium), technical positive controls (2 ng/ml TGF- β 1 recombinant protein), technical inhibitor controls (2 ng/ml TGF- β 1 + SB431542, 10 μ M), and experimental controls were used.

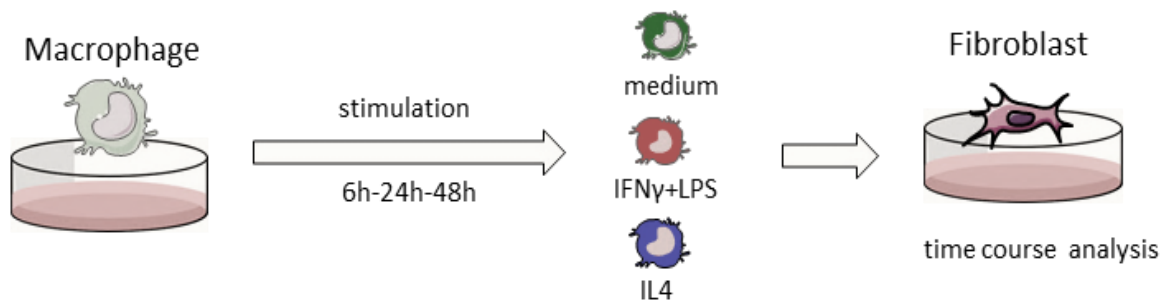


Figure 8. Schematic graph of mechanistic studies

RAW264.7 are seeded in 12 well plates for 24h, and then stimulated with pro and anti-inflammatory cytokines for 6, 24 and 48 h. Cell lysate was used for gene expression analysis. Cell medium was used for activity assay, ELISA measurements, and for stimulation of fibroblasts

3.10 Statistical analysis

Data represent mean \pm SEM. For the comparison between 2 groups, the statistical significance was assessed by a non-parametric t-test (Mann-Whitney); for the comparison between 3 and more groups, the difference was evaluated by one-way ANOVA followed by a post-test (Kruskal-Wallis) or by a Tukey's multiple -test. Furthermore, the Stable group was compared to each BOS group via a non-parametric t-test (Mann-Whitney), since the group of Stable LTx patients is independent from BOS group. Median values are showed. Differences were considered to be statistically significant at $P < 0.05$.

4. RESULTS AND FIGURES

4.1 Demographics of patients involved in the study

Patients that underwent lung transplantation (LTx) were considered in this study and were classified as Stable LTx (S), if they were clinically stable during the entire study period (n=20), and as BOS (BOS), if they showed a significant decline of the lung function (n=22). Age, gender and the underlying lung disease of each patient were defined at the start of the study. All patients underwent double lung transplantation (DLTx), which, as previously mentioned, represents the most used approach because of the high rate of survival (15). Patients with BOS were monitored during the study, and BAL samples were collected, for most of patients, at different stages of the disease (**Table 14**).

All BALFs that were used in this study were collected and stored from 2004 until 2014. For this analysis, patients with clear signs of BOS and Stable LTx patients were selected from our archive. All patients underwent double lung transplantation (DLTx) and were analyzed retrospectively. Pre-transplant underlying diseases were categorized into chronic obstructive pulmonary disease (COPD), interstitial lung disease (ILD), cystic fibrosis and pulmonary hypertension (PH). BOS was defined as a chronic decline in FEV₁ by 20% from baseline FEV₁ (FEV₁ /FEV₁ baseline <80%) that was present for a minimum of 3 weeks according to the current recommendations. Baseline FEV₁ (FEV₁baseline) was defined as the mean of the two best measurements of FEV₁ post-transplant, at least 3 weeks apart. Patients with BOS potentially caused by confounding conditions were excluded from the analysis. After lung transplantation during hospital stay and rehabilitation lung function analysis are performed weekly. After discharge, lung function tests are performed once per month for the first post-surgery year and at least once every 3 months afterwards. LTx patients were followed up in our center and every lung function test was performed with a spirometry and body-plethysmography. Since our samples were collected from a longitudinal study, we could classify as BOS-0, patients that were stable at the time of BAL collection, but developed later BOS-1 or higher. Stable LTx is a patient who has not developed CLAD for at least 5 years since the BAL sample was collected.

Table 14. Demographics of lung transplanted patients from Munich cohort (cohort 1)

Patients were clustered according to their gender, (F) for female and (M) for male, and according to the underlying diseases; COPD referred to chronic obstructive pulmonary disease, ILD/LF referred to interstitial lung diseases/lung fibrosis, CF referred to cystic fibrosis, and PH referred to pulmonary hypertension

	Stable	BOS
Number of patients	20	22
Age (years)	43 ± 8	47 ± 12
Sex (F/M)	13 F/ 7M	8 F/ 14 M
Underlying disease	ILD 8 COPD 2 CF 6 PH 4	ILD/LF 11 COPD 1 CF 4 PH 6
Procedure (SLTx/DLTx)	All DLTx	All DLTx
Days after LTx	669 ± 396	996 ± 572
Grade at BAL	All 0	BOS 0 n=20 (90%) BOS 1 n= 12 (54.5%) BOS 2 n=10 (45.5%) BOS 3 n=17 (77.3%)

In order to diagnose a pathological state, LTx patients were clinically evaluated. Clinical evaluations were based on lung function parameters and lung imaging. Along with the widely accepted definition of parameters that define BOS patients (JHLT Registry 2018), our cohort patients showed a significant decrease of the forced expiratory volume in the first second (FEV₁%) (**Figure 9A**), while no change in total lung capacity TLC% was observed (**Figure 9B**). These two parameters are crucial to distinguish BOS from RAS (107) (31) (104) (29).

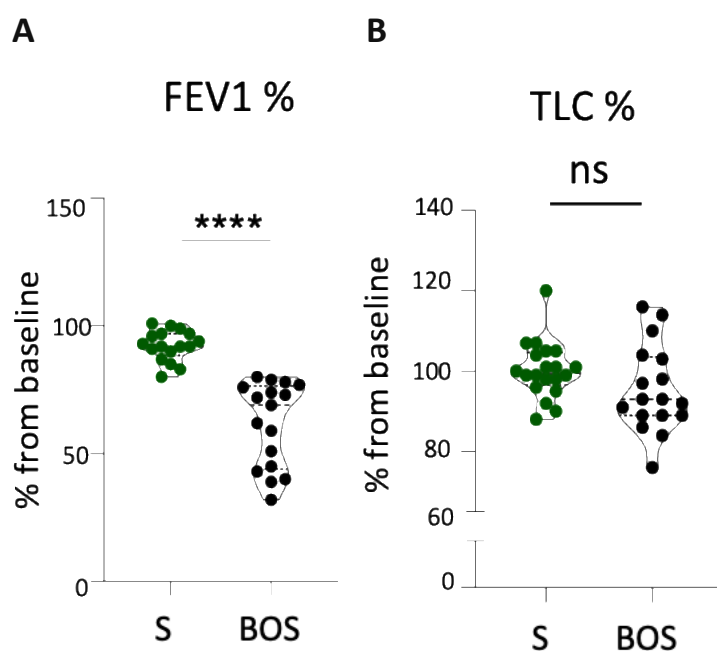


Figure 9. Lung function measurement of LTx patients

(A) Analysis of the forced expiratory volume in 1 second decline (FEV₁ %) in (S) and BOS patients; (B) Analysis of total lung capacity percentage (TLC %) in Stable (S) and BOS patients. Violin plot graphs show mean values +/- SD. Statistical significance was assessed using T-test student, Mann-Whitney U test (****P < 0.0001) (A, B)

Since macrophages are described to have a dual role in the lung immunology, BAL alveolar macrophage (MΦ) cell count was evaluated. Interestingly, we observed a remarkable decrease of the macrophage cell population at stage 2 of the disease, that recovered at the later stage of the disease BOS stage 3 (**Figure 10**). Patients were solely selected according to the lung function analysis, and not according to the differential BAL count. Some of the Stable (S) patients had a low percentage number of macrophages, because of a temporary increase of neutrophils that was treated with Azithromycin. Stable patients remained clinically stable over a long period of time (>5 years).

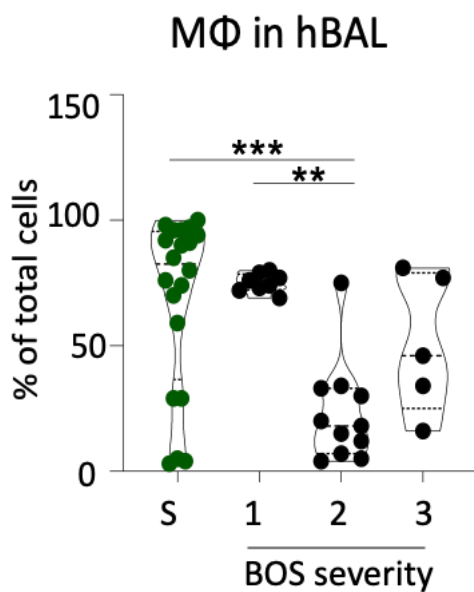


Figure 10. BAL alveolar macrophage cell count

*Quantification of alveolar macrophage percentage detected in BAL from Stable (S) and BOS patients, at different stages of the disease (Munich cohort). Violin plots show mean values. Statistical significance was assessed using via one-way ANOVA, Kruskal Wallis (** $P < 0.005$; *** $P < 0.0003$)*

Bronchoalveolar lavage (BAL) has been widely used to evaluate inflammatory biomarkers in the lung airways; moreover, the total protein content in BALF has been associated with the inflammatory response in the airways (108) (105). Therefore, BALF samples from Stable and BOS patients were analysed at different stages of the disease. No change in the protein content was found over the progression of the disease, neither between stable either in BOS patients (**Figure 11**).

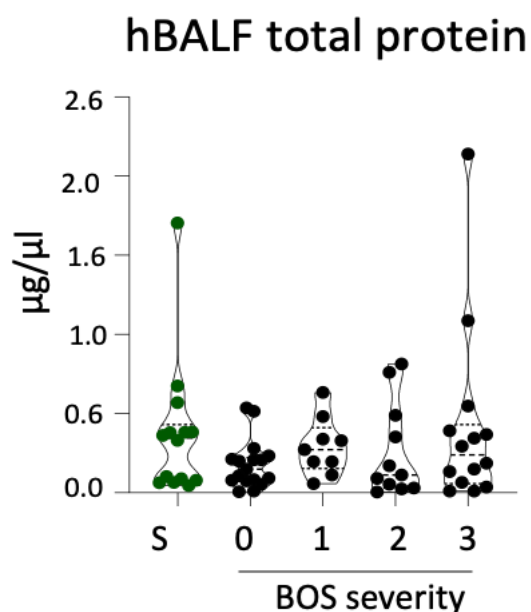


Figure 11. Total protein concentration in BALF of LTx patients

Analysis of the total protein concentration in BALF from Stable (S) and BOS patients (BOS), at different stages of the disease (Munich cohort). Violin plots show mean values. Statistical significance was assessed using one-way ANOVA, Kruskal Wallis

Due to the lack of lung tissue from this Munich cohort at the time of BALF collection as well as at the later stage of the disease, a second human cohort of LTx patients (France cohort) was considered. Unfortunately, lung tissue sampling was achieved only from the advanced stage of the disease (BOS-3). Lung sections were obtained by excision of explanted grafts from LTx patients before re-transplantation (re-LTx) and embedded in paraffin for tissue analysis. Age, gender, underlying disease, type of surgery and post-surgery complications were defined for each patient at the time of the lung tissue collection (**Table 15**).

Moreover, the human control sections used for histology were derived from healthy parts of lungs from non-transplanted donors, Healthy donors (HD).

Table 15. Demographics of lung transplanted patients from France cohort (cohort 2)

Underlying disease	LTx type	Age, Sex	Rejection grade	Therapy	Complications	Time before reLTx
PAH	Heart-lung	31, F	All stage 3	Immunosuppressive	Aspergillus aereus	
PAH histiocytosis	SLTx	42, F		Immunosuppressive	Edema Staphylococcus aereus Infection	
IPD	DLTx	41, F		Immunosuppressive	Aspergillus aereus Fibrotic pneumopathy	7 years
Not known	Heart-lung	F		Immunosuppressive		6 years
PAH		41, F		Immunosuppressive	Infection	2 years

4.2 Newly formed collagen levels increased in BOS patients

Patients that developed BOS are characterized by marked tissue collagen deposition that negatively affects long-term functional outcomes after LTx (107-108). Pro-collagen 1a1 is a component of a procollagen 1 molecule, and it is a well-described marker of fibroblast activation during lung fibrosis (109). COL1A1 gene encodes pro-collagen a1 chain, which combined with another pro-collagen a1 chain and with a pro-collagen a2 chain build up a molecule of Pro-collagen 1. Pro-collagen 1 molecules are processed in the extracellular space, where they organize into long and thin fibrils that cross-link around cells in a mature form (collagen 1), which is following responsible for the lung tissue fibrosis. The levels of soluble pro-collagen 1a1 were assessed in the BALF of LTx patients using an enzyme-linked immunosorbent assay. When comparing BOS LTx patients with Stable (S) patients, a large increase of newly formed pro-collagen 1a1 was found in BALF from BOS patients (7.4 fold-change, $P=0.0003$) (**Figure 12A**). Pro-collagen-1a1 levels were already high at stage-1 of the disease (655.02 pg/ml in BOS-1 vs 98.8 pg/ml in S, $P=0.0009$), and stage-2 of the disease (425.31 pg/ml in BOS-2 vs 98.8 pg/ml in S, $P=0.029$), and peaked at stage-3 (1081.74 pg/ml in BOS-3 vs 98.8 in S, $P=0.0048$) when compared with Stable LTx patients (**Figure 12B**). No significant differences were found between the BOS groups after using a Mixed effects model analysis followed by a Tukey's multiple comparisons test.

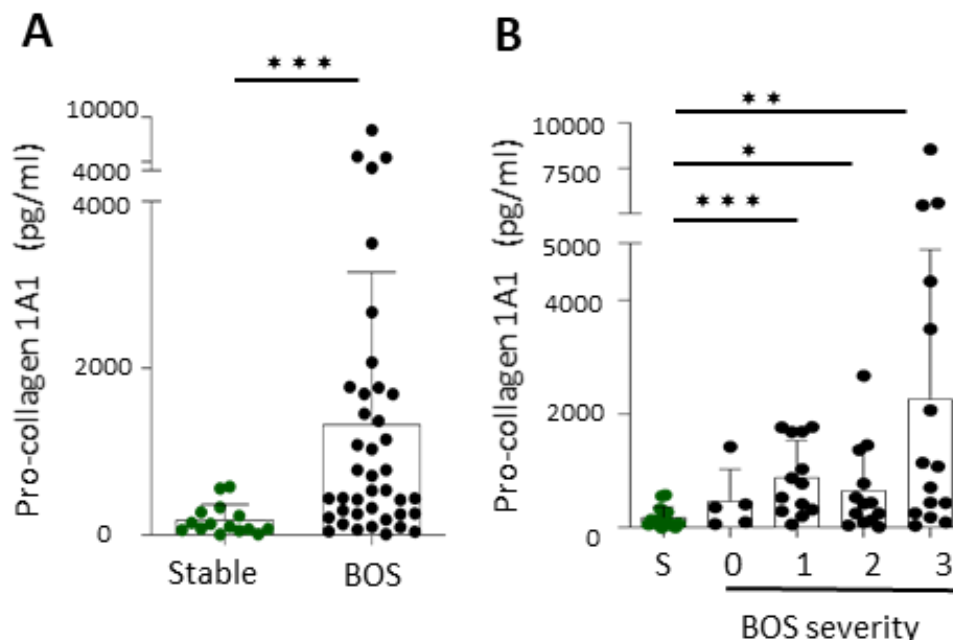


Figure 12. Newly formed pro-collagen 1A1 levels increased at early stage of BOS disease

(A, B) Quantification via ELISA of secreted pro-collagen 1a1 in bronchoalveolar lavage fluid (BALF), from Stable (S), and from BOS patients (BOS). Bar graphs show mean values \pm SD. Statistical significance was assessed using Mann-Whitney U test ($***P < 0.0003$) (A), and one-way ANOVA, Kruskal Wallis ($*P < 0.05$; $**P < 0.005$) (B)

Most importantly, pro-collagen 1a1 levels negatively correlated with FEV₁% values after LTx (P= 0.0018) (**Figure 13**). These results suggest that fibroblast activation during BOS development occurs at early stages of the disease.

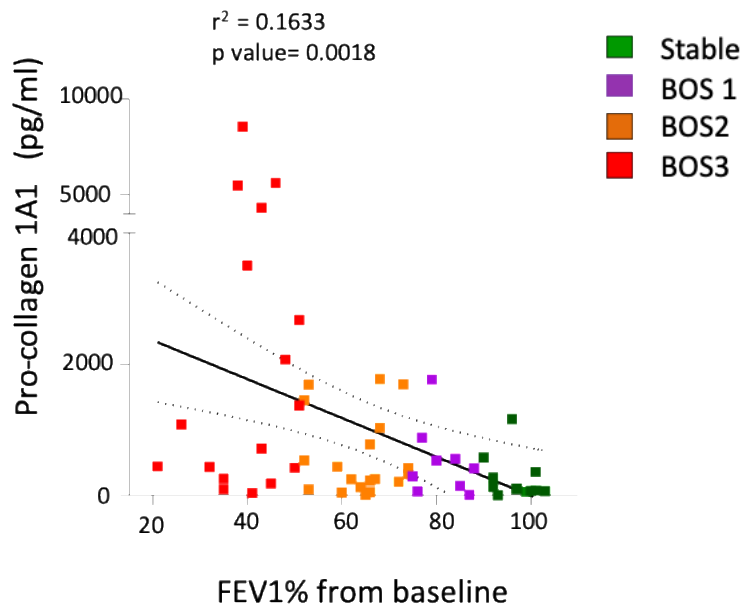


Figure 13. Newly formed collagen secretion correlated with the pulmonary function

Linear correlation between pro-collagen 1a1 secreted in BALF and FEV₁ % of Stable and BOS patients; BOS0 patients are excluded for the analysis because of no change in FEV₁% from the baseline. The different stages of the disease are highlighted using a colour code that stays consistent in all figures of this study: green for Stable patients (S), purple for BOS patients at stage 1 of the disease; orange for BOS patients at stage 2 of the disease, and purple for BOS patients at stage 3 of the disease

4.3 Cystatin C levels decreased in BOS patients

Previous studies have shown Cystatin-C (CysC), an endogenous regulator of the activity of several cathepsins, was able to prevent activation and proliferation of fibroblasts in injured lung tissue and in cancer cells (86-87). Therefore, CysC levels were assessed in explanted human lung tissue by immunostaining. Lung tissue from BOS stage-3 patients (cohort 2, **Table 15**) showed a remarkable decrease in CysC expression (35.3 positive cells/20 FOV in H, vs 14.3 positive cells/20 FOV in BOS-3, P= 0,011) (**Figure 14A-B**) compared to Healthy donors (HD) patients, and mainly localized in macrophages using Galectin-3 staining as macrophages marker (**Figure 15**).

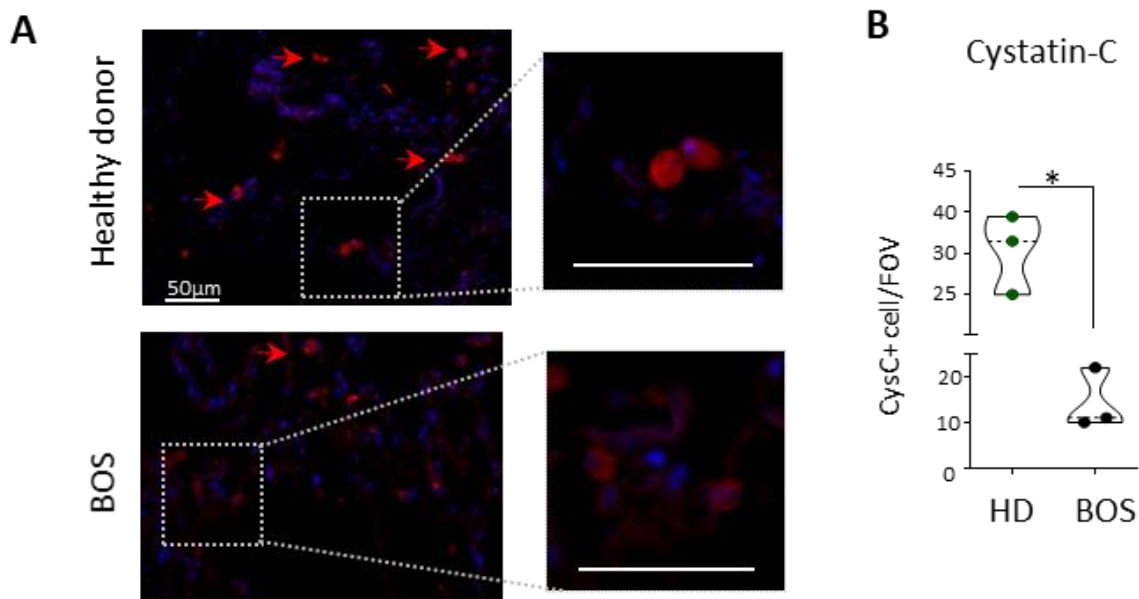


Figure 14. CysC protein expression decreased in BOS lung tissue

(A) Representative immunofluorescence staining of Cystatin-C (CysC), in red, in human lung tissue, from Healthy donors (HD) and BOS stage-3 patients (scale bar of 50µm); (B) Quantification of CysC-positive cells in 20 fields of view (FOV) in human lung tissue. Violin plots show mean values +/- SD. Statistical significance was assessed using Mann-Whitney U test (* $P < 0.05$)

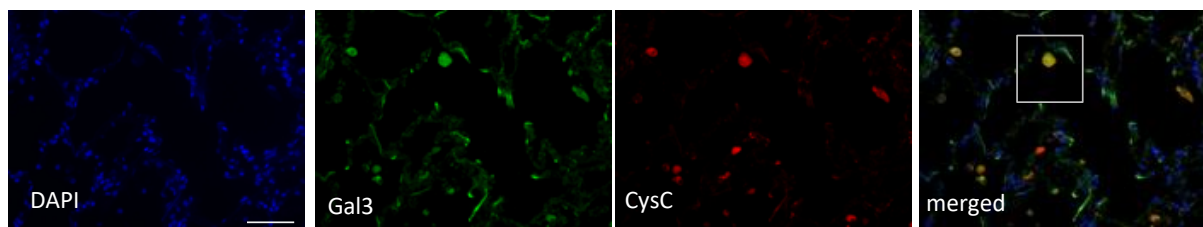


Figure 15. CysC expression in macrophages in the lung tissue of Healthy donors

Representative immunofluorescence staining of Cystatin-C (CysC) in lung tissue of Healthy donor patients (scale bar of 50µm). Nuclear staining (in blue), Gal3 macrophage staining (green), and CysC staining (red)

4.4 Cathepsin B activity increased in BOS patients

Cathepsin B (CatB) activity was reported to be involved in tissue fibrosis (83-84). We hypothesized that the activity of CatB in BALF from BOS patients was dysregulated as a consequence of decreased levels of CysC. CatB activity in BALF of LTx patients (cohort 1) was measured by using a FRET-based activity assay. BALF from BOS patients were compared to Stable patients. A substantial increase of CatB activity was observed in BOS patients (21.3 ng/ml in BOS vs 3.05 ng/ml in H, $P = 0.0001$) (**Figure 16A**), (16.9 ng/ml in BOS-0 vs 2.69 ng/ml in S, $P < 0.0001$) compared to Stable LTx patients (**Figure 16B**). Moreover, similarly with pro-collagen levels, CatB activity also negatively correlated with FEV₁% values from

baselines after BOS development already at early stage of the disease, indicating that CatB maybe contribute to the disease progression (P= 0.014) (**Figure 17**).

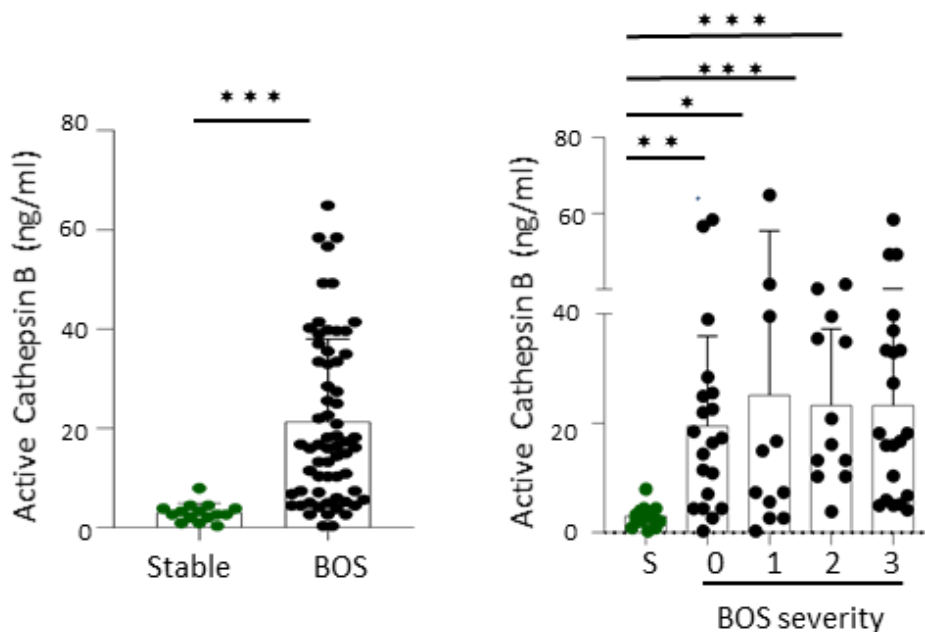


Figure 16. CatB activity increased in BOS

(A, B) Quantification of Cathepsin-B (CatB) activity in human BALF via a FRET-probe based activity assay adding 10 μ M of Z-Arg-Arg-AMC substrate to the reaction buffer. CatB concentration was measured with serial dilutions of CatB recombinant protein. Bar graphs show mean values +/- SD. Statistical significance was assessed using Mann-Whitney U test (****P < 0.0001) (A), and one-way ANOVA, Kruskal Wallis (*P < 0.05; **P < 0.005; ***P < 0.0003; ****P < 0.0001) (B)

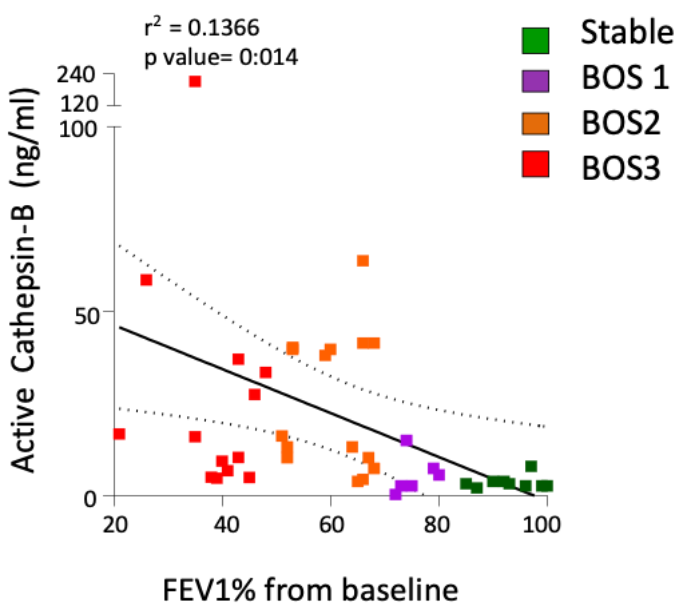


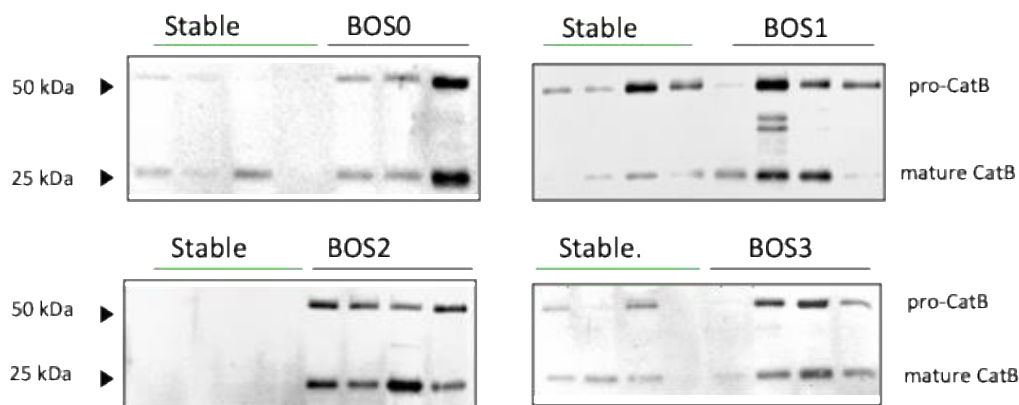
Figure 17. The increase of CatB activity was associated with a poor lung function

Linear correlation between pro-collagen 1a1 secreted in BALF and FEV1 % of Stable and BOS patients; BOS0 patients are excluded for the analysis because of no change in FEV1% decline. The different stages of the disease are highlighted using a colour code that stays consistent in all figures of this study: green for Stable patients (S), purple for BOS patients at stage 1 of the disease; orange for BOS patients at stage 2 of the disease, and purple for BOS patients at stage 3 of the disease

4.5 Cathepsin B expression increased in BOS patients

Since the presence of active Cathepsin B depends on different post-translational mechanisms (96), it was investigated whether also the translation of CatB was regulated during BOS development after LTx. Remarkably, total CatB protein level was significantly increased in BALF from BOS patients (4.5 fold change, $P < 0.005$), as well as the pro-form of CatB (pro-CatB) (2.7 fold change, $P < 0.05$), and the mature form of CatB (mature CatB) (2 fold change, $P < 0.05$) compared to Stable patients (**Figure 18A-B**).

A



B

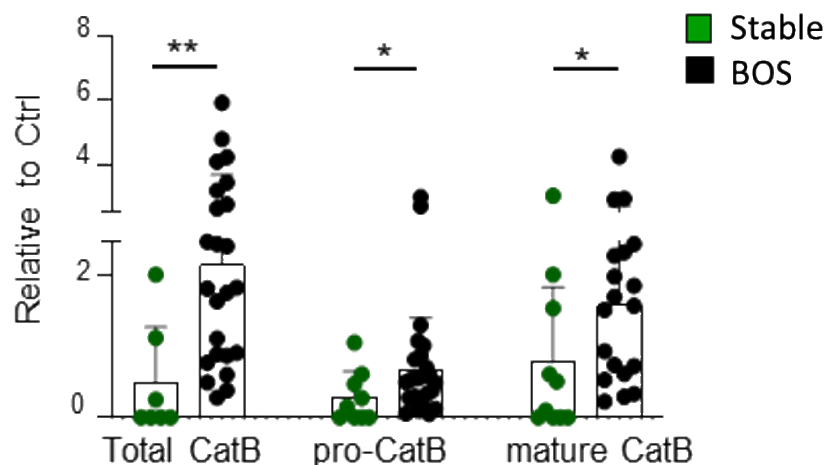


Figure 18. CatB protein expression increased in BOS

(A) Representative Western blots of human BALF samples from Stable and BOS patients. (B) Quantification of protein levels of total CatB, pro-CatB and mature CatB determined and quantified according to the molecular weight. Bar graphs shows mean values \pm SD. Statistical significance was assessed using T-student test, Mann-Whitney U test ($*P < 0.05$; $**P < 0.005$) (B)

Similarly, the localization and expression of CatB in explanted lung tissue from BOS stage-3 patients (cohort 2, **Table 15**) showed a marked increase of CatB expression when compared

with Stable LTx patients (**Figure 19** upper panel). Interestingly, we observed a significant increase of collagen deposition in areas of CatB localization (as showed in **Figure 19** lower panel).

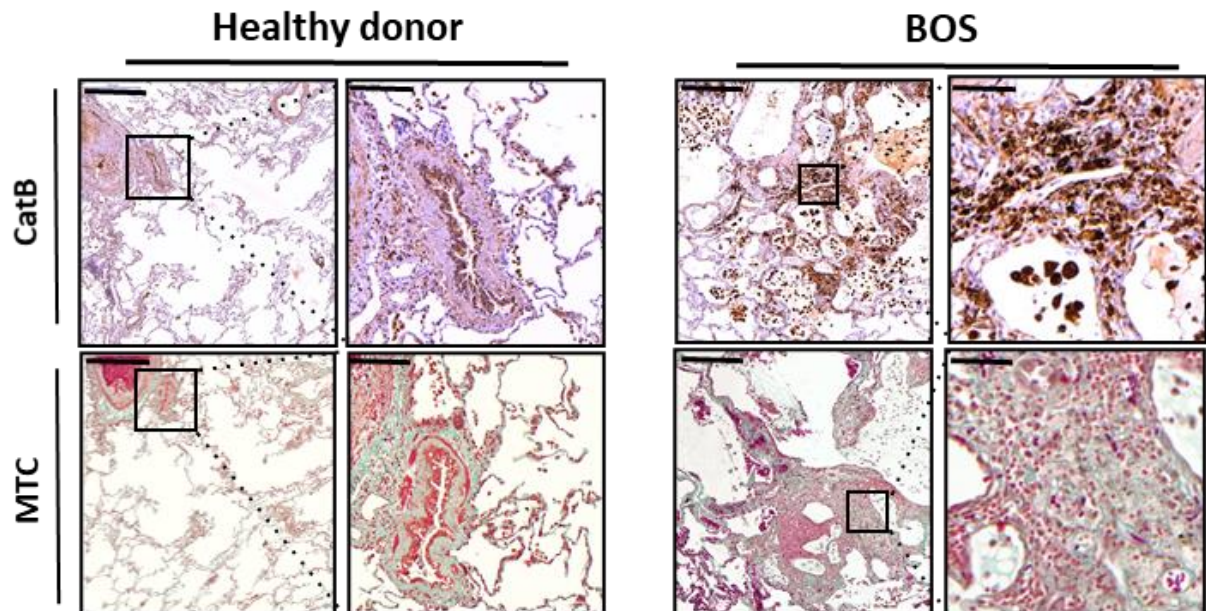


Figure 19. CatB protein expression increased in lung tissue of BOS patients

Paraffin-embedded lung tissue was obtained from Healthy donors and from BOS stage-3 patients and from stable LTx patients. Representative immunostaining of CatB expression in human lung tissue (upper panel) (scale bar of 100 μ m); Representative staining of collagen deposition in human lung tissue (lower panel) (scale bar of 100 μ m) via Masson Trichrome staining (MTC)

The presence of causality between CatB activity and pro-collagen 1a1 levels over the progression of BOS was evaluated, Interestingly, a synergistic increase of CatB activity together with the secretion of pro-collagen 1a1 was observed along BOS development (**Figure 20**). Taken together, these results indicate that CatB can trigger the collagen biosynthesis, which plays a key role in the progression of BOS.

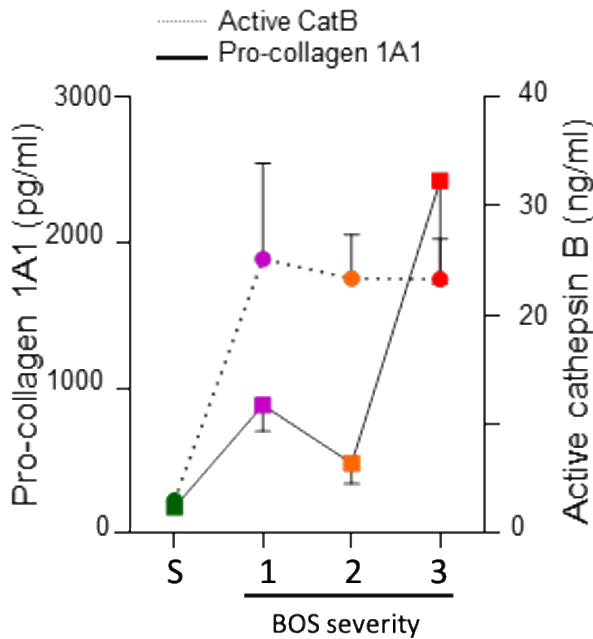


Figure 20. CatB and pro-collagen secretion increased over the progression of BOS

Evaluation of CatB and pro-collagen 1a1 expression over BOS progression (+/- SEM). Dotted line represents the activity of CatB (ng/ml), and continuous line represents the protein level of procollagen 1a1 (pg/ml). CatB activity and procollagen 1a1 levels were measured in BALF collected from LTx patients. The different stages of the disease are highlighted using a colour code that stays consistent in all figures of this study: green for Stable patients (S), purple for BOS patients at stage 1 of the disease; orange for BOS patients at stage 2 of the disease, and purple for BOS patients at stage 3 of the disease

4.6 Enhanced Cathepsin B activity in IPF patients

In this study, BALF samples were analysed from LTx patients with a different history of underlying disease (**Table 14**). We questioned whether the history of pulmonary disease, before LTx, was affecting the activity of CatB during BOS development. Interestingly, this investigation revealed a substantial increase of CatB activity in patients previously diagnosed for lung fibrosis (LF/IPF) (53.9 ng/ml in BOS vs 7.3 ng/ml in H, $P= 0.0047$) (**Figure 21A**), rather than for other diseases (**Figure 21B**). Remarkably, BOS patients diagnosed for LF showed decreased CysC levels in BALF samples compared with LF patients without signs of rejection (23.3 ng/ml in BOS vs 81.57 ng/ml in H, $P= 0.0048$) (**Figure 21C**), but not in other underlying diseases (**Figure 21D**).

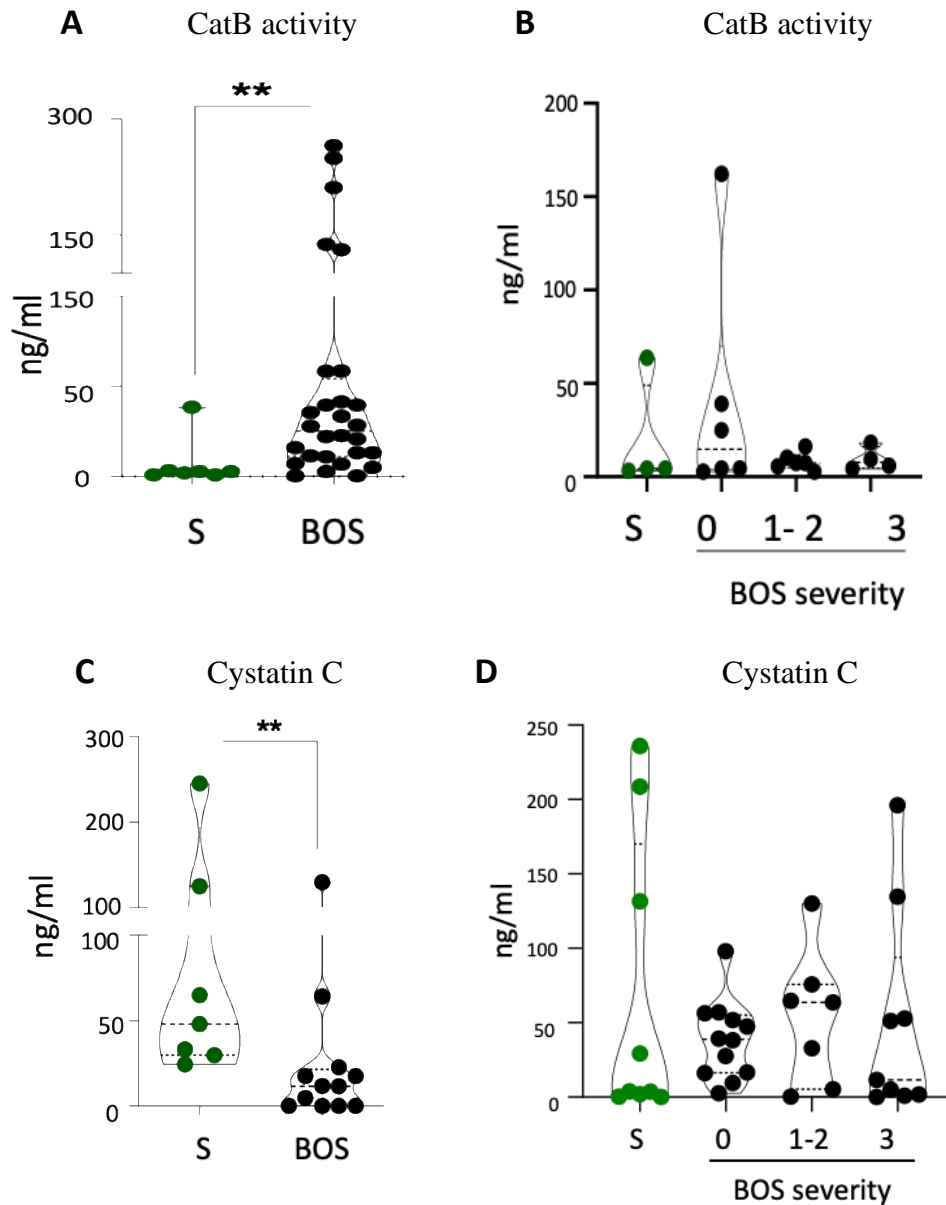


Figure 21. CatB activity and CysC levels are impaired in patients with lung fibrosis

Analysis of CatB activity and CysC levels according to the underlying diseases. (A) Quantification of CatB activity via a FRET-probe based activity assay in BALF from patients who were affected by lung fibrosis (LF); (B) and in patients affected by other underlying diseases (cystic fibrosis, CF, and pulmonary hypertension, PH);(C) Quantification of CysC levels via ELISA in BALF from patients who were affected by lung fibrosis (LF); (D) and in patients affected by other underlying diseases (cystic fibrosis, CF, and pulmonary hypertension, PH). Violin plots show mean values. Statistical significance was assessed using Mann-Whitney U test (** $P < 0.005$) (A, C), and one-way ANOVA (B, D).

4.7 Infiltrating macrophages are the main source of CatB in BOS

The localization of CatB have been investigated by immunohistochemistry. One hallmark of BOS is the influx of immune cells into the allograft lung, and particularly mononuclear cells such as T and B cells as well as macrophages were showed increased in areas surrounding

airways and vessels (30). Specifically, macrophages, stained here for Gal3, have been shown to express CatB in the lung tissue of patients with BOS (**Figure 22**).

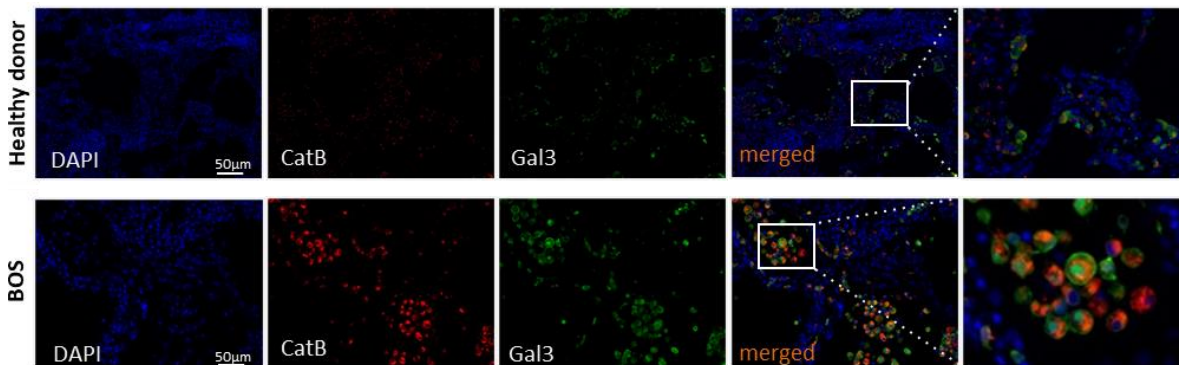


Figure 22. Macrophages were the main source of CatB in lung tissue of BOS patients

Representative immunofluorescence staining of cathepsin B (in red), and of macrophage marker, Galectin 3 (in green) in human lung tissue from Healthy donors and BOS stage-3 patients (scale bar of 50 μ m)

In addition, CatB expression was investigated in lung tissue from our previously established mouse model of LTx (52), comparing syngeneic mice (B6 \rightarrow B6) with a model of early stage of BOS (HLA \rightarrow B6), 2 months after LTx. Similar to human LTx lungs, alveolar macrophages were identified as the main source of CatB, in areas surrounding the airways and vessels (**Figure 23**).

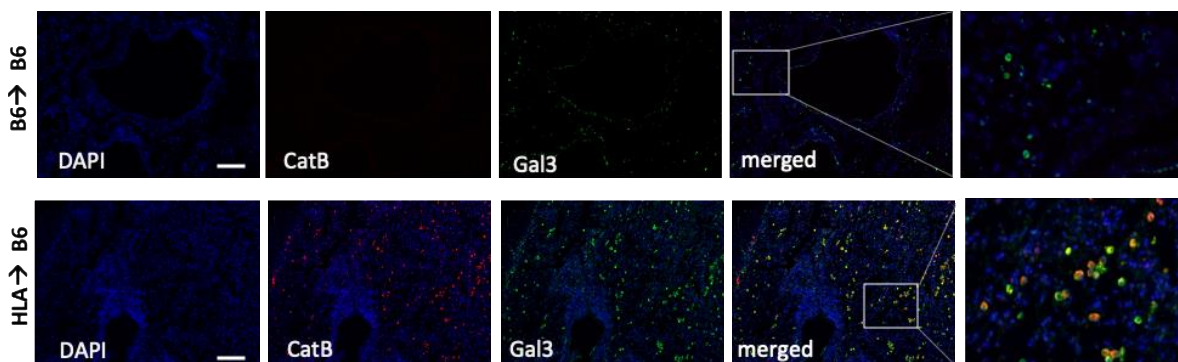


Figure 23. Macrophages were the main source of CatB in lung tissue of the mouse model of BOS

Left lungs from B6, and HLA mice were orthotopically transplanted into B6 mice and analysed 2 months after LTx (B6 \rightarrow B6 n= 4, HLA \rightarrow B6 n= 4). Representative immunofluorescence staining for CatB (red) and for macrophage marker, Gal3 (green) (scale bar of 50 μ m) in murine lung tissue

Furthermore, to understand whether CatB-macrophages were recruited or donor-specific, left lung tissue from HLA \rightarrow B6 mice was stained for HLA.A2, which is only expressed on the surface of donor cells, and for CatB. Interestingly, only recipient-derived macrophages, that

were negative for HLA.A2, expressed CatB. This finding suggests that recipient monocyte-derived macrophages are the main source of CatB (**Figure 24**).

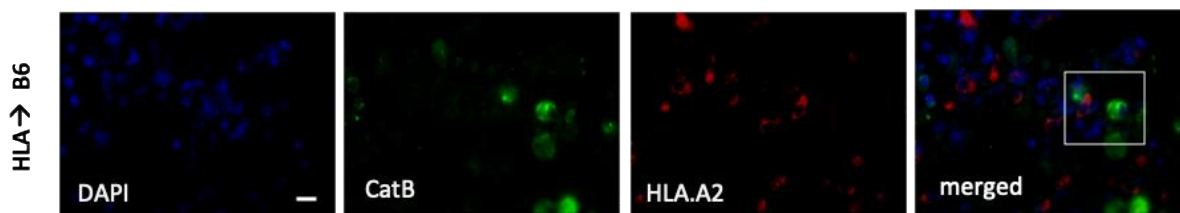


Figure 24. Macrophages expressing CatB were recipient-derived

Representative immunofluorescence staining for cathepsin-B (in green) and left lung donor-derived antigen, HLA.A2 (red) in lung tissue from HLA→B6, 2 months after LTx.

Furthermore, quantitative analysis of macrophages cell number by immunofluorescence staining of lung tissue from LTx mice revealed a significant increase of macrophages cell number (324 macrophages/FOV in BOS mice vs 97 macrophages/FOV in Ctrl mice; $P=0.0079$) (**Figure 25A**) as well as CatB-positive cells (110 CatB positive cells/FOV in BOS mice, vs 5 CatB positive cells/FOV in Ctrl mice; $P=0.04$) (**Figure 25B**) in HLA→B6 mice compared to B6→B6 control mice.

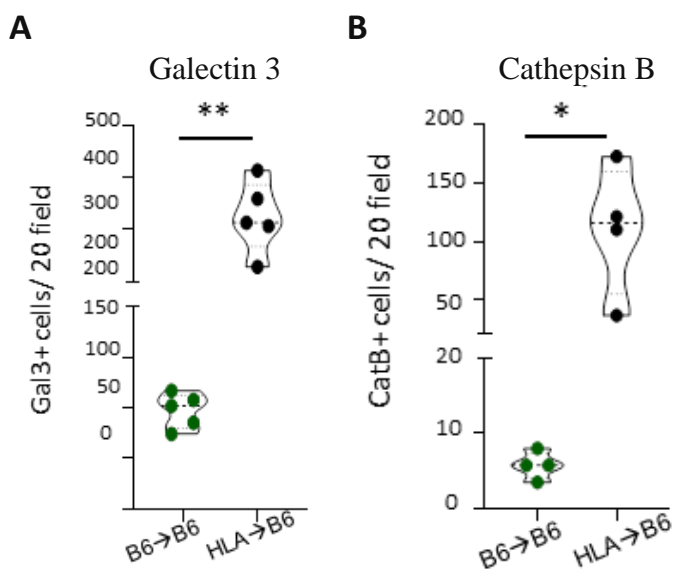


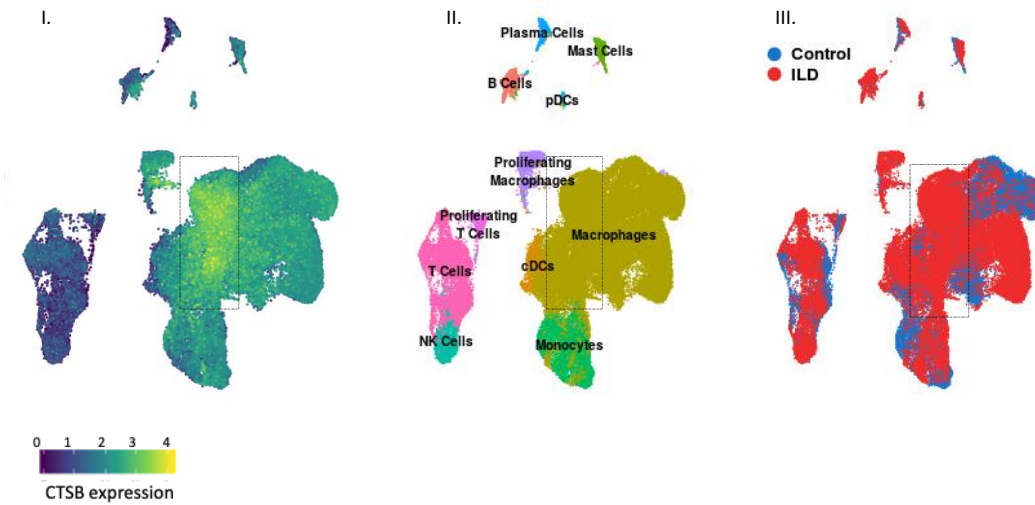
Figure 25. Macrophages and CatB-positive cells increased in BOS

(A) Quantification of Galectin-3 positive cells in 20 randomly selected fields of view (FOV); (B) Quantification of CatB positive cells in 20 randomly selected fields of view. Values were normalized to the total area. Violin plots show mean values. Statistical significance was assessed using Mann-Whitney U test ($*P<0.05$; $**P<0.005$)

In strong agreement with our findings, recent single cell RNA seq-analysis from two independent research groups have confirmed macrophages as the predominant source of CatB in lungs from lung fibrosis patients before LTx. Of relevance, CatB expression was highly expressed in macrophages deriving from fibrotic areas of explanted lungs of patients affected by idiopathic pulmonary fibrosis (as shown in **Figure 26A-B**).

A

Immune cells

**B**

Immune Cells

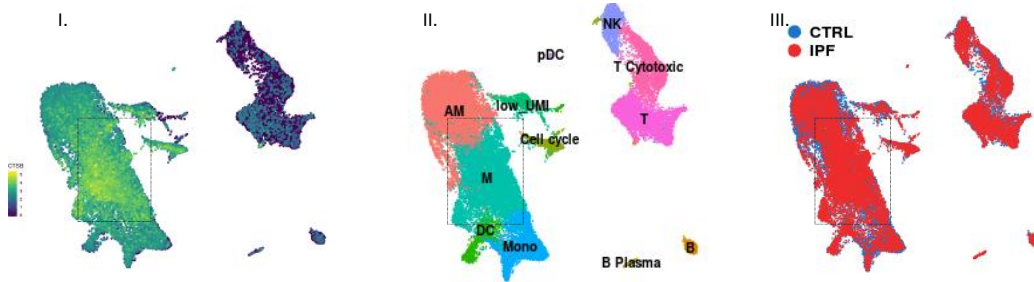
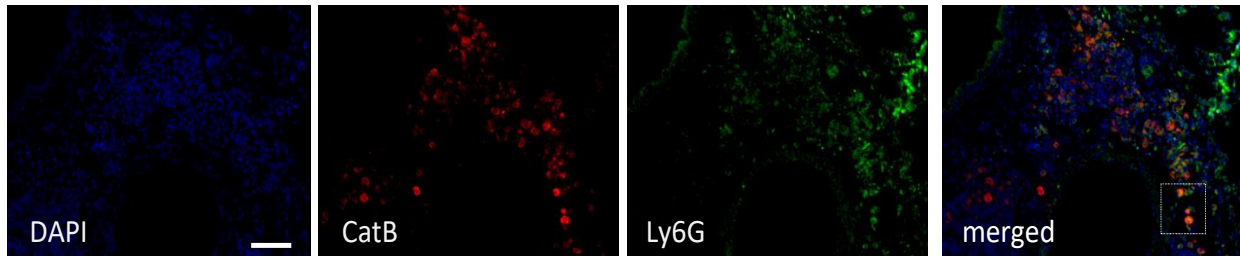


Figure 26. Macrophages were the main source of CatB in lung fibrosis patients

(A) Combined *t*-distributed stochastic neighbour embedding (*t*-SNE) analysis of single-cell transcriptomes from three normal (control), three idiopathic pulmonary fibrosis (IPF) patients (110) and (B) from 10 non-fibrotic control and 20 PF lungs. Analysis of 114,396 cells identified 31 distinct cell types. single-cell suspensions from peripheral lung tissue removed at the time of lung transplant surgery from patients with IPF ($n=12$) and no fibrotic control ($n=10$) (111). Cathepsin-B (labelled as CTSB) gene expression in immune cells in IPF patients compared with controls

Beside macrophages, T and B cells were described to infiltrate allograft lung tissue already at early stage of the rejection (51), while alveolar neutrophils have been indicated as BOS predictors, and as biomarkers of BOS progression (45). Therefore, the expression of CatB was investigated in T, B cells as well as in neutrophils using immunofluorescence staining and specific marker for each cell population. Interestingly, only few neutrophils showed a slight localization of CatB in the mouse model of LB (**Figure 27A**), whereas T and B cells were negative for CatB (**Figure 27B**).

A



B

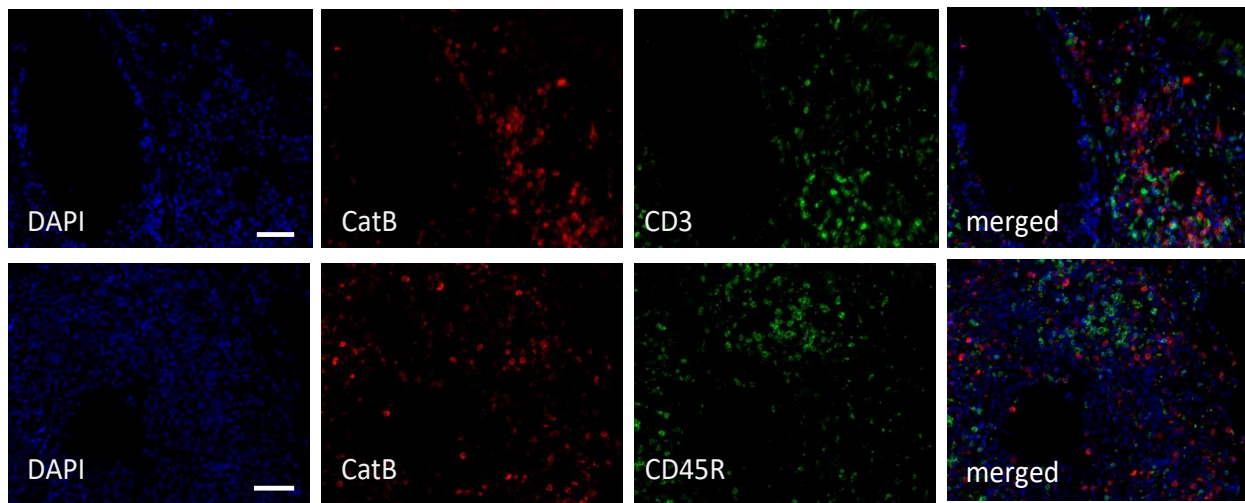


Figure 27. CatB was slightly expressed in neutrophils

Left lungs from HLA mice were orthotopically transplanted into B6 mice and analysed 2 months after LTx (n=4). (A) Representative immunofluorescence staining of CatB (red), and neutrophils, Ly6G-positive (green) in lung tissue (scale bar of 50 μ m); (B) Representative immunofluorescence staining of CatB (red), and T-cell marker, stained for CD3 (green) (upper panel), and B-cell marker, stained for CD45R (green) in murine BOS lung tissue (lower panel)

4.8 Cathepsin B expression increases in a murine model of LB

Since human BOS patients and our mouse model of LB showed a marked increase of CatB expression in BALF and lung tissue, respectively, the contribution of CatB during the progression of the disease was investigated, in a time-dependent manner, in the orthotopic mouse model of LTx. Here, for the first time, we provided a comprehensive understanding of BOS pathogenesis on the cellular and molecular level, by using lung tissue and BALF samples at different stages of the disease.

Left lungs from wildtype mice (B6) and HLA-A2-knock-in (HLA) mice were orthotopically transplanted into B6 recipient mice and analysed at days 7, 14, and 28 after LTx (**Figure 28**).

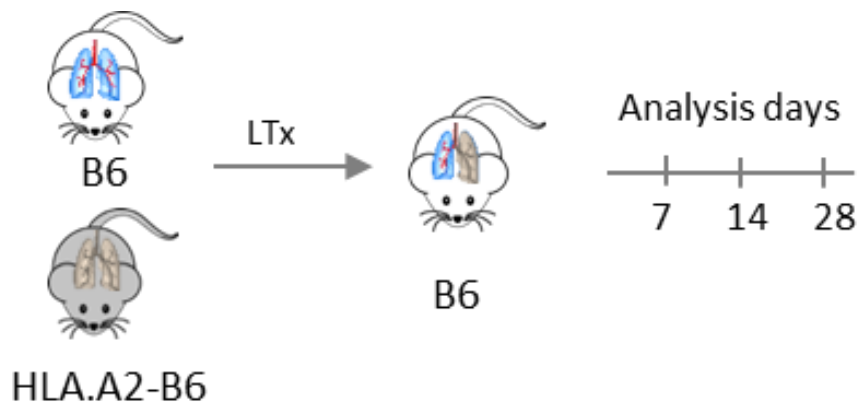


Figure 28. Experimental design of the orthotopic mouse lung transplantation model

Experimental design of a time-course orthotopic murine left lung transplantation (LTx) model. Left lungs from B6 and HLA were orthotopically transplanted into B6 mice and sacrificed at day 7, 14, and 28 after LTx. Lung tissue and BALF were analysed over time

In order to evaluate the progression of the disease, left lung tissue from B6→B6 and HLA→B6 mice were stained and quantified for collagen and inflammation in a time-dependent manner. Left lung tissue from mice reminiscent of human BOS showed a time-dependent increase of peribronchiolar and perivascular inflammation together with a progressive peribronchiolar fibrosis (**Figure 29A-B**).

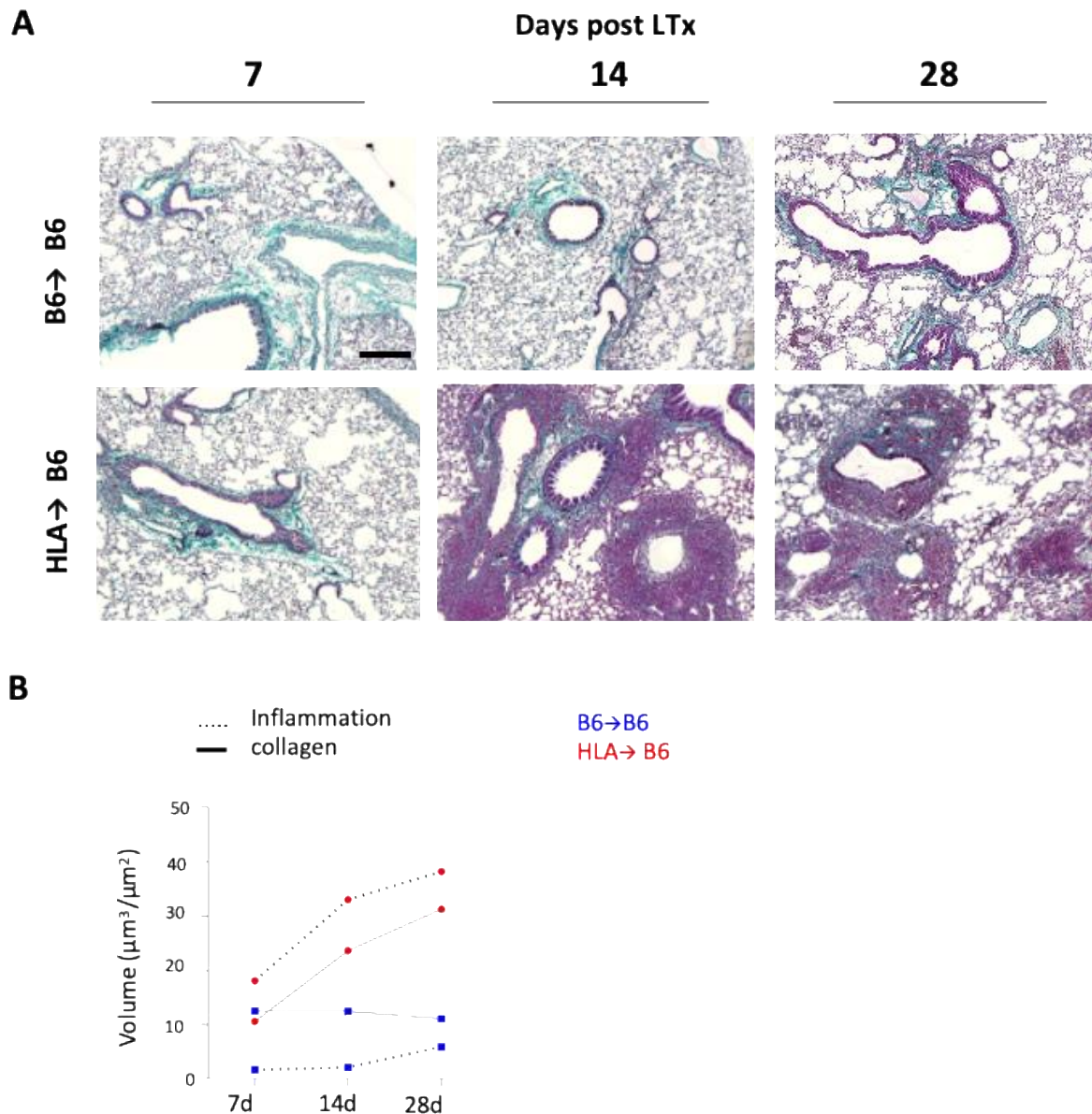


Figure 29. Inflammation and fibrosis started at early stage of BOS development

(A) Representative pictures of murine left lung tissue stained for inflammation and for collagen by using Masson trichrome staining protocol (scale bar of $200\mu\text{m}$); (B) Quantification of collagen and inflammation of (A) was performed via a computer-assisted stereology analysis (CAST). Values are represented as mean value and expressed as volume on surface ($\mu\text{m}^3/\mu\text{m}^2$)

To determine the expression of CatB over the progression of the disease, left lung tissue from the mouse model of LB was stained for CatB by immunofluorescence in a time-dependent manner. Consistent with human data (**Figure 14B**) an increase of CatB expression at 14 days post-LTx was detected in lung tissue and BALF of LB mice already after 14 days post-LTx (**Figure 30, 31A and B**).

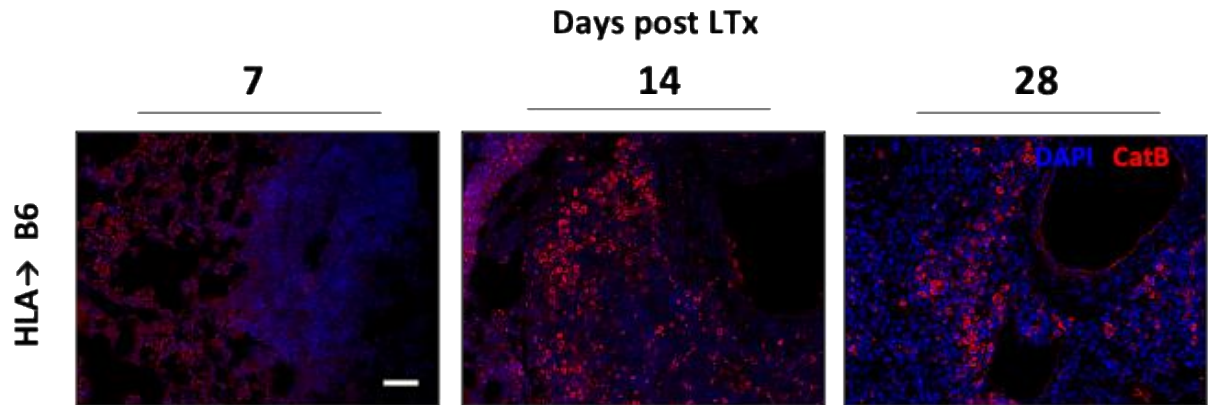


Figure 30. CatB expression increased during BOS progression

Representative immunofluorescence staining of CatB (red) in areas surrounding airways and vessel in lung tissue of a mouse model of BOS (scale bar of 50 μ m)

Since CatB expression is positively associated with collagen deposition, we investigated the expression of collagen-1 and fibronectin-1, two ECM components, in lung tissue and BALF over the progression of the disease. Remarkably, the expression of collagen-1 increased in LB lung tissue after 14 days post LTx (**Figure 31A**). Fibronectin-1 (FN1), which is needed for the assembly of the collagen matrix and shown to play an important role in fibrosis (112), was also increased after 14 days post LTx in BOS mice (**Figure 31A-B**).

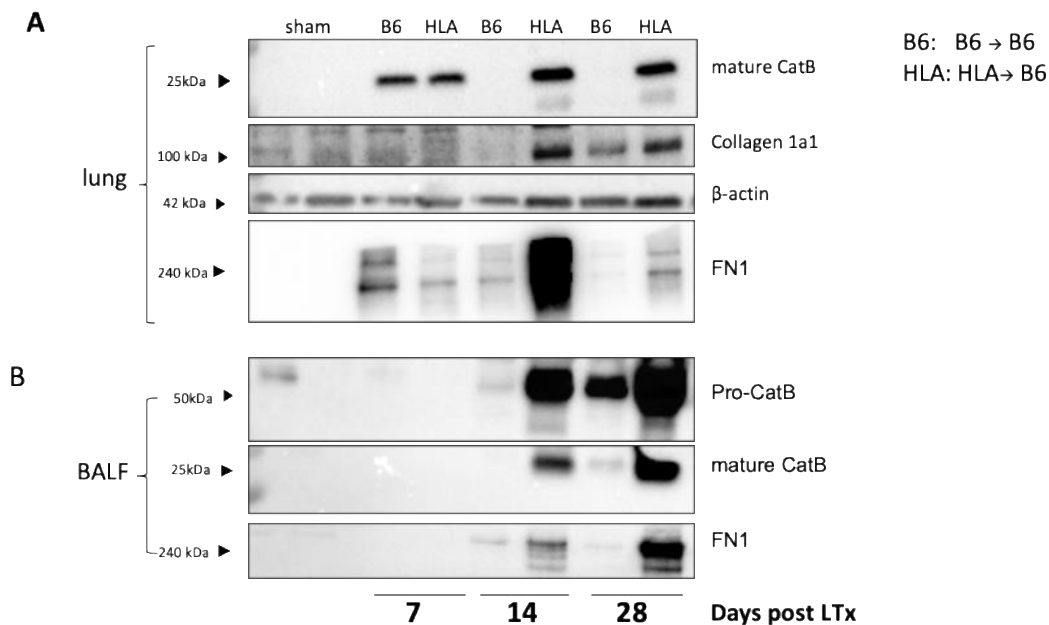


Figure 31. Extracellular matrix proteins and CatB increased during BOS progression

(A) Representative Western blots of Cathepsin-B, collagen 1 and fibronectin 1 (FN1) expression in murine lung tissue lysates from B6→B6 and HLA→B6 at different time points; (B) and in BALF. Equal amount of total protein was loaded for lung tissue analysis (15 μ g), and equal volume was loaded for BALF analysis. Pro-forms and mature forms of Cathepsin-B were detected according to the molecular weight

4.9 Genetic deletion of Cathepsin-B protected lungs from BOS development

To elucidate whether CatB plays a role in the development of BOS, HLA.A2/B6 left lungs were transplanted into B6 or *Ctsb*^{-/-} recipient mice, and lung function, tissue inflammation and collagen deposition after 28 days were analysed (**Figure 32**).

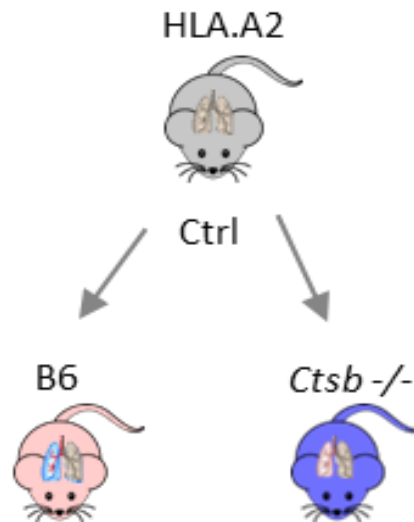


Figure 32. Experimental design of the orthotopic mouse LTx model for functional studies

*Experimental design of orthotopic left lung transplantation (LTx) in mice. CatB knock-out mice (*Ctsb*^{-/-}) were used as recipient of HLA.A2 left lungs and were compared with wild-type B6 recipients. Mice were sacrificed 28 days after LTx, to analyse lung function, lung tissue inflammation and fibrosis*

First, similar to human patients, the lung function of recipient mice was evaluated at day 28 post-LTx. CatB-deficient mice demonstrated improved lung compliance (0.017 ml/cmH₂O in *Ctsb*^{-/-} mice, vs 0.0069 ml/cmH₂O in BOS mice; P= 0.011), as well as a higher inspiratory lung capacity (0.31 ml in *Ctsb*^{-/-} mice, vs 0.13 ml in BOS mice) in comparison to LB mice (**Figure 33A-B**). Furthermore, *Ctsb*^{-/-} mice were protected from enhanced airway resistance (1.5 cmH₂O/ml in *Ctsb*^{-/-} mice, vs 9.39 cmH₂O/ml in BOS mice, P= 0.029), and tissue elastance (57.55 ml/cmH₂O in *Ctsb*^{-/-} mice, vs 124.6 ml/cmH₂O in BOS mice, P= 0.026) (**Figure 33C-D**), indicating that CatB participated in BOS pathogenesis.

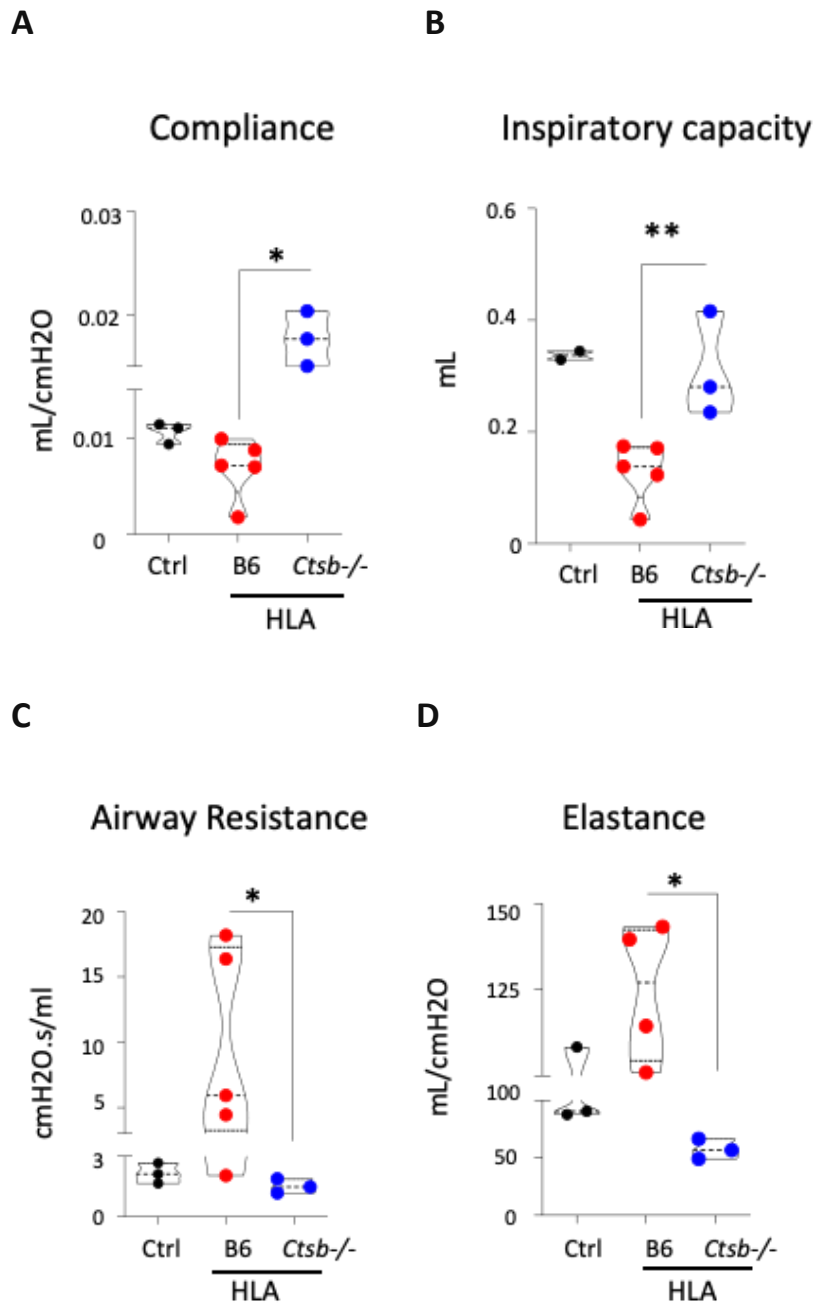


Figure 33. *CatB* deficient mice were protected from lung dysfunction

In vivo measurements of left lung function via Flexivent, 28 days after LTx. At least three measurements for each parameter were recorded. Measurements were normalized to the body weight of the recipient mouse. Violin plots show mean values \pm SD. Statistical significance was assessed using one-way ANOVA, Kruskal Wallis (* $P < 0.05$; ** $P < 0.005$)

In order to investigate whether the observed protective effect on lung function depends on reduced collagen accumulation, lung tissue sections were evaluated for collagen expression and inflammation. In agreement with the improvement of the lung function, left lungs from *Ctsb*^{-/-} showed mild signs of fibrosis in peribronchial areas and all over the lung tissue (**Figure**

34A), compared to the BOS mice. Importantly, *Ctsb*^{-/-} mice revealed reduced septal inflammation and fibrosis (**Figure 34B**). Strikingly, genetic deletion of CatB in recipient mice efficiently protected the transplanted graft from BOS progression.

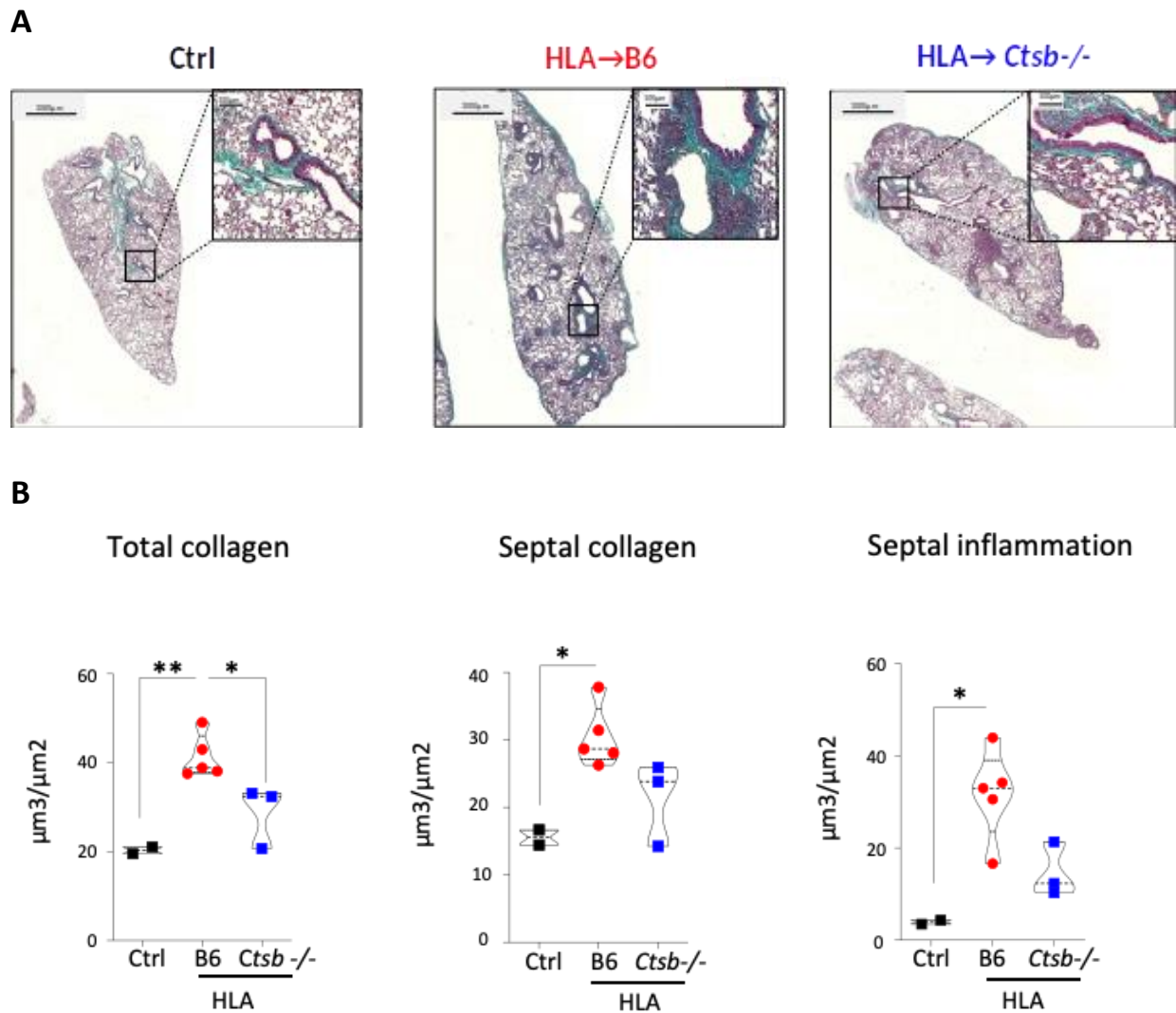


Figure 34. *CatB* deficient mice were protected from lung fibrosis

(A) Representative pictures of collagen and inflammation are shown for each group (1000µm, left panel; 100 µm, right panel); (B) Quantification of inflammation and collagen of left lung tissue, in areas surrounding airways, vessel and septum, was performed via computer-assisted stereology (CAST). Violin plots show mean values +/- SD. Statistical significance was assessed using one-way ANOVA, Kruskal Wallis (* $P < 0.05$; ** $P < 0.005$)

However, genetic deletion of CatB did not affect macrophage infiltration into the lung (**Figure 33**). Taken together, these data demonstrate that, in our mouse model of LB, the release of CatB rather than macrophages number induced BOS development.

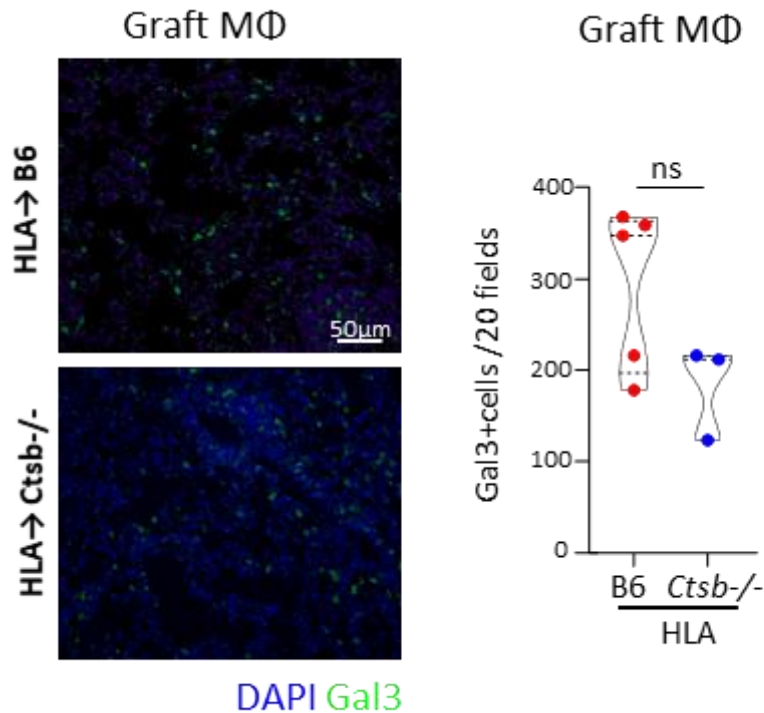


Figure 35. Genetic deletion of *CatB* did not affect macrophage infiltration

Quantification of macrophage cell number in left lung tissue at 28 days after LTx via computer-assisted stereology (CAST). (A) Representative immunofluorescence staining of Gal3, marker for macrophages (green) in lung tissue of LTx mice (scale bar of 50 μ m). (B) Quantification of Gal3-positive cells (A). Violin plots represent mean values. Statistical significance was assessed using Mann-Whitney U test

4.10 Cathepsin B expression in pro-inflammatory macrophages

CatB-positive macrophages significantly increased in areas affected by fibrosis. To further investigate the molecular function of CatB, we stimulated macrophage cell lines towards a pro-inflammatory, M1 phenotype, with IFN- γ and LPS, or anti-inflammatory, M2 phenotype, with IL4 (**Figure 36**). Unstimulated macrophages, M0, were used as control. Interestingly, the *in vitro* study showed that only M1 macrophages experienced a marked increase of CatB mRNA after 24h of IFN- γ and LPS stimulation (**Figure 37A**); similarly, also the activity of CatB was found notably increased in the medium of M1 macrophages (**Figure 37B**).

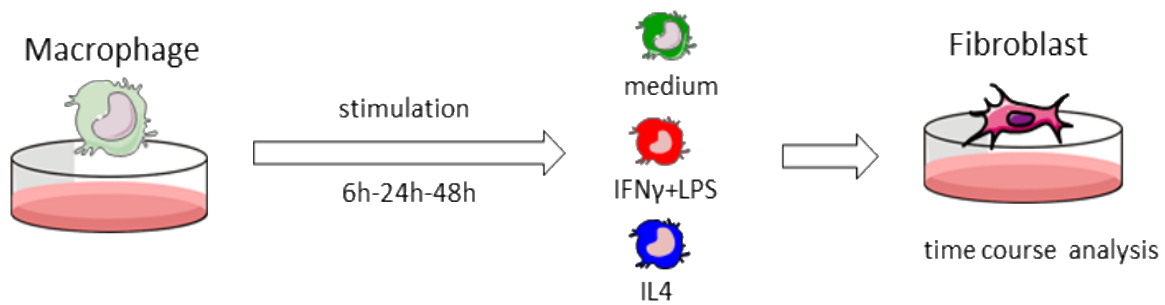


Figure 36. Experimental design of the *in vitro* model of BOS

Experimental design of macrophage (Raw264.7) polarization with IFN- γ (20 ng/ml), LPS (1 μ g/ml), IL-4 (20 ng/ml) and medium alone. Macrophage cell supernatant was used to analyse CatB activity, active TGF β 1 levels, and for further treatment of fibroblasts (MEF)

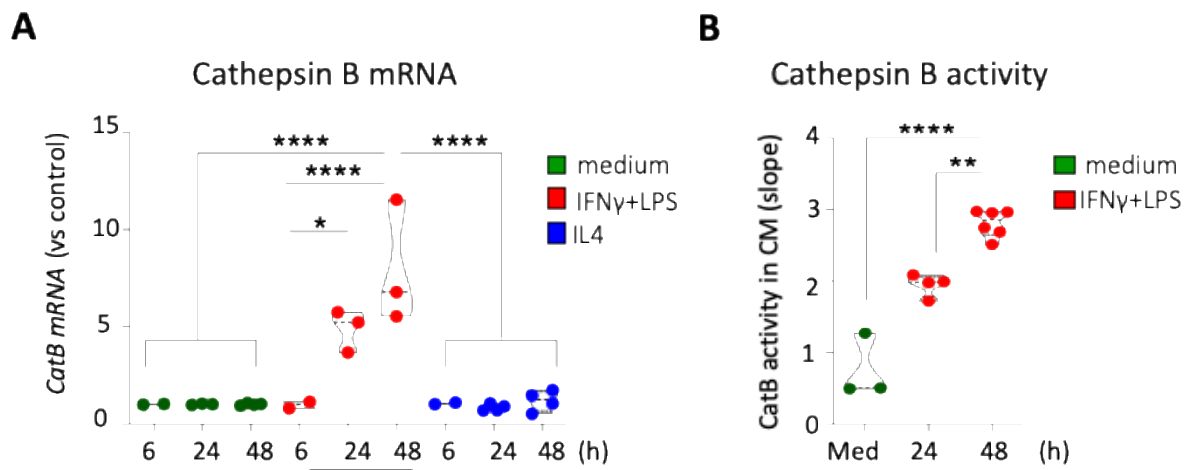
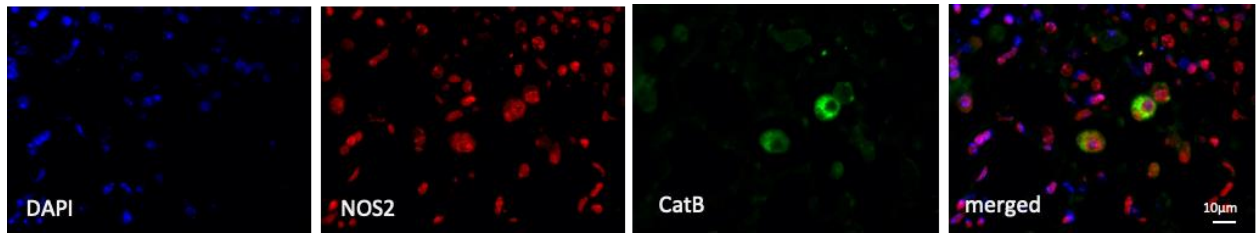


Figure 37. CatB expression and activity increased in inflammatory M1 macrophages

Macrophage cell lysate was used for gene expression analysis; (A) Gene expression analysis of murine *Ctsb* in macrophages under different stimulations and time points; (B) Quantification of CatB activity in macrophage cell supernatant via a FRET-probe based activity assay. Violin plots represent mean values \pm SD. Statistical significance was assessed using one-way ANOVA, Kruskal Wallis (B, C) (* $P < 0.05$; ** $P < 0.005$; **** $P < 0.0001$)

Since the *in vitro* study showed that pro-inflammatory macrophages were the source of CatB, the expression of CatB was further addressed in the lung tissue of the mouse model of LB by immunofluorescence. Left lung tissue from HLA \rightarrow B6 mice was stained for NOS2, a marker of pro-inflammatory macrophages, and for CD206, a marker of anti-inflammatory macrophages, together with CatB. Strikingly, CatB expression was found, similar to the *in vitro* analysis, localized in pro-inflammatory M1 macrophages (**Figure 38A-B**).

A



B

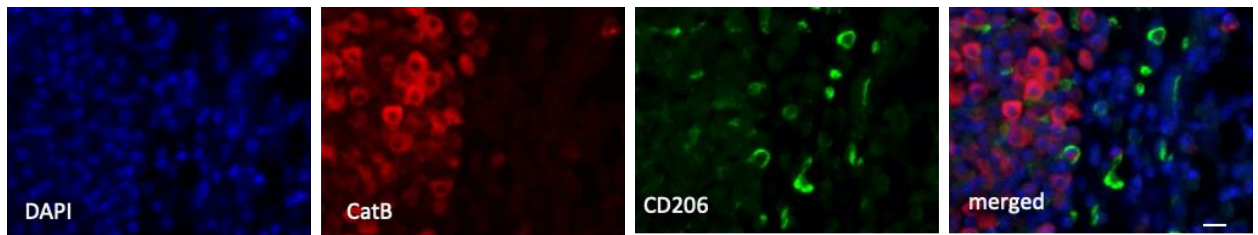


Figure 38. *CatB* was expressed in pro-inflammatory macrophages in the mouse model of BOS

(A) Representative immunofluorescence staining of *CatB* (green) and of M1 macrophages marker, *NOS2* (red) (scale bar of 50 μm), and (B) of *CatB* (red) and M2 macrophages marker, *CD206* (green) expression in the left lung of the murine model of BOS (scale bar of 10 μm)

4.11 Cathepsin-B contributed to fibroblast activation via TGFβ1-maturation

Pro-inflammatory M1 macrophage-derived cytokines (TNF-α, IL1-β) were previously shown to be highly released into the BALF of BOS patients (113).

Since macrophages were shown to be an important source of TGF-β1 in lung (111), the gene expression of *tgfb1* under different stimulation conditions was analysed in the *in vitro* model. A significant increase of *tgfb1* gene expression was confirmed in M1 polarized macrophages, but not in other macrophages (**Figure 39**).

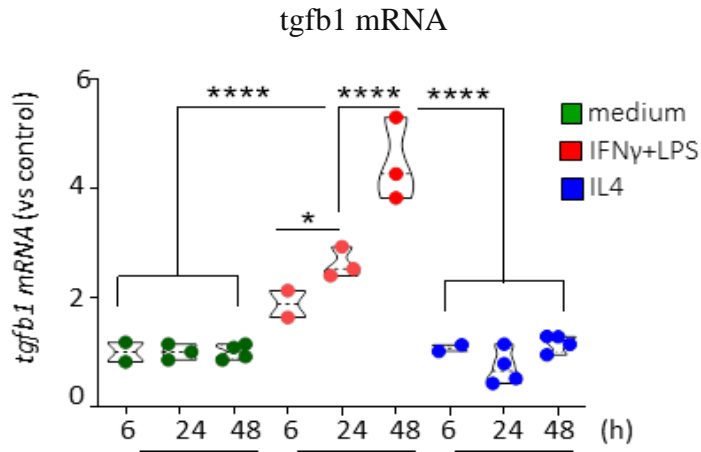


Figure 39. TGF- β 1 expression increased in M1 macrophages

Gene expression analysis of murine *tgfb1* in macrophages at different times of differentiation. Violin plots show mean values \pm SD. Statistical significance was assessed using one-way ANOVA, Kruskal Wallis (* $P < 0.05$; **** $P < 0.0001$)

To perform mechanistic studies, the effect of a specific CatB inhibitor (CA074) on CatB's activity was evaluated in the cell medium of M1 macrophages at different time points. CA074 successfully inhibited the activity of CatB in the cell medium up to 48h (**Figure 40A**). Next, we addressed the question whether CatB was regulating the maturation of latent free TGF- β 1 (pro-TGF- β 1) released from M1 macrophages. Interestingly, pre-treatment of M1 macrophages with CA074 resulted in the inhibition of pro-TGF- β 1 processing (**Figure 40B**).

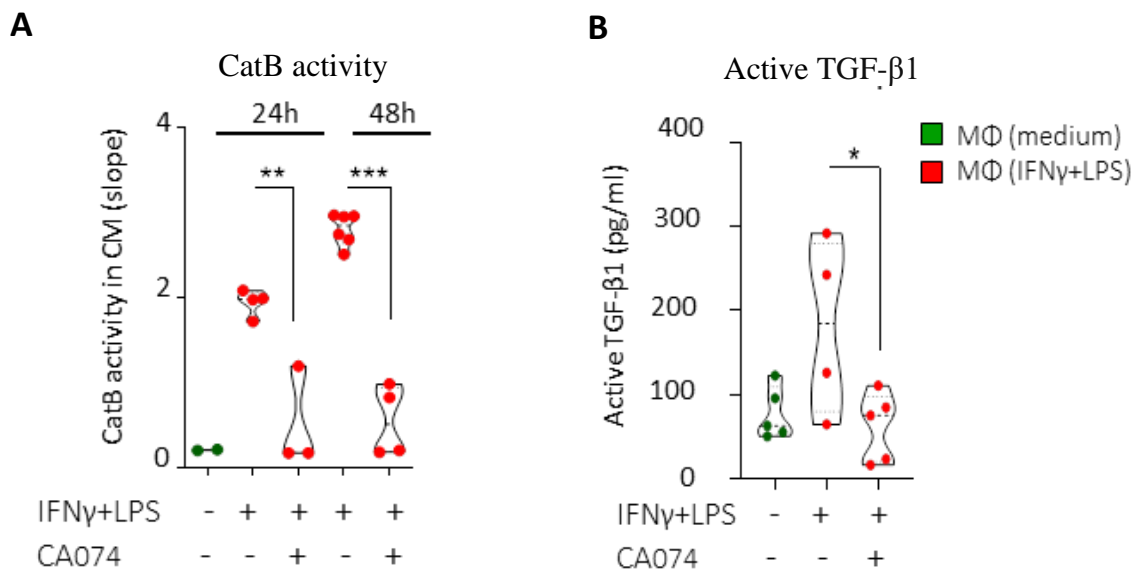
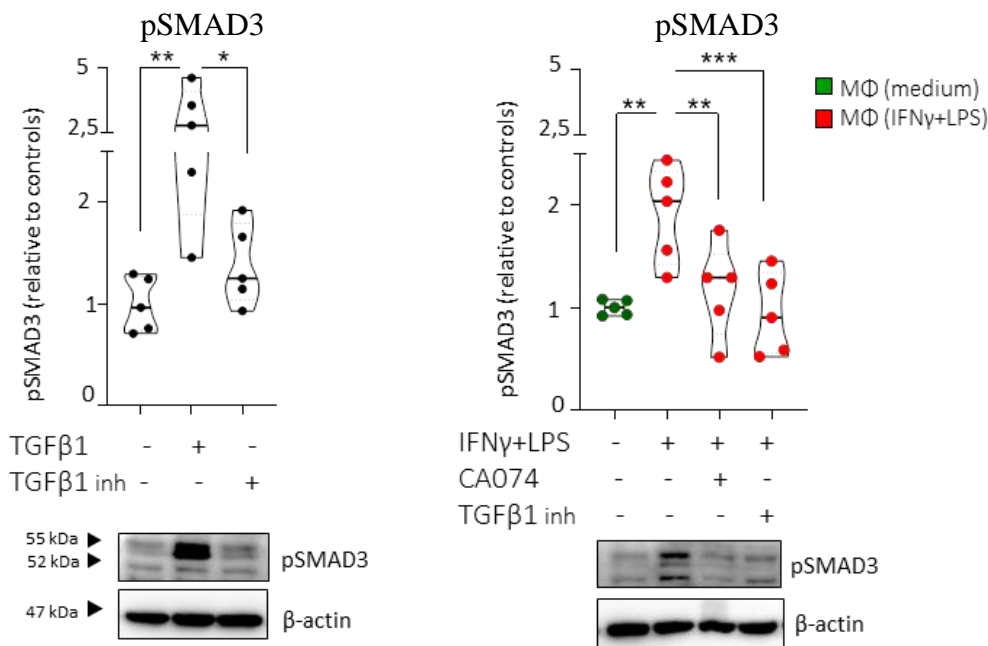


Figure 40. TGF- β 1 maturation was affected by CatB inhibitor

(A) Quantification of CatB activity via a FRET-based activity assay and (B) Quantification of active TGF β 1 via ELISA in cell supernatant of macrophage-pretreated with CA074 (10 μ M), or DMSO, and stimulated for 24h and 48h with IFN- γ (20 ng/ml) and LPS (1 μ g/ml). Violin plots show mean values \pm SD. Statistical significance was assessed using one-way ANOVA, Kruskal Wallis (A, B, C) and Turkey's multiple test (D-E) (* $P < 0.05$; ** $P < 0.005$; *** $P < 0.0003$)

To further validate the regulation of CatB-induced fibrosis, fibroblasts were treated with macrophage-derived cell medium. Since the phosphorylation of SMAD3 (pSMAD3) proteins is the main marker of the canonical TGF- β 1 signaling pathway activation, and promotes the transcription of ECM proteins, the signal of pSMAD3 after fibroblasts treatment was evaluated. Cell medium from stimulated M1 macrophages and unstimulated macrophages, with and without CatB and TGF- β 1 receptor inhibitor, was used to stimulate fibroblasts for 30 minutes. The phosphorylation of pSMAD3 was analysed in fibroblast cell lysate by western blotting. Strikingly, fibroblasts showed a significant increase in TGF- β 1-dependent activation after being stimulated with M1-derived cell medium, which was specifically mediated by CatB (**Figure 41**). Taken all together, our data demonstrate that M1 macrophages secrete CatB and by that cause the TGF- β 1-mediated activation of fibroblasts.



5. DISCUSSION

Several cellular and molecular markers of BOS have been described, in particular, the increased number of macrophages, neutrophils and lymphocytes (51), as well as soluble mediators (47). However, little is known about the fibro-proliferative mechanism and potential triggers that promote this process in areas surrounding airways.

The aim of this doctoral thesis was to investigate potential targets and mechanisms involved in the development of the BOS disease.

Cathepsin B (CatB) is a cysteine protease with unique properties. Contrary to other proteases, CatB is able to act as exopeptidase as well as endopeptidase, and exerts its activity under acidic and neutral pH conditions (102). Its enzymatic activity is broad, targeting highly similar substrates, preferentially in cleavage sites after basic and hydrophobic residues (114).

However, the contribution of CatB in the BOS development has not yet been investigated, we therefore aimed to determine the functional role of CatB in BOS development.

Our study brought to our knowledge that 1) CatB activity and expression are increased in BOS patients; 2) and that negatively associated with the lung function; 3) pro-inflammatory and recipient-derived macrophages were the main source of CatB; 4) CatB release resulted in a TGF- β 1-dependent activation of peri-bronchiolar collagen production.

The lack of knowledge about BOS development in human patients depends on several factors. One of the major reasons for this scientific gap is the limitation of human samples for research as well as the lack of a reproducible mouse model of BOS combined with the technical challenges of murine LTx. Translational studies are restricted to the usage of bronchoalveolar lavage fluid (BALF) and peripheral blood of LTx patients. Reliable lung tissue sampling is mainly available from patients that have already reached a very late stage of the disease, rendering it hard to investigate early-events for predictive studies. In this project, we performed a longitudinal study. BALF samples were stored longitudinally in the research bioarchive and then retrospectively selected for this study. In total, 22 BOS patients, and BALFs available at different BOS stages were selected and compared to 20 Stable LTx patients who did not develop BOS-related symptoms for at least 5 years after BALF collection (**Table 14**). BOS stages and relative BALF samples were grouped according to the % decline in FEV₁ values: they were grouped in BOS-0 patients that were stable at the time of BAL collection, but developed later BOS-1 or higher; in BOS-1 when the FEV₁ value was between 66-80%; in BOS-2 when the FEV₁ value was between 51-65%; and in BOS-3 when the FEV₁ value was \leq 50% (**Table 1**) (23, 28). Patients with infection as cause for lung function decline were not included in the study. Acute cellular rejection >A1 was not present in any of BOS

samples at the time of BAL collection. Lung tissue sections were obtained from BOS stage-3 patients, from a second human cohort (**Table 15**). This, coupled with our mouse lung transplantation model (52) that simulates the early stages of BOS development, enabled us to identify potential drivers of the disease that enter in play at very early stage.

We demonstrated a substantial increase of CatB activity in the BALF of BOS patients, starting already at BOS stage-0 (**Figure 16**). In accordance with our finding, a previous study showed a marked increase of CatB activity in BALF samples of mice, during the early phase of bleomycin-induced fibrosis, prompting the involvement of CatB in lung fibrosis (94). Importantly, the expression of CatB increased over the disease progression in BOS patients as well as in our mouse model of BOS (**Figure 28, 29**). This observation is comparable to previous studies performed in samples from patients and mice suffering from advanced liver fibrosis (5).

We then investigated the main source of CatB in BOS lung tissue. In cancer, CatB expression was demonstrated in infiltrating macrophages within metastatic areas, and its activity was crucial for tumor invasiveness, suggesting CatB as key-player in lung tumor progression (115). Interestingly, we showed that CatB expression was primarily found in pro-inflammatory recipient-derived macrophages in areas affected by marked signs of fibrosis and inflammation in BOS patients as well as in mice (**Figure 22-24**). We could further confirm *in vitro* that CatB-producing macrophages were predominantly pro-inflammatory M1 macrophages (**Figure 38**).

Previous studies have shown that the lung tissue of patients with BOS is characterized by a marked mononuclear infiltration in the areas surrounding the distal airways, together with a dense accumulation of collagen (116). However, histological information is widely reported at the latest stage of the disease (BOS stage 3) but not at earlier stages. Although, surveillance bronchoscopy, including BAL and transbronchial biopsy (TBB), is also part of the routine follow up in several centers, as well as in ours, lung tissue collected by TBB is not routinely stored in the research bio-archive, but only used for diagnosis purposes. Therefore, we were not able to directly compare BALF and TBB over the progression of BOS disease. In this study we used tissue sections that were obtained from the stage-3 of the disease, when lungs are explanted from BOS patients before re-LTx (116). The most relevant finding in our study is the observation of significant changes in disease-related factors in a time-dependent manner in our mouse model of BOS (**Figure 34**). Furthermore, we showed a time-dependent increase of newly formed collagen in BALF from BOS patients, that was increasing already at early stage of the disease (**Figure 12**), and negatively affected the pulmonary function of LTx

patients (**Figure 13**). Similarly, CatB activity was negatively correlated with the lung function after LTx (**Figure 17**).

The premature increase of CatB activity in the BALF (**Figure 16B**) suggested its contribution in promoting the biosynthesis of collagen. The increased levels of pro-collagen 1a1 were already reported by Keane et al. as a result of fibroproliferation of alveolar epithelial cells (117), as well as by King et al. in the BALF of patients with interstitial lung disease (118). Importantly, we showed that the increase of CatB activity occurred already at a very early stage of the disease (BOS-0), and later the production of collagen started (BOS-1), suggesting CatB as a potential trigger of the incessant production of collagen in BOS development. This observation is of particular importance since CatB and collagen levels in BALF could potentially be used in the future as simple and fast detectable biomarkers for earlier diagnosis of BOS.

Another very strikingly finding was that CatB-deficient mice showed a reduced peri-bronchial collagen production and graft protection against the development of BOS (**Figure 32-34**). However, the lack of CatB did not affect the recruitment of macrophages into the allograft (**Figure 35**), proposing CatB as player in the BOS development. With our mouse model of LTx, we could definitively demonstrate that the exclusive lack of CatB was sufficient to prevent collagen deposition and BOS development.

Due to the extensive immunosuppressive therapy, impaired mucous-clearance and continuous exposure to external microbes, BOS patients have shown high incidence of bacterial infection before and/or during the progression of the disease, that has been associated with an increased release of inflammatory mediators, such as LPS (120) and IFN γ (121-122). In our study, to simulate the *in vivo* mechanism, we therefore used LPS and IFN γ as main triggers for pro-inflammatory macrophages (**Figure 36**) (123).

In order to address the role of CatB in the development of the BOS disease, we simulated the *in vivo* mechanism of chronic rejection by using an *in vitro* system (**Figure 36**). Macrophages were used as source of CatB, while fibroblasts were used as effector cells and source of collagen. Importantly, we demonstrated that pro-inflammatory macrophages were the main source of CatB in the *in vitro* as well as in the *in vivo* model of rejection (**Figure 37A-38**). Furthermore, using a specific inhibitor of CatB-activity, called CA074, we displayed that CatB, once released in the extracellular space, binds TGF- β 1 and converts it into its active form (**Figure 40**) to promote fibroblasts activation (**Figure 41**). Although there is no clear knowledge about the physical interaction between CatB and TGF- β 1, we speculate that CatB preferentially binds TGF- β 1 on the Arginine-residuals (100) of the cleavage site, and by that promotes the dissociation of the latent protein (LAP) from the active sequence of TGF- β 1.

This finding already suggests CatB inhibition as a promising therapeutic target in the treatment of BOS. However, we have to take into account that other factors (85) might play a role in the development of BOS progression.

The autocrine effect of CatB in TGF- β 1 driven activation of fibroblasts was previously reported in *in vitro* studies (103). Fibroblasts from IPF patients showed higher levels and activity of CatB when compared with healthy patients; moreover, CatB activity enhanced the activation of TGF- β signalling and by that promoted the production of collagen in IPF patients (103).

By addressing the role of macrophage-derived CatB in BOS, we demonstrated that the paracrine signalling of CatB was necessary to activate latent TGF- β 1. Interestingly, a previous study confirmed the ability of pro-inflammatory M1 macrophages in inducing fibroblast activation; although, the key mediator was not investigated (119).

In-depth analysis of CatB activity revealed a marked increase in BOS patients with a history of pulmonary fibrosis (**Figure 21A**), and not in other underlying diseases (**Figure 21B**). We believe there is a systemic bioavailability of CatB in those patients, which depends on the pro-inflammatory macrophages that are recruited into the allograft after LTx. In accordance with our findings, recent single cell-transcriptome analysis, from two independent groups, showed a substantial increase of CatB levels in lungs that were explanted from patients with lung fibrosis (**Figure 26**). Consistently, we observed in the same group of patients with BOS a concomitant reduction in CysC (**Figure 21C**), and not in other underlying diseases (**Figure 21D**). Therefore, we think that the increase of CatB activity in BALF from LTx patients with underlying lung fibrosis results from the lack of the negative regulation from its endogenous regulator (CysC). Interestingly, previous findings demonstrated the presence of lung fibrosis as consequence of CysC deficiency (88).

According to the findings achieved in the present study, and in the light of the increasing demand of personalized medicine, we here suggest the usage of a CatB inhibitor for BOS patients with a history of lung fibrosis, although is not yet investigated in clinical studies.

On the preclinical level, several chemical inhibitors of CatB activity have been described. CatB inhibition is widely investigated in the context of tumor, since it is strongly suggested as driving factor of tumor progression in several solid organs (124-125), as well as in the lung (126). Commercially available and newly synthesized drugs have been tested *in vitro* and *in vivo* models. Among these, Ca074, has been described as a specific inhibitor of CatB activity also in a preclinical study, preventing tissue fibrosis in rat (127).

Moreover, a recent study has developed new construct that conjugated a CatB inhibitor to a liposomal nanocarrier (LNC-NS-629), which is able to target extracellular and intracellular

CatB in an irreversible way. Moreover, this drug was showed to efficiently reach macrophages and inhibit its target (128). Based on all our findings, we suggest this compound as a potential therapy for LTx patients to prevent BOS progression; for instance, by using a drug liposome aerosol-based system to specifically target the lung, we could use lower concentration of the drug, prevent local irritation, increase the bioavailability of the drug and increase potency with reduced systemic toxicity. This approach would improve the efficiency of therapeutic approaches (129).

In this work, we successfully obtained a reasonable number of BALF samples from LTx patients, most of those referring to a different stage of BOS disease (**Table 14**), giving the opportunity of investigating disease-related targets along the progression of the disease; however, we were limited from the heterogeneity of LTx patients. The BALF Munich cohort was mainly composed of patients with a history of lung fibrosis. In order to strengthen our findings for clinical application, a larger number of cases (around 10) per underlying disease is preferred, in order to obtain results that are clinically useful. Moreover, the use of a second human cohort is suggested in order to estimate whether different therapeutic strategies affect our findings.

In conclusion, based on our results, in human as well as in mice, this study clearly shows the crucial role of macrophage-produced CatB in the TGF β -1 mediated production of collagen by fibroblasts already at early stages of BOS, suggesting CatB as early marker of BOS progression.

6. REFERENCES

- 1: Crapo JD, Broaddus VC, Brody AR, et al., American Thoracic Society. *Am J Respir Crit Care Med* 2003; 168(2):250-4
- 2: Iwasaki A, Medzhitov R., Control of adaptive immunity by the innate immune system. *Nat Immunol* 2015; 16(4):343–353
- 3: Lobo LJ, Aris RM, Schmitz J, et al., Donor-specific antibodies are associated with antibody-mediated rejection, acute cellular rejection, bronchiolitis obliterans syndrome, and cystic fibrosis after lung transplantation. *JHLT* 2013; 32(1):70–77
- 4: Snyder LD, Wang Z, Chen DF, et al., Implications for human leukocyte antigen antibodies after lung transplantation: a 10-year experience in 441 patients. *Chest* 2013; 144(1):226–233
- 5: Meyer KC, Recent advances in lung transplantation. *F1000Res* 2018; 7
- 6: Snell GI, Levvey BJ, Levin K, et al., Donation after Brain Death versus Donation after Circulatory Death: Lung Donor Management Issues. *Semin Respir Crit Care Med* 2018; 39(2):138–147
- 7: Costa J, Shah L, Robbins H, et al., Use of Lung Allografts From Donation After Cardiac Death Donors: A Single-Center Experience. *Ann Thorac Surg* 2018; 105(1):271–278
- 8: Ruttens D, Martens A, Ordies S, et al., After Lung Transplantation From Circulatory-Dead Donors: A Single-Center Experience. *Transplantation* 2017; 101(11):2691–2694
- 9: Toronto Lung Transplant Group, Unilateral lung transplantation for pulmonary fibrosis. *N Engl J Med* 1986; 314(18):1140–1145
- 10: Dark JH, Patterson GA, Al-Jilaihawi AN, et al., Experimental en bloc double-lung transplantation. *Ann Thorac Surg* 1986; 42(4):394–398
- 11: Birsan T, Zuckermann A, Artemiou O, et al., Functional results and long-term outcome after bilateral lung transplantation for pulmonary hypertension. *Wiener klinische Wochenschrift* 1998; 110(2):45–52
- 12: Patterson GA, Todd TR, Cooper JD, et al., Airway complications after double lung transplantation. *J Thorac Cardiovasc Surg* 1990; 99(1):14–21
- 13: Noirclerc MJ, Metras D, Vaillant A, et al., Bilateral bronchial anastomosis in double lung and heart-lung transplantations. *Eur J Cardiothorac Surg* 1990; 4(6):314–317
- 14: Pasque MK, Cooper JD, Kaiser LR, et al., Improved technique for bilateral lung transplantation: rationale and initial clinical experience. *Ann Thorac Surg* 1990; 49(5):785–791
- 15: Fakhro M, Ingemansson R, Skog I, et al., 25-year follow-up after lung transplantation at Lund University Hospital in Sweden: superior results obtained for patients with cystic fibrosis. *Interact Cardiovasc Thorac Surg* 2016; 23(1):65–73
- 16: Egan TM, Murray S, Bustami RT, et al. Development of the new lung allocation system in the United States. *Am J Transplant.* 2006;6(5 Pt 2):1212-1227
- 17: Verleden GM, Dupont L, Yserbyt J, et al., Recipient selection process and listing for lung transplantation. *J Thorac Dis* 2017; 9(9):3372–3384
- 18: De Meester J, Smits JM, Persijn GG, et al., Listing for lung transplantation: life expectancy and transplant effect, stratified by type of end-stage lung disease, the Eurotransplant experience. *J Heart Lung Transplant* 2001; 20(5):518–524
- 19: Kotloff RM, Thabut G., Lung transplantation. *Am J Respir Crit Care Med* 2011; 184(2):159–171

- 20: Van Raemdonck D, Neyrinck A, Cypel M, et al., Ex-vivo lung perfusion. *Transpl Int* 2015; 28(6):643–656
- 21: Hosenpud JD, Bennett LE, Keck BM, et al., The Registry of the International Society for Heart and Lung Transplantation: seventeenth official report-2000. *J Heart Lung Transplant* 2000; 19(10):909–931
- 22: Criée CP, Sorichter S, Smith HJ, et al., Body plethysmography-its principles and clinical use. *Respir Med* 2011; 105(7):959–971
- 23: Morrish WF, Herman SJ, Weisbrod GL, et al., Bronchiolitis obliterans after lung transplantation: findings at chest radiography and high-resolution CT. *Radiology* 1991; 179(2):487–490
- 24: Collins J., Imaging of the chest after lung transplantation. *J Thorac Imaging* 2002; 17(2):102–112
- 25: Leung AN, Fisher K, Valentine V, et al., Bronchiolitis obliterans after lung transplantation: detection using expiratory HRCT. *Chest* 1998; 113(2):365–370
- 26: Stewart S, Fishbein MC, Snell GI, et al., Revision of the 1996 working formulation for the standardization of nomenclature in the diagnosis of lung rejection. *J Heart Lung Transplant* 2007; 26(12):1229–1242
- 27: Frost AE, Jammal CT, Cagle PT., Hyperacute rejection following lung transplantation. *Chest* 1996; 110(2):559–562
- 28: Ingulli E. et al., Mechanism of cellular rejection in transplantation. *Pediatr Nephrol* 2010, 25:61-74
- 29: Glanville AR, et al. Severity of lymphocytic bronchiolitis predicts long-term outcome after lung transplantation. *Am J Respir Crit Care Med*.2008; 177:1033–40.
- 30: Meyer KC, Raghu G, Verleden GM, et al., An international ISHLT/ATS/ERS clinical practice guideline: diagnosis and management of bronchiolitis obliterans syndrome. *Eur Respir J* 2014; 44(6):1479–1503
- 31: Estenne M, Maurer JR, Boehler A, et al., Bronchiolitis obliterans syndrome 2001: an update of the diagnostic criteria. *J Heart Lung Transplant* 2002;21(3):297–31
- 32: Sato M, Waddell TK, Wagnetz U, et al., Restrictive allograft syndrome (RAS): a novel form of chronic lung allograft dysfunction. *J Heart Lung Transplant* 2011; 30(7):735–742
- 33: Verleden SE, Von Der Thüsen J, Van Herck A, et al., Identification and characterization of chronic lung allograft dysfunction patients with mixed phenotype: A single-center study. *Clin Transplant* 2020; 34(2):e13781
- 34: Verleden SE, Vos R, Vanaudenaerde BM, Verleden GM., Chronic lung allograft dysfunction phenotypes and treatment. *J Thorac Dis*. *J Thorac Dis* 2017; 9(8):2650-2659
- 35: Barker AF, Bergeron A, Rom WN, Hertz MI, Obliterative bronchiolitis. *N Engl J Med* 2014; 370(19):1820-1828
- 36: Burke CM, Theodore J, Dawkins KD, et al., Post-transplant obliterative bronchiolitis and other late lung sequelae in human heart-lung transplantation. *Chest* 1984; 86(6):824-829
- 37: Schlesinger C, Meyer CA, Veeraghavan S, Koss MN., Constrictive (obliterative) bronchiolitis: diagnosis, etiology, and a critical review of the literature. *Ann Diagn Pathol* 1998; 2(5):321-324
- 38: Buttgerit F, da Silva JA, Boers M, et al., Standardised nomenclature for glucocorticoid dosages and glucocorticoid treatment regimens: current questions and tentative answers in rheumatology. *Ann Rheum Dis* 2002; 61(8):718-722

- 39: Knoop C, Antoine M, Vachiéry JL, et al., FK 506 rescue therapy for irreversible airway rejection in heart-lung transplant recipients: report on five cases. *Transplant Proc* 1994; 26(6):3240-3241
- 40: Borro JM, Bravo C, Solé A, et al., Conversion from cyclosporine to tacrolimus stabilizes the course of lung function in lung transplant recipients with bronchiolitis obliterans syndrome. *Transplant Proc* 2007; 39(7):2416-2419
- 41: Vos R, Vanaudenaerde BM, Ottevaere A, et al., Long-term azithromycin therapy for bronchiolitis obliterans syndrome: divide and conquer? *J Heart Lung Transplant* 2010; 29(12):1358-1368
- 42: Zhang B, Bailey WM, Kopper TJ, et al., Azithromycin drives alternative macrophage activation and improves recovery and tissue sparing in contusion spinal cord injury. *J Neuroinflammation* 2015; 12:218
- 43: Hodge, S., Hodge, G., Brozyna, S., et al., Azithromycin increases phagocytosis of apoptotic bronchial epithelial cells by alveolar macrophages. *European Respiratory Journal* 2006; 28(3):486-495
- 44: Hachem R, Corris P., Extracorporeal Photopheresis for Bronchiolitis Obliterans Syndrome After Lung Transplantation. *Transplantation* 2018; 102(7):1059-1065
- 45: Vanaudenaerde BM, et al. A dichotomy in bronchiolitis obliterans syndrome after lung transplantation revealed by azithromycin therapy. *Eur Respir J*. 2008; 32:832–43
- 46: Devouassoux, G., Drouet C, Pin I, Alveolar neutrophilia is a predictor for the bronchiolitis obliterans syndrome, and increases with degree of severity. *J Transplant Immunol* 2002; 10(4):303-310
- 47: Verleden SE, Ruttens D, Vos R, et al., Differential cytokine, chemokine and growth factor expression in phenotypes of chronic lung allograft dysfunction. *Transplantation* 2015; 99(1):86-93
- 48: Beck J, Oellerich M, Schulz U, et al., Donor-Derived Cell-Free DNA Is a Novel Universal Biomarker for Allograft Rejection in Solid Organ Transplantation. *Transplant Proc* 2015; 47(8):2400-2403
- 49: Gimino VJ, Lande JD, Berryman TR, King RA, Hertz MI. Gene expression profiling of bronchoalveolar lavage cells in acute lung rejection. *Am J Respir Crit Care Med* 2003; 168:1237–1242
- 50: Jungraithmayr W, Weder W. The technique of orthotopic mouse lung transplantation as a movie-improved learning by visualization. *Am J Transplant*. 2012 Jun;12(6):1624-6
- 51: Sato M, Hirayama S, Hwang DM, et al., The role of intrapulmonary de novo lymphoid tissue in obliterative bronchiolitis after lung transplantation. *J Immunol* 2009; 182(11):7307-7316
- 52: Smirnova NF, Conlon TM, Morrone C, et al., Inhibition of B cell-dependent lymphoid follicle formation prevents lymphocytic bronchiolitis after lung transplantation. *JCI Insight* 2019; 4(3): e123971
- 53: Martin TR, Frevert CW., Innate immunity in the lungs. *Proc Am Thorac Soc* 2005; 2(5):403-411
- 54: Mosser DM, Edwards JP., Exploring the full spectrum of macrophage activation. *Nat Rev Immunol* 2010; 10(6):460
- 55: Morales-Nebreda L, Misharin AV, et al., The heterogeneity of lung macrophages in the susceptibility to disease. *Eur Respir Rev* 2015; 24(137):505-509

- 56: Hashimoto D, Chow A, Noizat C, et al., Tissue-resident macrophages self-maintain locally throughout adult life with minimal contribution from circulating monocytes. *Immunity* 2013; 38(4):792-804
- 57: Hussell T, Bell TJ., Alveolar macrophages: plasticity in a tissue-specific context. *Nat Rev Immunol* 2014; 14(2):81-93
- 58: Xue J, Schmidt SV, Sander J, et al., Transcriptome-based network analysis reveals a spectrum model of human macrophage activation. *Immunity* 2014; 40(2):274-288
- 59: Gaudino SJ, Kumar P., Cross-Talk Between Antigen Presenting Cells and T Cells Impacts Intestinal Homeostasis, Bacterial Infections, and Tumorigenesis. *Front Immunol* 2019; 10:360
- 60: Koenig A, Thauinat O., Lymphoid Neogenesis and Tertiary Lymphoid Organs in Transplanted Organs. *Front Immunol* 2016; 7:646
- 61: Liu W, Xiao X, Demirci G, et al., Innate NK cells and macrophages recognize and reject allogeneic nonself in vivo via different mechanisms. *J Immunol* 2012; 188(6):2703-2711
- 62: Stewart S, Winters GL, Fishbein MC, et al., Revision of the 1990 working formulation for the standardization of nomenclature in the diagnosis of heart rejection. *J Heart Lung Transplant* 2005; 24(11):1710-1720
- 63: Beckmann N, Cagnet C, Fringeli-Tanner M, et al., Macrophage labeling by SPIO as an early marker of allograft chronic rejection in a rat model of kidney transplantation. *Magn Reson Med* 2003; 49(3):459-467
- 64: Azuma H, Nadeau KC, Ishibashi M, et al., Prevention of functional, structural, and molecular changes of chronic rejection of rat renal allografts by a specific macrophage inhibitor. *Transplantation* 1995; 60(12):1577-1582
- 65: Pilmore HL, Painter DM, Bishop GA, Early up-regulation of macrophages and myofibroblasts: a new marker for development of chronic renal allograft rejection. *Transplantation* 2000; 69(12):2658-2662
- 66: Scalea JR, Tomita Y, Lindholm CR, et al., Transplantation Tolerance Induction: Cell Therapies and Their Mechanisms. *Front Immunol* 2016; 7:87
- 67: Liu W, Xiao X, Demirci G, Madsen J, et al., Innate NK cells and macrophages recognize and reject allogeneic nonself in vivo via different mechanisms. *J Immunol* 2012; 188(6):2703-2711
- 68: Oberbarnscheidt, Martin H., et al., Non-self recognition by monocytes initiates allograft rejection. *J Clin Invest* 2014; 124(8):3579-3589
- 69: Qi F, Adair A, Ferenbach D, et al., Depletion of cells of monocyte lineage prevents loss of renal microvasculature in murine kidney transplantation. *Transplantation* 2008; 86(9):1267-1274
- 70: Bräsen JH, Khalifa A, Schmitz J, et al., Macrophage density in early surveillance biopsies predicts future renal transplant function. *Kidney Int* 2017; 92(2):479-489
- 71: Bergler T, Jung B, Bourier F, et al., Infiltration of Macrophages Correlates with Severity of Allograft Rejection and Outcome in Human Kidney Transplantation. *PLoS One* 2016; 11(6): e0156900
- 72: Matheson PJ, Dittmer ID, Beaumont BW, et al., The macrophage is the predominant inflammatory cell in renal allograft intimal arteritis. *Transplantation* 2005; 79(12):1658-1662
- 73: Osterholzer JJ, Olszewski MA, Murdock BJ, et al., Implicating exudate macrophages and Ly-6C(high) monocytes in CCR2-dependent lung fibrosis following gene-targeted alveolar injury. *J Immunol* 2013; 190(7):3447-3457

- 74: Piguet PF, Ribaux C, Karpuz V, et al., Expression and localization of tumor necrosis factor-alpha and its mRNA in idiopathic pulmonary fibrosis. *Am J Pathol* 1993; 143(3):651-655
- 75: Raghu G, Brown KK, Costabel U, et al., Treatment of idiopathic pulmonary fibrosis with etanercept: an exploratory, placebo-controlled trial. *Am J Respir Crit Care Med* 2008; 178(9):948-955
- 76: Lappalainen U, Whitsett JA, Wert SE, et al., Interleukin-1beta causes pulmonary inflammation, emphysema, and airway remodeling in the adult murine lung. *Am J Respir Cell Mol Biol* 2005; 32(4):311-318
- 77: Gasse P, Mary C, Guenon I, et al., IL-1R1/MyD88 signaling and the inflammasome are essential in pulmonary inflammation and fibrosis in mice. *J Clin Invest* 2007; 117(12):3786-3799
- 78: Todd JL, Palmer SM., Bronchiolitis obliterans syndrome: the final frontier for lung transplantation. *Chest* 2011; 140(2):502-508
- 79: Rockey DC, Bell PD, Hill JA., Fibrosis--a common pathway to organ injury and failure. *N Engl J Med* 2015; 372(12):1138-1149
- 80: Wynn TA., Fibrotic disease and the T(H)1/T(H)2 paradigm. *Nat Rev Immunol* 2004; 4(8):583-594
- 81: Hinz B, Phan SH, Thannickal VJ, et al., The myofibroblast: one function, multiple origins. *Am J Pathol* 2007; 170(6):1807-1816
- 82: Rockey DC, Housset CN, Friedman SL., Activation-dependent contractility of rat hepatic lipocytes in culture and in vivo. *J Clin Invest* 1993; 92(4):1795-1804
- 83: Meng XM, Nikolic-Paterson DJ, Lan HY., TGF- β : the master regulator of fibrosis. *Nat Rev Nephrol* 2016; 12(6):325-338
- 84: Manchanda M, Das P, Gahlot GPS, et al., Cathepsin L and B as Potential Markers for Liver Fibrosis: Insights From Patients and Experimental Models. *Clin Transl Gastroenterol* 2017; 8(6): e99
- 85: Horan GS, Wood S, Ona V, et al., Partial inhibition of integrin alpha(v)beta6 prevents pulmonary fibrosis without exacerbating inflammation. *Am J Respir Crit Care Med* 2008; 177(1):56-65
- 86: Mu D, Cambier S, Fjellbirkeland L, et al., The integrin alpha(v)beta8 mediates epithelial homeostasis through MT1-MMP-dependent activation of TGF-beta1. *J Cell Biol* 2002; 157(3):493-507
- 87: Girolami I, Veronese N, Smith L, et al., The Activation Status of the TGF- β Transducer Smad2 Is Associated with a Reduced Survival in Gastrointestinal Cancers: A Systematic Review and Meta-Analysis. *Int J Mol* 2019; 20(15):3831
- 88: Sokol JP, Neil JR, Schiemann BJ, et al., The use of cystatin C to inhibit epithelial-mesenchymal transition and morphological transformation stimulated by transforming growth factor-beta. *Breast Cancer Res* 2005; 7(5): R844-853
- 89: Kim, Young-Im, et al., Epithelial cell-derived cytokines CST3 and GDF15 as potential therapeutics for pulmonary fibrosis. *Cell death & disease* 2018; 9(5):1-14
- 90: Rawlings, Neil D., and Alan J. Barrett., Evolution of proteins of the cystatin superfamily. *J Mol* 1990; 30(1):60-71
- 91: Tenstad O, Roald AB, Grubb A, Renal handling of radiolabelled human cystatin C in the rat. *J Clin Lab Invest* 1996; 56(5):409-414

- 92: Rudzińska M, Parodi A, Soond SM, et al., The Role of Cysteine Cathepsins in Cancer Progression and Drug Resistance. *Int J Mol Sci* 2019; 20(14):3602
- 93: Bode W, Engh R, Musil D, et al., The 2.0 Å X-ray crystal structure of chicken egg white cystatin and its possible mode of interaction with cysteine proteinases. *EMBO J* 1988; 7(8):2593-2599
- 94: Kasabova M, Villeret B, Gombault A, et al., Discordance in cathepsin B and cystatin C expressions in bronchoalveolar fluids between murine bleomycin-induced fibrosis and human idiopathic fibrosis. *Respir Res* 2016; 17(1):118
- 95: Martin SL, Moffitt KL, McDowell A, et al., Association of airway cathepsin B and S with inflammation in cystic fibrosis. *Pediatric pulmonology* 2010; 45(9):860-868
- 96: Müntener K, Zwicky R, Csucs G, et al., Exon skipping of cathepsin B: mitochondrial targeting of a lysosomal peptidase provokes cell death. *J Biol Chem* 2004; 279(39):41012-41017
- 97: Roshy S, Sloane BF, Moin K, Pericellular cathepsin B and malignant progression. *Cancer Metastasis Rev* 2003; 22(23):271-286
- 98: Illy C, Quraishi O, Wang J, et al., Role of the occluding loop in cathepsin B activity. *J Biol Chem* 1997; 272(2):1197-1202
- 99: Musil D, Zucic D, Turk D, et al., The refined 2.15 Å X-ray crystal structure of human liver cathepsin B: the structural basis for its specificity. *EMBO J* 1991; 10(9):2321-2330
- 100: Imeida PC, Nantes IL, Chagas JR, et al., Cathepsin B activity regulation. Heparin-like glycosaminoglycans protect human cathepsin B from alkaline pH-induced inactivation. *J Biol Chem* 2001; 276(2):944-951
- 101: Cotrin SS, Puzer L, de Souza Judice WA, et al., Positional-scanning combinatorial libraries of fluorescence resonance energy transfer peptides to define substrate specificity of carboxydipeptidases: assays with human cathepsin B. *Anal Biochem* 2004; 335(2):244-252
- 102: Mort J S, Anneliese D. Recklies, and A. Robin Poole, Extracellular presence of the lysosomal proteinase cathepsin B in rheumatoid synovium and its activity at neutral pH. *The Official Journal of the American College of Rheumatology* 1984; 27(5):509-515
- 103: Kasabova M, Joulin-Giet A, Lecaille F, et al., Regulation of TGF- β 1-driven Differentiation of Human Lung Fibroblasts EMERGING ROLES OF CATHEPSIN B AND CYSTATIN C. *J Biol Chem* 2014; 289(23):16239-16251
- 104: El-Gamel A, Sim E, Hasleton P, et al., Transforming growth factor beta (TGF-beta) and obliterative bronchiolitis following pulmonary transplantation. *J Heart Lung Transplant* 1999; 18(9):928-837
- 104: Aubin Vega M, Chupin C, Pascariu M, et al., Dexamethasone fails to improve bleomycin-induced acute lung injury in mice. *Physiol Rep* 2019; 7(21): e14253
- 105: Kelly KE, Hertz MI, Mueller DL. T-cell and major histocompatibility complex requirements for obliterative airway disease in heterotopically transplanted murine tracheas. *Transplantation* 1998; 66:764-771
- 106: McDyer JF. Human and murine obliterative bronchiolitis in transplant. *Proc Am Thorac Soc.* 2007;4(1):37-43
- 107: Verleden GM, Glanville AR, Lease ED, et al., Chronic lung allograft dysfunction: Definition, diagnostic criteria, and approaches to treatment-A consensus report from the Pulmonary Council of the ISHLT. *J Heart Lung Transplant* 2019; 38(5):493-503

- 108: Müller C, Andersson-Sjöland A, Schultz HH, et al., Early extracellular matrix changes are associated with later development of bronchiolitis obliterans syndrome after lung transplantation. *BMJ Open Respir Res* 2017; 4(1): e000177
- 109: Westra IM, et al., Human precision-cut liver slices as a model to test antifibrotic drugs in the early onset of liver fibrosis. *Toxicol In Vitro* 2016; 35:77-85
- 110: Habermann AC, Gutierrez AJ, Linh T B, Single-cell RNA-sequencing reveals profibrotic roles of distinct epithelial and mesenchymal lineages in pulmonary fibrosis 2019
- 111: Adams TS, Schupp DC, Poli S, et al., Single Cell RNA-seq reveals ectopic and aberrant lung resident cell populations in Idiopathic Pulmonary Fibrosis
- 112: Sottile J, Hocking DC, Fibronectin polymerization regulates the composition and stability of extracellular matrix fibrils and cell-matrix adhesions. *Mol Biol Cell* 2002; 13(10):3546-3559
- 113: Borthwick LA, Corris PA, Mahida R, et al., TNF α from classically activated macrophages accentuates epithelial to mesenchymal transition in obliterative bronchiolitis. *Am J Transplant* 2013; 13(3):621-633
- 114: Vidak E, Javoršek U, Vizovišek M, Turk B, Cysteine Cathepsins and their Extracellular Roles: Shaping the Microenvironment. *Cells* 2019; 8(3):264
- 115: Vasiljeva O, Papazoglou A, Krüger A, et al., Tumor cell-derived and macrophage-derived cathepsin B promotes progression and lung metastasis of mammary cancer. *Cancer Res* 2006; 66(10):5242-5250
- 116: Weigt SS, DerHovanessian A, Wallace WD, et al., Bronchiolitis obliterans syndrome: the Achilles' heel of lung transplantation. *Semin Respir Crit Care Med* 2013; 34(3):336-351
- 117: Keane MP, Donnelly S C, Belperio J A, Imbalance in the expression of CXC chemokines correlates with bronchoalveolar lavage fluid angiogenic activity and procollagen levels in acute respiratory distress syndrome. *J Immunol* 2002; 169(11):6515-6521
- 118: King TE Jr, Mortenson RL, Bronchoalveolar lavage in patients with connective tissue disease. *J Thorac Imaging* 1992; 7(3):26-48
- 119: Hindman, B. and Q. Ma, Carbon nanotubes and crystalline silica stimulate robust ROS production, inflammasome activation, and IL-1 β secretion in macrophages to induce myofibroblast transformation. *Arch Toxicol* 2019; 93(4):887-907
- 120: Yomota M, Yanagawa N, Sakai F, et al., Association between chronic bacterial airway infection and prognosis of bronchiolitis obliterans syndrome after hematopoietic cell transplantation. *Medicine* 2019; 98(1): e13951
- 121: Hodge G, Hodge S, Nguyen PT, et al., Bronchiolitis obliterans syndrome is associated with increased p-glycoprotein expression and loss of glucocorticoid receptor from steroid-resistant proinflammatory CD8 $^+$ T cells. *Clin Exp Immunol* 2018; 192(2):242-250
- 122: Hodge G, Hodge S, Bronchiolitis obliterans syndrome is associated with increased p-glycoprotein expression and loss of glucocorticoid receptor from steroid-resistant proinflammatory CD8 $^+$ T cells. *Int J Mol Sci* 2018; 20(6):1511
- 123: Chen S, Keller I, Vosyka O, et al, Polarization of alveolar macrophages is regulated by the immunoproteasome. *Eur Respir J* 2014; 44: P879
- 124: Murata M, Miyashita S, Yokoo C, et al., Novel epoxysuccinyl peptides. Selective inhibitors of cathepsin B, in vitro. *FEBS Lett* 1991; 280(2):307-310
- 125: Vasiljeva O, Reinheckel T, Peters C, et al., Emerging roles of cysteine cathepsins in disease and their potential as drug targets. *Curr Pharm Des* 2007; 13(4):387-403

- 126: Seymour LW, Ferry DR, Kerr DJ, et al., Phase II studies of polymer-doxorubicin (PK1, FCE28068) in the treatment of breast, lung and colorectal cancer. *Int J Oncol* 2009; 34(6):1629-1636
- 127: Zhang L, Fu XH, Yu Y, et al., Treatment with CA-074Me, a Cathepsin B inhibitor, reduces lung interstitial inflammation and fibrosis in a rat model of polymyositis. *Lab Invest* 2015; 95(1):65-77
- 128: Mikhaylov G, Klimpel D, Schaschke N, et al., Selective targeting of tumor and stromal cells by a nanocarrier system displaying lipidated cathepsin B inhibitor. *Angew Chem Int Ed Engl* 2014; 53(38):10077-10081
- 129: Waldrep JC, New aerosol drug delivery systems for the treatment of immune-mediated pulmonary diseases. *Drugs Today* 1998;34(6):549–561

7. LIST OF TABLES

<i>Table 1. BOS severities according to the decline of FEV1</i>	<i>16</i>
<i>Table 2. Solutions, reagents and cell culture media used in the study.....</i>	<i>27</i>
<i>Table 3. Composition of buffers and stock solutions.....</i>	<i>29</i>
<i>Table 4. qPCR primers used in this study</i>	<i>30</i>
<i>Table 5. Primary antibodies used in this study</i>	<i>31</i>
<i>Table 6. Secondary antibodies used in this study.....</i>	<i>32</i>
<i>Table 7. List of commercial kits used in the study.....</i>	<i>32</i>
<i>Table 8. List of devices used in the study</i>	<i>33</i>
<i>Table 9. FRET substrate used in this study</i>	<i>34</i>
<i>Table 10. Recombinant proteins used in this study</i>	<i>34</i>
<i>Table 11. FRET reaction buffer composition</i>	<i>38</i>
<i>Table 12. FRET reaction solution for recombinant protein.....</i>	<i>38</i>
<i>Table 13. FRET reaction solution for sample</i>	<i>39</i>
<i>Table 14. Demographics of lung transplanted patients from Munich cohort (cohort 1).....</i>	<i>48</i>
<i>Table 15. Demographics of lung transplanted patients from France cohort (cohort 2).....</i>	<i>50</i>

8. LIST OF FIGURES

<i>Figure 1. Schematic representation of single lung transplantation.....</i>	<i>8</i>
<i>Figure 2. Underlying lung diseases incidence in adult patients before LTx.....</i>	<i>10</i>
<i>Figure 3. Lung imaging via high resolution computer tomography.....</i>	<i>14</i>
<i>Figure 4. Histological comparison between BOS and RAS tissue.....</i>	<i>16</i>
<i>Figure 5. Macrophage polarization.....</i>	<i>19</i>
<i>Figure 6. Histological features of BOS.....</i>	<i>20</i>
<i>Figure 7. Schematic description of TGF-β1 signaling.....</i>	<i>21</i>
<i>Figure 8. Schematic graph of mechanistic studies.....</i>	<i>46</i>
<i>Figure 9. Lung function measurement of LTx patients.....</i>	<i>48</i>
<i>Figure 10. BAL alveolar macrophage cell count.....</i>	<i>49</i>
<i>Figure 11. Total protein concentration in BALF of LTx patients.....</i>	<i>50</i>
<i>Figure 12. Newly formed pro-collagen 1A1 levels increased at early stage of BOS disease.....</i>	<i>51</i>
<i>Figure 13. Newly formed collagen secretion correlated with the pulmonary function.....</i>	<i>52</i>
<i>Figure 14. CysC protein expression decreased in BOS lung tissue.....</i>	<i>53</i>
<i>Figure 15. CysC expression in macrophages in the lung tissue of Healthy donors.....</i>	<i>53</i>
<i>Figure 16. CatB activity increased in BOS.....</i>	<i>54</i>
<i>Figure 17. The increase of CatB activity was associated with a poor lung function.....</i>	<i>54</i>
<i>Figure 18. CatB protein expression increased in BOS.....</i>	<i>55</i>
<i>Figure 19. CatB protein expression increased in lung tissue of BOS patients.....</i>	<i>56</i>
<i>Figure 20. CatB and pro-collagen secretion increased over the progression of BOS.....</i>	<i>57</i>
<i>Figure 21. CatB activity and CysC levels are impaired in patients with lung fibrosis.....</i>	<i>58</i>
<i>Figure 22. Macrophages were the main source of CatB in lung tissue of BOS patients.....</i>	<i>59</i>
<i>Figure 23. Macrophages were the main source of CatB in lung tissue of the mouse model of BOS.....</i>	<i>59</i>
<i>Figure 24. Macrophages expressing CatB were recipient-derived.....</i>	<i>60</i>
<i>Figure 25. Macrophages and CatB-positive cells increased in BOS.....</i>	<i>60</i>
<i>Figure 26. Macrophages were the main source of CatB in lung fibrosis patients.....</i>	<i>61</i>
<i>Figure 27. CatB was slightly expressed in neutrophils.....</i>	<i>62</i>
<i>Figure 28. Experimental design of the orthotopic mouse lung transplantation model.....</i>	<i>63</i>
<i>Figure 29. Inflammation and fibrosis started at early stage of BOS development.....</i>	<i>64</i>
<i>Figure 30. CatB expression increased during BOS progression.....</i>	<i>65</i>
<i>Figure 31. Extracellular matrix proteins and CatB increased during BOS progression.....</i>	<i>65</i>
<i>Figure 32. Experimental design of the orthotopic mouse LTx model for functional studies.....</i>	<i>66</i>

<i>Figure 33. CatB deficient mice were protected from lung dysfunction.....</i>	<i>67</i>
<i>Figure 34. CatB deficient mice were protected from lung fibrosis</i>	<i>68</i>
<i>Figure 35. Genetic deletion of CatB did not affect macrophage infiltration</i>	<i>69</i>
<i>Figure 36. Experimental design of the in vitro model of BOS</i>	<i>70</i>
<i>Figure 37. CatB expression and activity increased in inflammatory M1 macrophages.....</i>	<i>70</i>
<i>Figure 38. CatB was expressed in pro-inflammatory macrophages in the mouse model of BOS.....</i>	<i>71</i>
<i>Figure 39. TGF-β1 expression increased in M1 macrophages.....</i>	<i>72</i>
<i>Figure 40. TGF-β1 maturation was affected by CatB inhibitor.....</i>	<i>72</i>
<i>Figure 41. CatB promoted fibroblast activation</i>	<i>73</i>

9. LIST OF PUBLICATIONS

1. Götzfried J* & Smirnova NF*, **Morrone C**, Korkmaz B, Yildirim AÖ, Eickelberg O, Jenne DE. *Preservation with $\alpha 1$ -antitrypsin improves primary graft function of murine lung transplants*. J Heart Lung Transplant. 2018 Aug;37(8):1021-1028
2. Smirnova NF, Conlon TM, **Morrone C**, Dorfmueller P, Humbert M, Stathopoulos GT, Umkehrer S, Pfeiffer F, Yildirim AÖ, Eickelberg O. *Inhibition of B cell-dependent lymphoid follicle formation prevents lymphocytic bronchiolitis after lung transplantation*. JCI Insight. 2019 Feb 7;4(3): e123971.
3. Rehm SRT, Smirnova NF, **Morrone C**, Götzfried J, Feuchtinger A, Pedersen J, Korkmaz B, Yildirim AÖ, Jenne DE. *Premedication with a cathepsin C inhibitor alleviates early primary graft dysfunction in mouse recipients after lung transplantation*. Sci Rep. 2019 Jul 9;9(1):9925.
4. Sarker RSJ* & Conlon TM*, **Morrone C**, Srivastava B, Konyalilar N, Verleden SE, Bayram H, Fehrenbach H, Yildirim AÖ. *CARMI regulates senescence during airway epithelial cell injury in COPD pathogenesis*. Am J Physiol Lung Cell Mol Physiol. 2019 Nov 1;317(5): L602-L614
5. Bölükbas DA, Datz S, Meyer-Schwickerath C, **Morrone C**, Doryab A, Gößl D, Vreka M, Yang L, Argyo C, van Rijt SH, Lindner H, Eickelberg O, Stoeger T, Schmid O, Lindstedt S, Stathopoulos GT, Bein T, and Wagner DE, Meiners S. *Organ-restricted vascular delivery of nanoparticles for lung cancer therapy*. Advanced Therapeutics 2020 April.
6. Umkehrer S, **Morrone C**, Dinkel J, Kaiser L, Smirnova NF, Yildirim AÖ, Reiser MF, Herzen J, Pfeiffer F, Hellbach K. *Phase-contrast imaging for the detection of large airway pathologies: A proof-of-principle study of a murine model for lung transplantation*. Scientific Reports 2020
7. **Rehm SRT* & Morrone C***, Smirnova NF, Doryab A, Weiß SAI, Schmid O, Yildirim A Ö, and Jenne DE. Lung preservation during cold storage and ex-vivo perfusion by Cystatin-C. *Under submission*
8. **Morrone C**, Smirnova NF, Jeridi A, Kneidinger N, Jenne DE, Eickelberg O, and Yildirim AÖ. Cathepsin-B promotes collagen biosynthesis driving the progression of Bronchiolitis Obliterans Syndrome. *Under re-submission*

* equal contribution to the work

ACKNOWLEDGMENT

I have finally reached the end of this chapter, coloured of beautiful moments and of some gray lines that all make this experience unique.

I can't believe that I have reached the end of this journey, that I hardly desired in the beginning after 2 years of search.

Everything I have reached and learned was not possible without the help and the support of several people.

I am grateful to **Oliver Eickelberg** for giving me the opportunity to play my game, and to start my PhD in his group.

I am very thankful to **Natalia Smirnova**, who was my supervisor for almost 2 years, for the guidance, enthusiasm and extensive scientific discussions. This experience has conveyed to me the importance of thinking independently about my project, managing each step, working hard, without neglecting the efficiency.

Special appreciation and immense gratitude go to a special person, **Aicha Jeridi**, our young PostDoc, for her excellent scientific and personal support and for the extensive scientific discussions, that I already miss. Above all, a big thank you for the great effort in editing my thesis. Thank you, Aicha!!

A special thanks goes to my supervisor, **Oender Yildirim**, for welcoming me in his lab and for the committed supervision of my project. Despite our personal challenges, he had always been open to discussion.

I would also thank **Nikolaus Kneidinger** and **Alexey Dashkevich** for their advice and clinical support along my project.

Furthermore, I feel glad for all the colleagues I got the chance to share with beautiful experiences. A warm thanks to **Gizem** and **Carol** (in NH), and **Arunima**, **Mario** and **Steffi** (in GH) for the time spent together and for being good friends in difficult periods. A kind thanks to **Tom** for being always there for precious scientific suggestions.

Many thanks to **Wolfgang Jungraithmayr** for giving me the great opportunity to join the fantastic course on mouse lung transplantation; and to **John McDyer** for being a great mentor in lung transplantation.

Moreover, I enjoyed the collaboration with the ingenious **Ali Dorjab**, **Salome Rehm** and Prof. **Dieter Jenne**.

I want to express my immense gratitude to my mum, **Mina**, and my brother, **Daniele**, for having constantly believed in me.